

İSTANBUL TECHNICAL UNIVERSITY ★ INSTITUTE OF INFORMATICS

**ASSIMILATION OF GPS-RO ATMOSPHERIC PROFILE DATA: A CASE
STUDY OF A MEDITERRANEAN LOW PRESSURE SYSTEM**

**M.Sc. Thesis by
Şeyda TANRIÖVER**

Department : Advanced Technologies

Programme : Satellite Remote Sensing and Communication

June 2009

İSTANBUL TECHNICAL UNIVERSITY ★ INSTITUTE OF INFORMATICS

**ASSIMILATION OF GPS-RO ATMOSPHERIC PROFILE DATA: A CASE
STUDY OF A MEDITERRANEAN LOW PRESSURE SYSTEM**

**M.Sc. Thesis by
Şeyda TANRIÖVER
(705051008)**

**Date of submission : 29 June 2009
Date of defence examination: 02 June 2009**

**Supervisor (Chairman) : Prof. Dr. Mikdat KADIOĞLU (ITU)
Members of the Examining Assoc. Prof. Dr. Yurdanur SEZGİNER
Committee : ÜNAL (ITU)
Assoc. Prof. Dr. Tayfun KINDAP (ITU)**

June 2009

İSTANBUL TEKNİK ÜNİVERSİTESİ ★ BİLİŞİM ENSTİTÜSÜ

**GPS-RO ATMOSFERİK PROFİL VERİSİNİN ASİMİLASYONU: BİR
AKDENİZ ALÇAK BASINÇ SİSTEMİNİN VAKA ANALİZİ**

**YÜKSEK LİSANS TEZİ
Şeyda TANRIÖVER
(705051008)**

Tezin Enstitüye Verildiği Tarih : 29 Haziran 2009

Tezin Savunulduğu Tarih : 2 Haziran. 2009

**Tez Danışmanı : Prof. Dr. Mikdat KADIOĞLU (İTÜ)
Diğer Jüri Üyeleri : Doç. Dr. Yurdanur SEZGİNER ÜNAL (İTÜ)
Doç. Dr. Tayfun KINDAP (İTÜ)**

Haziran 2009

FOREWORD

I would like to thank to my supervisor Prof. Dr. Mikdat Kadiođlu for his guidance and support. I would like to express my deep appreciation and thanks to Dr. Altuđ Aksoy for his advices, ideas and cooperation. I would also thank to Abdullah Kahraman and Deniz Ural for their helps. This study is performed using the hardware at the Meteorological Modelling Laboratory. Thus I am indebted to Department of Meteorological Engineering for this opportunity.

Finally, I want to present my gratefulness to my dearest family especially my mother for their encouragement and aids during my study.

June 2009

Şeyda Tanrıöver
Meteorological Engineer

TABLE OF CONTENTS

	<u>Page</u>
ABBREVIATIONS	ix
LIST OF TABLES	xi
LIST OF FIGURES	xiii
SUMMARY	xvii
ÖZET	xix
1. INTRODUCTION	1
1.1 Historical Overview on GPS-RO Data Assimilation Studies and Purpose of the Thesis	3
2. DATA ASSIMILATION	5
2.1 3DVAR Data Assimilation.....	8
3. MODELLING 20 MARCH 2007 MEDITERRANEAN LOW PRESSURE SYSTEM WITH WRF (ARW)	13
3.1 Overview on Advanced Research WRF Modeling System	13
3.2 Description of the Case	14
3.2.1 GPS-RO data availability.....	20
3.3 Sensitivity to Physical Parameterizations	21
4. ASSIMILATION OF GPS-RO BY USING WRF- 3DVAR	31
4.1 GPS Radio Occultation	31
4.1.1 Brief description of the COSMIC system.....	33
4.2. WRF- 3DVAR.....	34
4.2.1 Running WRF- 3DVAR.....	34
4.2.2 Observation preprocessor (OBSPROC)	36
4.2.3 Background error statistics (gen_be)	38
4.2.4 WRF-Var diagnostics.....	39
5. RESULTS AND DISCUSSIONS	41
5.1 Overall Average RMS and Mean Errors.....	41
5.2 Vertical Average RMS and Mean Errors Gradient.....	47
5.3 Examples of Positive Impact of Data Assimilation on Forecasts.....	53
REFERENCES	71
APPENDICES	75
CURRICULUM VITAE	93

ABBREVIATIONS

AO	: Observation Minus Analysis
BUFR	: Binary Universal Form for the Representation of Meteorological Data
CDAAC	: COSMIC Data Analysis and Archive Center
COSMIC	: Constellation Observing System for Meteorology Ionoshepre & Climate
ECMWF	: European Centre for Medium-Range Weather Forecasts
EUMETSAT	: European Organisation for the Exploitation of Meteorological Satellites
GFS	: Global Forecast System
GPS-RO	: Global Positioning System- Radio Occultation
LEO	: Low Earth Orbit
NCAR	: National Center for Atmospheric Research
NCEP	: National Centers for Environmental Prediction
NMC	: National Meteorological Center
NWP	: Numerical Weather Prediction
OBSPROC	: Observation Preprocessor
OI	: Observation Minus Initial
OMA	: Observation Minus Analysis
OMB	: Observation Minus Background
PSAS	: Physical Space Analysis System
RRTM	: Rapid Radiative Transfer Model
TACC	: Taiwan Analysis Center for COSMIC
WPS	: WRF Preprocessing System
WRF	: Weather Research and Forecasting
WRF-ARW	: Advanced Research WRF
WRF-VAR	: WRF Variational Data Assimilation System
VAR	: Variational Assimilation

LIST OF TABLES

	<u>Page</u>
Table 3.1: Parameterizations tried in sensitivity analysis (Wang et al., 2008)	21
Table 3.2: 8 different physics options variations used in WRF runs of sensitivity analysis	22
Table 3.3: RMSE and bias statistics of verification of the most accurate WRF forecast with Kain-Fritsch Scheme, Eta microphysics, Rapid Radiative Transfer Model Scheme, Dudhia Scheme Physics Options.....	23
Table 4.1: Information about WRF-Var input files	35
Table 4.2: The number of GPS-RO soundings during the case.....	37
Table 5.1: Verification results for each forecast.....	43
Table 5.2: Vertical RMS and mean error gradients of all 18 hour forecasts for both GPS-RO assimilated and not assimilated initial conditions.....	49
Table 5.3: Vertical RMS and mean error gradients of 18 hour forecasts with initial times 00Z or 12Z for both GPS-RO assimilated and not assimilated initial conditions.....	50
Table 5.4: Vertical RMS and mean error gradients of 18 hour forecasts with initial times 06Z or 18Z for both GPS-RO assimilated and not assimilated initial conditions.....	51
Table A.1 : RMSE and BIAS Statistics for Variables of cu_physics= 1, mp_physics= 3 Parameterizations Verifications.....	81
Table A.2 : RMSE and BIAS Statistics for Variables of cu_physics= 2, mp_physics= 3 Parameterizations Verifications.....	81
Table A.3 : RMSE and BIAS Statistics for Variables of cu_physics= 3, mp_physics= 3 Parameterizations Verifications.....	82
Table A.4 : RMSE and BIAS Statistics for Variables of cu_physics= 5, mp_physics= 5 Parameterizations Verifications.....	82
Table A.5 : RMSE and BIAS Statistics for Variables of cu_physics= 3, mp_physics= 5 Parameterizations Verifications.....	83
Table A.6 : RMSE and BIAS Statistics for Variables of cu_physics= 1, mp_physics= 5 ra_lw_physics= 99 Parameterizations Verifications ...	83
Table A.7 : RMSE and BIAS Statistics for Variables of cu_physics= 1, mp_physics= 5 ra_lw_physics= 99 ra_sw_physics= 9	84

LIST OF FIGURES

	<u>Page</u>
Figure 1.1 : NCEP Operational S1 Scores at 36 and 72 hour over North America (500hPa).....	1
Figure 1.2 : NCEP Operational S1 Scores: Mean Sea Level Pressure Over North America.....	2
Figure 2.1 : Schematic of grid points (circles), observations (squares), and radius of influence around a grid point 'i' signed with a black circle (Kalnay, 2003).....	6
Figure 2.2 : Typical global 6-h analysis cycle performed four times a day (00, 06, 12, 18 UTC).....	7
Figure 2.3 : Typical regional analysis cycle. Regional models needs boundary conditions coming from global forecasts.....	8
Figure 2.4 : Summurized history of the main data assimilation algoritms (Bouttier and Courtier, 1999).....	9
Figure 2.5 : Illustiration of the variational cost-function minimization in a two variable model space (Bouttier and Courtier, 1999).....	10
Figure 3.1 : WRF system components (Skamarock et al., 2008).....	13
Figure 3.2 : 500 hPa Geopotential Height and Sea Level Pressure (hPa), 20 March 2007.....	15
Figure 3.3 : 500 hPa Geopotential Height and Sea Level Pressure (hPa), 21 March 2007.....	15
Figure 3.4 : 500 hPa Geopotential Height and Sea Level Pressure (hPa), 22 March 2007.....	16
Figure 3.5 : Satellite image for the region on 22.03.2007 00:00 GMT (Turkish State Meteorological Service).....	16
Figure 3.6 : Radar image on 22.03.2007 00:00 GMT (Turkish State Meteorological Service).....	18
Figure 3.7 : WRF 18 h forecasts of total precipitation in past 6 hours valid at 06 UTC 22 March 2007.....	18
Figure 3.8 : Total precipitation in past 24 hours (Turkish State Meteorological Service).....	19
Figure 3.9 : Cosmic data avaiability during formation and evaluation period of the Mediterranean low pressure system.....	20
Figure 3.10 : Total occultation distribution for 2007.077 to 2007.083.....	21
Figure 3.11 : Mean sea level pressure difference of the forecast and the observation at 12z on 20.03.2007 with usage of Kain-Fritsch Scheme, WRF Single-Moment 3-class scheme , Rapid Radiative Transfer Model Scheme, Dudhia Scheme Physics Options.....	24
Figure 3.12 : Mean sea level pressure difference of the forecast and the observation at 12z on 20.03.2007 with usage of Betts-Miller-Janjic scheme , WRF Single-Moment 3-class scheme , Rapid Radiative Transfer Model Scheme, Dudhia Scheme Physics Options.....	24

Figure 3.13 :	Mean sea level pressure difference of the forecast and the observation at 12z on 20.03.2007 with usage of Grell-Devenyi ensemble scheme, WRF Single-Moment 3-class scheme , Rapid Radiative Transfer Model Scheme, Dudhia Scheme Physics Options.....	25
Figure 3.14 :	Mean sea level pressure difference of the forecast and the observation at 12z on 20.03.2007 with usage of Kain-Fritsch Scheme, Eta microphysics, Rapid Radiative Transfer Model Scheme, Dudhia Scheme Physics Options.....	25
Figure 3.15 :	Temperature (at 850 hPa level) difference of the forecast and the observation at 12z on 20.03.2007 with usage of Kain-Fritsch Scheme, WRF Single-Moment 3-class scheme , Rapid Radiative Transfer Model Scheme, Dudhia Scheme Physics Options.....	26
Figure 3.16 :	Temperature (at 850 hPa level) difference of the forecast and the observation at 12z on 20.03.2007 with usage of Betts-Miller-Janjic scheme , WRF Single-Moment 3-class scheme , Rapid Radiative Transfer Model Scheme, Dudhia Scheme Physics Options.....	27
Figure 3.17 :	Temperature (at 850 hPa level) difference of the forecast and the observation at 12z on 20.03.2007 with usage of Grell-Devenyi ensemble scheme,WRF Single-Moment 3-class scheme ,Rapid Radiative Transfer Model Scheme,Dudhia Scheme Physics Options..	27
Figure 3.18 :	Temperature (at 850 hPa level) difference of the forecast and the observation at 12z on 20.03.2007 with usage of Kain-Fritsch Scheme, Eta microphysics, Rapid Radiative Transfer Model Scheme, Dudhia Scheme Physics Options.....	28
Figure 3.19 :	Relative Humidity (at 700 hPa level) difference of the forecast and the observation at 12z on 20.03.2007 with usage of Kain-Fritsch Scheme, WRF Single-Moment 3-class scheme, Rapid Radiative Transfer Model Scheme, Dudhia Scheme Physics Options.....	29
Figure 3.20 :	Relative Humidity (at 700 hPa level) difference of the forecast and the observation at 12z on 20.03.2007 with usage of Betts-Miller-Janjic Scheme, WRF Single-Moment 3-class scheme, Rapid Radiative Transfer Model Scheme, Dudhia Scheme Physics Options.....	29
Figure 3.21 :	Relative Humidity (at 700 hPa level) difference of the forecast and the observation at 12z on 20.03.2007 with usage of Grell-Devenyi Ensemble Scheme, WRF Single-Moment 3-class scheme, Rapid Radiative Transfer Model Scheme, Dudhia Scheme Physics Options.....	30
Figure 3.22 :	Relative Humidity (at 700 hPa level) difference of the forecast and the observation at 12z on 20.03.2007 with usage of Kain-Fritsch Scheme, Ferrier microphysics, Rapid Radiative Transfer Model Scheme, Dudhia Scheme Physics Options.....	30
Figure 4.1 :	Geometry of a typical GPS occultation	31
Figure 4.2 :	Coverage of COSMIC GPS RO sounding in one day, Green dots are COSMIC. Red dots are radiosonde stations (Marshall& Yoe, 2005).....	33
Figure 4.3 :	Cosmic System Overview	34
Figure 4.4 :	The relationship between datasets (circles), and algorithms (rectangles) of the ARW system (Skamarock et al., 2008).....	35
Figure 4.5 :	Time window description for 3D-VAR.....	36

Figure 4.6 : Map_PLOT outputs which show the GPS-RO Occultations for given time windows	38
Figure 5.1 : Average RMS errors for 6, 12, 18, 24 hour forecasts of the study.....	44
Figure 5.2 : Average mean errors for 6, 12, 18, 24 hour forecasts of study	44
Figure 5.3 : Average RMS errors for 6, 12, 18, 24 hour forecasts with initial times 00Z and 12Z	45
Figure 5.4 : Average mean errors for 6, 12, 18, 24 hour forecasts with initial times 00Z and 12Z	46
Figure 5.5 : Average RMS errors for 6, 12, 18, 24 hour forecasts with initial times 06Z and 18Z	46
Figure 5.6 : Average mean errors for 6, 12, 18, 24 hour forecasts with initial times 06Z and 18Z	47
Figure 5.7 : Vertical average RMSE difference gradient for all 18 hour forecasts...48	
Figure 5.8 : Vertical average mean error difference gradient for all 18 hour forecasts.....	49
Figure 5.9 : Vertical average RMSE difference gradient for 18 hour forecasts with initial times 00Z or 12Z.....	50
Figure 5.10 : Vertical average mean error difference gradient for 18 hour forecasts with initial times 00Z or 12Z.....	51
Figure 5.11 : Vertical average RMSE difference gradient for 18 hour forecasts with initial times 06Z or 18Z	52
Figure 5.12 : Vertical average mean error difference gradient for 18 hour forecasts with initial times 06Z or 18Z.....	52
Figure 5.13 : (a) 20.03.2007 00:00 GMT forecast without assimilation, initialized at 19.03.2007 06:00 GMT. (b) 20.03.2007 00:00 GMT forecast with GPS-RO assimilation, initialized at 19.03.2007 06:00 GMT. (c) 20.03.2007 00:00 GMT analysis of GFS.....	53,54
Figure 5.14 : (a) 20.03.2007 06:00 GMT forecast without assimilation, initialized at 19.03.2007 12:00 GMT. (b) 20.03.2007 06:00 GMT forecast with GPS-RO assimilation, initialized at 19.03.2007 12:00 GMT. (c) 20.03.2007 06:00 GMT analysis of GFS.....	55,56
Figure 5.15 : (a) 20.03.2007 12:00 GMT forecast without assimilation, initialized at 19.03.2007 18:00 GMT. (b) 20.03.2007 12:00 GMT forecast with GPS-RO assimilation, initialized at 19.03.2007 18:00 GMT. (c) 20.03.2007 12:00 GMT analysis of GFS.....	57,58
Figure 5.16 : (a) 20.03.2007 12:00 GMT forecast without assimilation, initialized at 19.03.2007 18:00 GMT. (b) 20.03.2007 12:00 GMT forecast with GPS-RO assimilation, initialized at 19.03.2007 18:00 GMT. (c) 20.03.2007 12:00 GMT analysis of GFS.....	59,60
Figure 5.17 : (a) 20.03.2007 12:00 GMT forecast without assimilation, initialized at 19.03.2007 18:00 GMT. (b) 20.03.2007 12:00 GMT forecast with GPS-RO assimilation, initialized at 19.03.2007 18:00 GMT. (c) 20.03.2007 12:00 GMT analysis of GFS.....	61,62
Figure 5.18 : (a) 21.03.2007 12:00 GMT forecast without assimilation, initialized at 20.03.2007 18:00 GMT. (b) 21.03.2007 12:00 GMT forecast with GPS-RO assimilation, initialized at 20.03.2007 18:00 GMT. (c) 21.03.2007 12:00 GMT analysis of GFS.....	63,64
Figure 5.19 : (a) 21.03.2007 12:00 GMT forecast without assimilation, initialized at 20.03.2007 18:00 GMT. (b) 21.03.2007 12:00 GMT forecast with	

	GPS-RO assimilation, initialized at 20.03.2007 18:00 GMT. (c)	
	21.03.2007 12:00 GMT analysis of GFS.....	65,66
Figure 5.20 :	(a) 21.03.2007 18:00 GMT forecast without assimilation, initialized at	
	21.03.2007 00:00 GMT. (b) 21.03.2007 18:00 GMT forecast with	
	GPS-RO assimilation, initialized at 21.03.2007 00:00 GMT. (c)	
	21.03.2007 18:00 GMT analysis of GFS.....	67,68
Figure A.1 :	GPS-RO Occultation Distirubitions during the case	85, 86, 87, 88

ASSIMILATION OF GPS-RO ATMOSPHERIC PROFILE DATA: A CASE STUDY OF A MEDITERRANEAN LOW PRESSURE

SUMMARY

In this study the impacts of assimilation of GPS-RO data in numerical simulations of a Mediterranean low pressure system are evaluated. In 20 March 2007, a deep low-pressure centre formed over the Mediterranean Sea near the western Anatolia and later affected a large area of central and eastern Mediterranean region downstream. This system is simulated using the WRF-ARW model initialized with GFS analysis data. Several variations of physics options of WRF-ARW Version 3 are tried for sensitivity analysis of the case. GFS analyses are used for the verification of sensitivity. Finally Kain-Fritsch Scheme for cumulus parameterization, Eta microphysics for microphysics parameterization, Rapid Radiative Transfer Model Scheme for longwave radiation parameterization and Dudhia Scheme for shortwave radiation parameterizations are chosen for modelling the low pressure system accurately.

Using the WRF-VAR 3DVAR system, COSMIC (Constellation Observing System for Meteorology, Ionosphere & Climate) post-processed data are assimilated to the model. The WRF-Var system requires three input files to run: WRF first guess/boundary input-format files output from either WPS/real (cold-start) or WRF (warm-start), Observations (in ASCII format, PREBUFR or BUFR for radiance), and a background error statistics file (containing background error covariance). COSMIC wetPrf data are downloaded and prepared for Obsproc (WRF 3DVAR Observation Preprocessor) by decoding to little_r format from NETCDF format by using wefPrf decoder. The data outside the time range and domain are removed by Obsproc. Our domain-specific background error statistics are generated with the gen_be utility. Then, WRF-VAR is run. Before running a NWP forecast using the WRF model with WRF-Var analysis, the values and tendencies for each of predicted variables for the first time period in the lateral boundary condition file for domain-1 (wrfbdy_d01) must also be updated to be consistent with the new WRF-Var initial condition (analysis). This procedure is performed by the WRF-Var utility called da_updated_bc.exe.

In this study WRF is run for eleven analysis times initialized with GFS analyses only and for the same analysis times with the additional assimilation of GPS-RO observations. The 6, 12, 18 and 24 hour forecast results are verified against GPS-RO soundings. In total, 44 forecasts with GPS-RO assimilation and 44 forecasts with no GPS-RO assimilation initial conditions are compared. Improvements in these forecasts with the assimilated GPS-RO data are observed and the benefits of assimilating GPS-RO data in addition to the traditional observations assimilated by the GFS system are presented.

GPS-RO ATMOSFERİK PROFİL VERİSİNİN ASİMİLASYONU: BİR AKDENİZ ALÇAK BASINÇ SİSTEMİNİN VAKA ANALİZİ

ÖZET

Bu çalışmada GPS-RO verisinin bir Akdeniz alçak basınç sisteminin numerik simülasyonuna etkileri incelendi. 20 Mart 2007'de Akdeniz'in Batı Anadolu'ya yakın bölgelerinde derin bir alçak basınç merkezi oluştu ve doğu Akdeniz bölgesini etkisi altına aldı. Bu sistem WRF-ARW modeliyle, sınır ve başlangıç koşulları için GFS analiz verileri kullanılarak modellendi. Simülasyonu iyileştirmek için WRF-ARW modelinin 3. versiyonunun farklı parametrizasyon grupları kullanıldı. Parametrizasyon gruplarının sınanmasında GFS analizleri kullanıldı. Sonuç olarak kümülüs parametrizasyonu için Kain-Fritsch Scheme, mikrofizik parametrizasyonu için Eta microphysics, uzun dalga radyasyon parametrizasyonu için Rapid Radiative Transfer Model Scheme ve kısa dalga radyasyon parametrizasyonu için Dudhia Scheme kullanılarak sistem en iyi şekilde modellenmeye çalışıldı.

Daha sonra, WRF-VAR 3DVAR programı kullanılarak işlenmiş COSMIC (Constellation Observing System for Meteorology, Ionosphere & Climate) verileri modele asimile edildi. WRF-Var sistemi üç girdi dosyası ile çalışmaktadır. Bunlardan ilki soğuk başlangıç durumunda WPS/real in çıktısı olan, sıcak başlangıç durumunda WRF' un çıktısı olan bir WRF ilk tahmin/sınır dosyasıdır. İkincisi gözlem verilerini içeren ASCII formatında Obsproc'un çıktısı olan bir dosyadır. Sistemin çalışması için gerekli olan üçüncü girdi dosyası ise tahmin hata istatistikleri dosyasıdır.

Öncelikle COSMIC wetPrf verileri indirildi, wetPrf decoder programıyla formatları NETCDF'ten Little_r' a dönüştürüldü. Böylelikle veriler Obsproc (WRF 3DVAR Observation Preprocessor)'un okuyabileceği hale getirildi. Obsproc'la zaman aralığı ve domain dışındaki veriler ayıklandı. Gen_be programı kullanılarak vakaya ve domaine ait tahmin hata istatistikleri dosyası oluşturuldu. Gerekli girdi dosyaları hazırlandıktan sonra WRF-VAR çalıştırıldı. WRF-Var analizleri kullanılarak sayısal hava tahmin modeli çalıştırılmadan önce ana domain için sınır koşullarının da güncellenmesi gerekmektedir. Bu güncelleme işlemi için WRF-Var paketinde bulunan da_updated_bc.exe programı kullanıldı.

Çalışmada WRF on bir ayrı analiz zamanı için GPS-RO asimilasyonsuz ve GPS-RO asimilasyonlu başlangıç koşullarıyla (güncellenmiş sınır koşullarıyla) 24 saatlik çalıştırıldı. 6., 12., 18. ve 24. saat tahminleri o ana ait GPS-RO verileriyle karşılaştırıldı. Toplam 44 GPS-RO asimilasyonlu ve 44 GPS-RO asimilasyonsuz tahmin karşılaştırıldı. GPS-RO asimilasyonunun tahminlere katkıları gözlemlendi.

1. INTRODUCTION

A successful forecast requires two basic components; the first one is modeling the atmosphere realistically and the second one is defining initial conditions accurately since time integration of an atmospheric model is an initial-value problem (Lynch, 2008).

Operational numerical weather prediction has been performed by NCEP (formerly NMC, National Meteorological Center) since 1950s. Until 1973, forecasts were only carried out for the Northern Hemisphere, and globally thereafter. As a result of developments in the methods used for atmospheric observations and model properties, forecasts skills have been improved consistently throughout the years. Improvement in the NCEP forecast skill is shown in Figure 1.1 and 1.2.

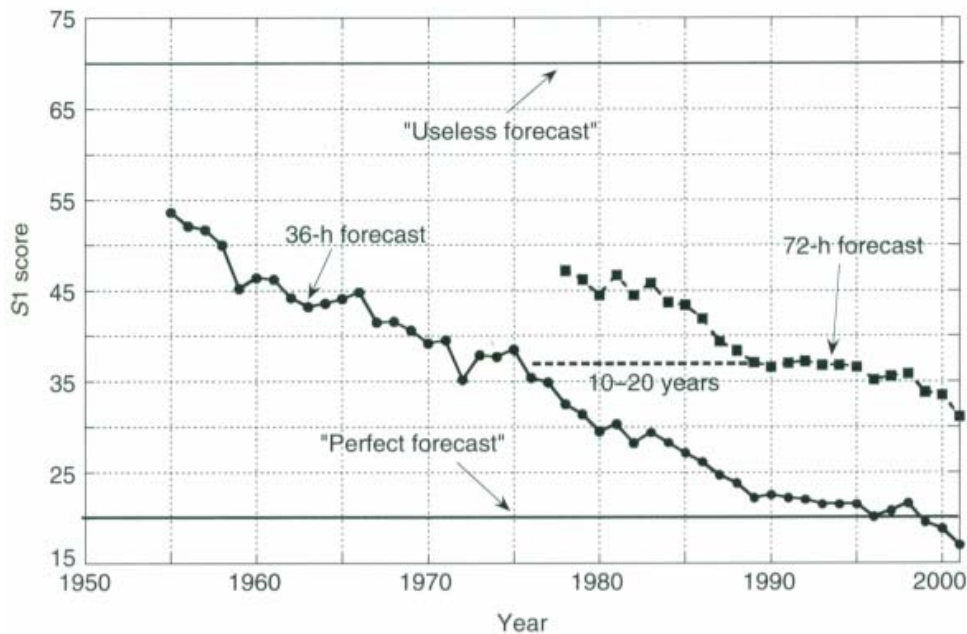


Figure 1.1 : NCEP Operational S1 Scores at 36 and 72 hour forecasts over North America (500hPa) (Kalnay, 2003)

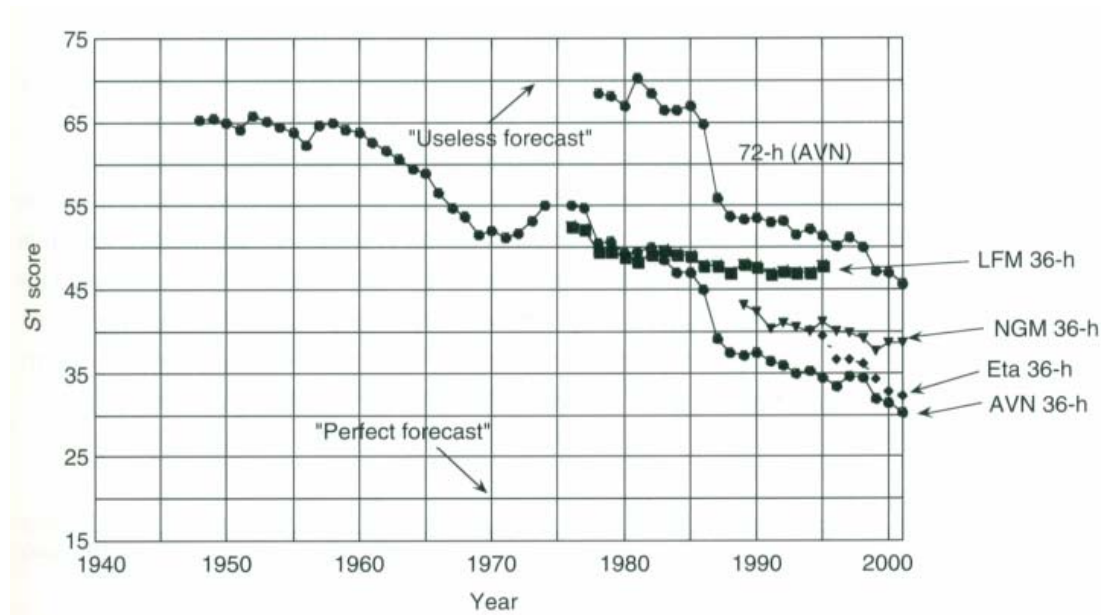


Figure 1.2 : NCEP Operational S1 Scores: Mean Sea Level Pressure Over North America (Kalnay, 2003)

Figure 1.1 shows the decrease of S1 score which measures the relative error in the horizontal gradient of the height of the 500 hPa constant pressure surface since 1955 to current day. As a result of empirical experiences at NMC, a S1 score of 70% or more assumed is interpreted as a useless inadequate forecast and a S1 score of 20% or less is assumed interpreted as a perfect forecast (Kalnay, 2003). Figure 1.2 shows the S1 score of NCEP for mean sea level pressure over North America.

Improvements in weather forecast skills are results of four main factors. They are improvements in computer technology, enhancements in model parameterizations, the increased data availability and more accurate data assimilation methods. The improvements in computer technology allow higher resolutions and fewer approximations in the numerical models. Enhancements in model parameterizations result better representations of small-scale physical processes (clouds, precipitation, moisture, radiation, etc.) in the models. More accurate data assimilation methods lead to more realistic initial conditions for the model (Kalnay, 2003).

1.1 Historical Overview on GPS-RO Data Assimilation Studies and Purpose of the Thesis

Forecast skill is limited at remote regions like oceans and seas, since the lack of data causes uncertainties in the initial conditions of the models. When five winters standard deviation of the 500-mb geopotential height difference between NCEP (National Centers for Environmental Prediction) and ECMWF (European Centre for Medium Range Forecast) global analyses are compared, the maximum differences of 500-mb geopotential height occurred at the regions where radiosonde observations are sparse such as the Pacific Ocean, the Atlantic Ocean, and the Polar regions in the northern hemisphere (Rabier et al., 1996).

Statistical comparisons of the GPS/MET retrieved refractivity and temperature profiles to global Numerical Weather Prediction (NWP) model analysis are the first studies that report positive impacts of radio occultation data on weather prediction systems. Statistics showed that the smaller differences between GPS/MET data and NWP model analysis were over data-dense (U.S., Europe) regions and the larger differences between GPS/MET data and NWP model analysis were over data-sparse (Pacific Ocean) regions.

There is no physical explanation for different errors of the GPS/MET data at those regions, so the quality of the NWP analysis which noticeably has much errors on data-sparse regions, must be the reason of this differences (Rocken et al., 1997). A similar study (Leroy, 1997) was made with time-averaged analyses of geopotential heights computed from GPS/MET (Ware et al. 1996) data and operational analyses over the same period from ECMWF. The results were the same; the biggest differences were over data-sparse regions like South Pacific Ocean (Leroy, 1997). Results of these studies imply that the GPS radio occultation data has a considerable positive impact on global analyses and global weather prediction.

COSMIC (Constellation Observing System for Meteorology Ionosphere & Climate) is a system that consists of eight Low Earth Orbit (LEO) satellites, the GPS constellation, and a ground segment that provides independent and accurate data over the Earth, with a total of 4000 soundings per day, uniformly distributed around the globe. In addition to its adequate horizontal resolution, with its high vertical resolution GPS radio occultation presents important information on the vertical

structure of temperature and pressure fields in the stratosphere and the troposphere. With improved descriptions of temperature, pressure and wind fields, important synoptic-scale atmospheric circulation systems (which are the drivers of surface cyclones and fronts, and their related weather) will be better described in the model initial conditions over the oceans and other data sparse regions (Kuo et al., 1997).

Significant cyclone activity occurs in the Mediterranean region, mainly during the cold season. As most of these cyclones form over the sea, spaceborne platforms are especially useful for observing these systems. Mediterranean Sea is a relatively data-sparse region in terms of conventional observations. The GPS technique is sensitive to the horizontal and temporal distribution of the precipitable water content in the atmosphere (e.g. Bevis et al. 1992; Rocken et al. 1995; Businger et al. 1996; Duan et al. 1996). The aim of this study is to analyse the impact of the 3DVAR assimilation of GPS measurements and conventional meteorological observations for one of these cyclone activities.

2. DATA ASSIMILATION

By using present conditions of the atmosphere as input, numerical weather prediction models simulate the evolution of the atmospheric processes, so as said before NWP is an initial-value problem. The success of the forecast is related to the determination of the initial conditions as correct as possible. The initialization of the forecast models is a very important and complex process. Currently, operational NWP centres produce initial conditions through a statistical combination of observations and short-range forecasts. This approach has been known as “data assimilation”, whose purpose is defined by Talagrand (1997) as “using all the available information, to determine as accurately as possible the state of the atmospheric (or oceanic) flow.”

In 1922 Richardson and in 1950 Charney et al. made hand interpolations of accessible observations to model grid points, and these fields of initial conditions were manually digitized. These were the first studies of data assimilation. The manual labor required to carry out such a task was immense and therefore an automated “objective analysis” was a necessity. In the subsequent decades, interpolation methods fitting data to grids were developed (e.g., Panofsky, 1949, Gilchrist and Cressman, 1954, Barnes, 1964, 1978). In figure 2.1 schematic of grid points (circles), observations (squares) which are irregularly distributed, and radius of influence around a grid point ‘i’ signed with a black circle are shown (Kalnay, 2003).

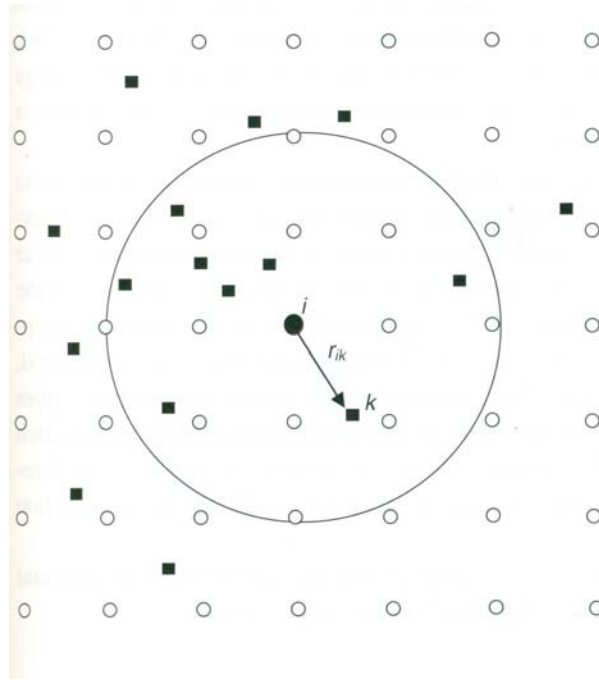


Figure 2.1 : Schematic of grid points (circles), observations (squares), and radius of influence around a grid point 'i' signed with a black circle (Kalnay, 2003)

There is a more important problem than the interpolation of observations to model grid points. The available data are not enough to initialize the current models. Modern primitive equation models have a huge number of degrees of freedom ($\sim 10^7$). For example, a latitude-longitude model with a resolution of 1° and 20 vertical levels would have $360 \times 180 \times 20 = 1.3 \times 10^6$ grid points. Also at least four prognostic variables (temperature, moisture, horizontal wind components) and surface pressure would have to be carried at each of these huge amounts of grid points. But typically 10^4 - 10^5 observations of the atmosphere are available for any given time window of ~ 3 hours and the spatial distribution of these observations is very nonuniform. For example, North America and Eurasia are relatively data rich regions and there are many regions on the globe where the observational coverage is poor.

Because of these, for preparing the initial conditions of the models, usage of additional information is a necessity so climatological information was used as first guess (also known as background field or prior information) (e.g., Gandin, 1963).

Then with the progress achieved in forecast skill, short-range forecasts began to be utilized as the first guesses in operational systems in what is called an “analysis cycle”.

The analysis cycle is an intermittent data assimilation system. Global operational systems generally use 6-h cycle performed four times a day. Information coming from observations has a dominant role in the definition of the analysis over data-rich regions. In data-poor regions, the forecast benefits from the information upstream. The forecast through the background error covariances is able to transport information from data-rich to data-poor regions, so data assimilation using a short-range forecast as a first guess has become known as four dimensional data assimilation (4DDA). 6-h forecasts over North Atlantic Ocean can be shown as an example, they are skillful because of the information coming from North America although oceans are relatively data-poor regions (Kalnay, 2003).

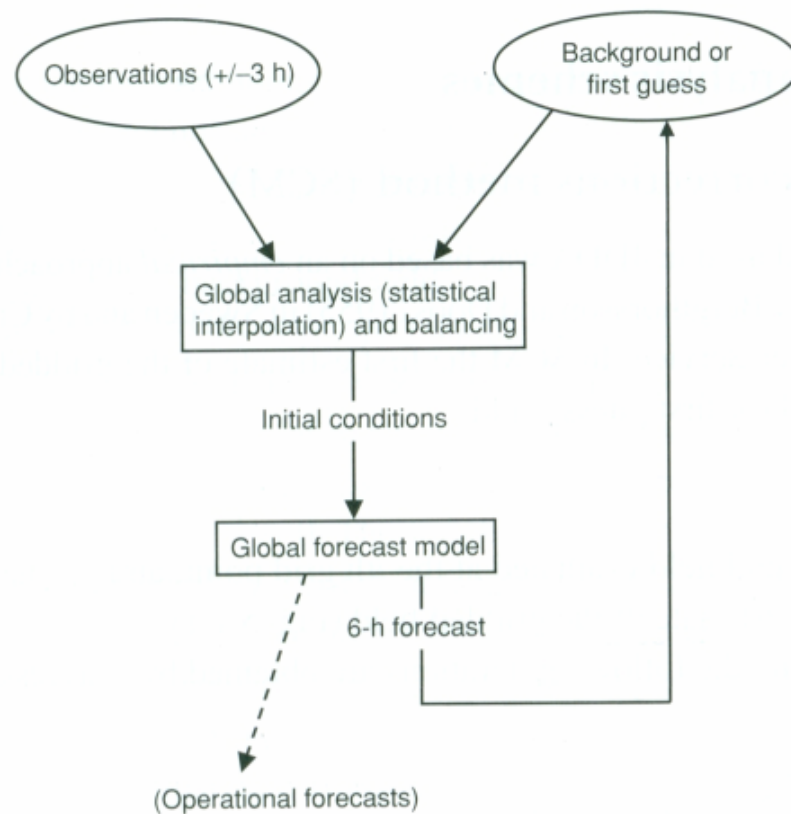


Figure 2.2 : Typical global 6-h analysis cycle performed four times a day (00, 06, 12, 18 UTC) (Kalnay, 2003).

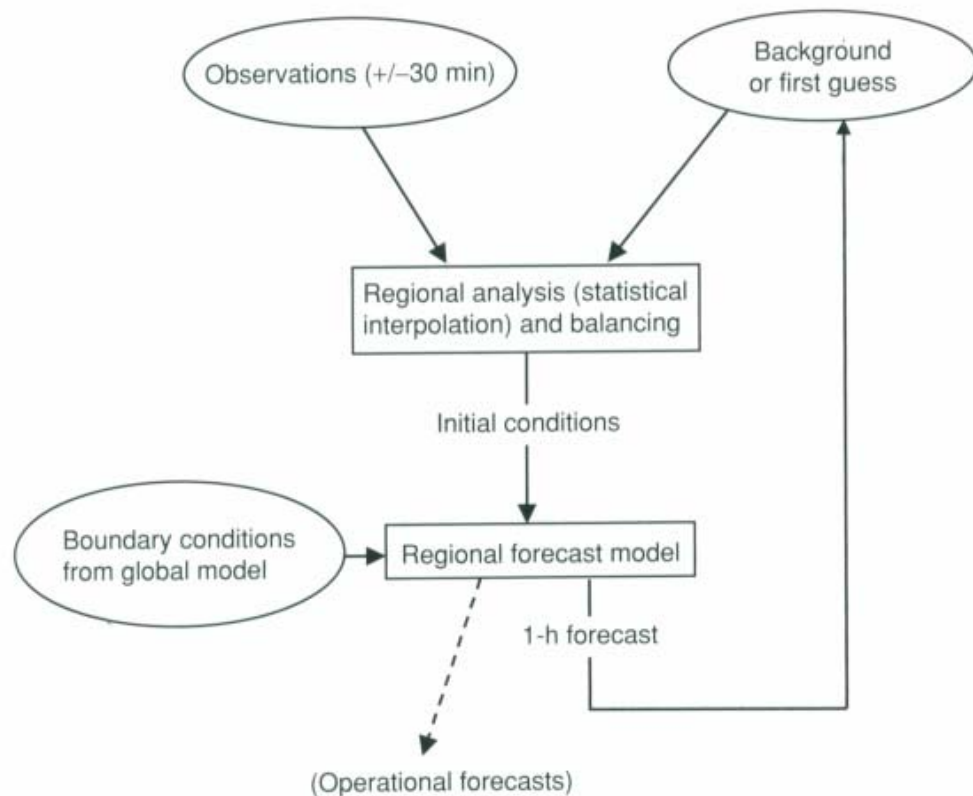


Figure 2.3 : Typical regional analysis cycle. Regional models need boundary conditions coming from global forecasts (Kalnay, 2003).

2.1 3DVAR Data Assimilation

There are numerous data assimilation methods in meteorology. Determination of the method is based on the available resources for data assimilation (computer and manpower). Data assimilation is a very time consuming process, and the time which is spent for data assimilation is a significant part of total NWP computing time. Therefore, time limitation is also important on data assimilation method selection, especially in operational environments.

Data assimilation methods can be classified into three main groups.

1. Empirical methods

Successive Correction Method (SCM)

Nudging

Physical Initialization (PI), Latent Heat Nudging (LHN)

2. Constant statistical methods

- Optimal interpolation (OI)
- 3-dimensional variational data assimilation (3DVar)
- 4-dimensional variational data assimilation (4DVar)
- 3. Adaptive statistical methods
 - Extended Kalman filter (EKF)
 - Ensemble Kalman filter (EnFK) (Kalnay, 2003)

The first data assimilation methods were called as "objective analyses". This was the opposite of "subjective analyses". Analyses were subjective in the past before data assimilation because meteorologists were calibrating the numerical weather predictions by using their operational expertise.

In Figure 2.4, the history of the main data assimilation algorithms is shown. Methods are divided into two groups according to their practicability to real time problems and ordered depending on their complexity and cost (Bouttier and Courtier, 1999).

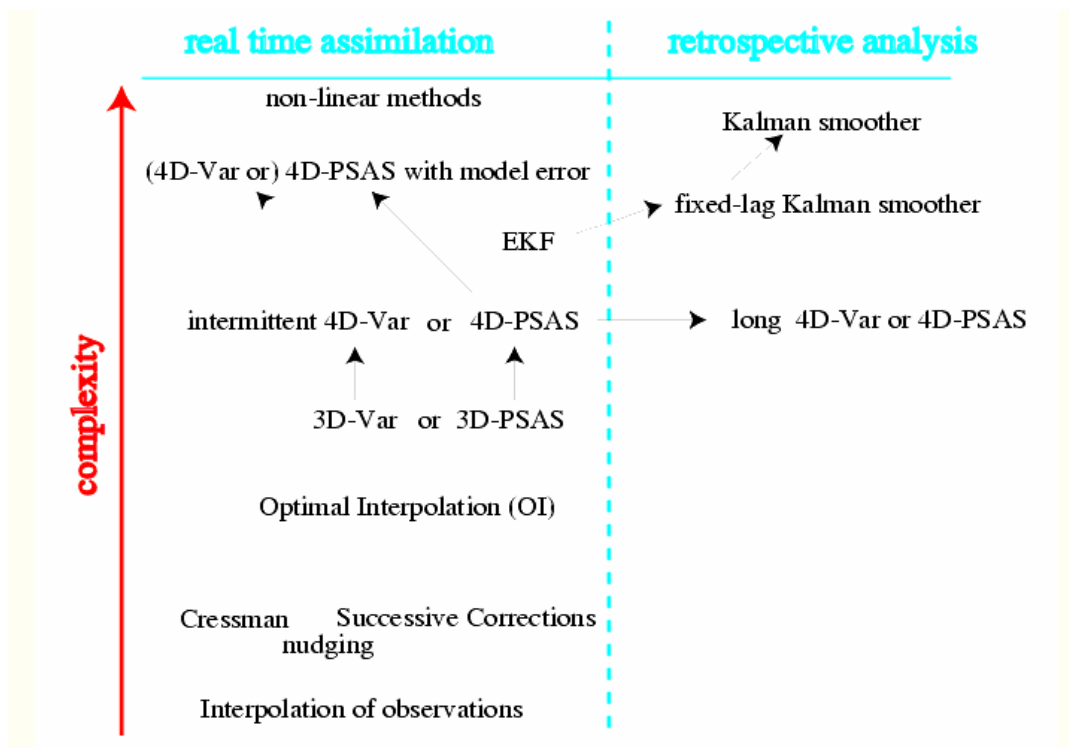


Figure 2.4: Brief history of the main data assimilation algorithms (Bouttier and Courtier, 1999)

In this study, the 3-dimensional variational data assimilation (3DVAR) technique is used. In variational data assimilation, the process of creating the analysis that is the production of an accurate image of the true state of the atmosphere at a given time, involves minimization of a prescribed cost function.

A typical cost function would be the sum of the squared deviations of the analysis values from the observations weighted by the accuracy of the observations, plus the sum of the squared deviations of the forecast fields and the analyzed fields weighted by the accuracy of the forecast. This has the effect of making sure that the analysis does not drift too far away from observations and forecasts that are known to usually be reliable. The variational problem can be summarized as the iterative minimization of $J(x)$ to find the analysis state x that minimizes $J(x)$ (Lorenc, 1986).

$$J(x) = 1/2(x - x_b)^T B^{-1}(x - x_b) + 1/2(H(x) - y_o)^T R^{-1}(H(x) - y_o) \quad (2.1)$$

x_b : First guess (or background)

y_o : Observations

B: Background error covariance matrix

R: Observation (instrumental) error covariance matrix

H: Observation operator used to transform the gridded analysis x to observation space ($y = H(x)$)

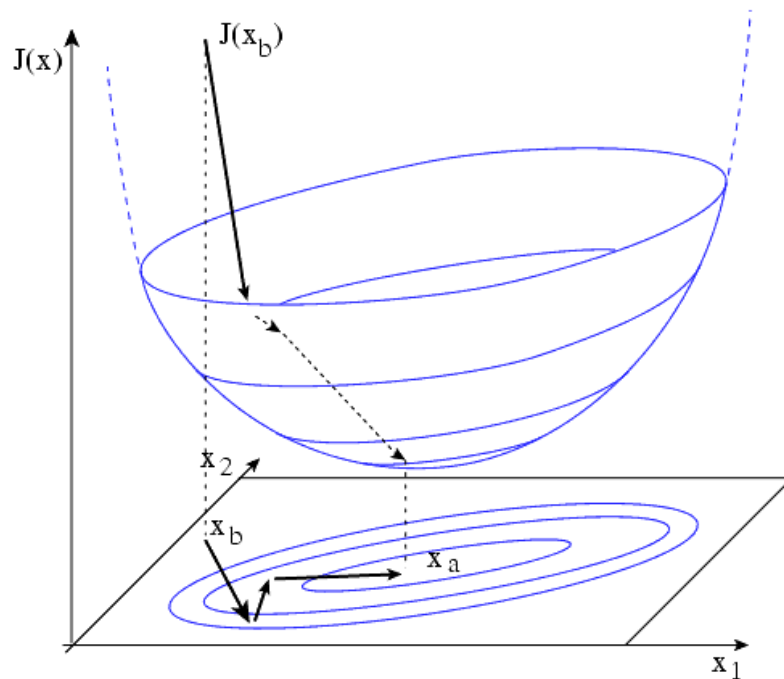


Figure 2.5: Illustration of the variational cost-function minimization in a two-variable model space (Bouttier and Courtier, 1999)

In Figure 2.5 an illustration of the variational cost-function minimization in a two variable model space is shown. As seen in the figure, the quadratic cost function has

the shape of a paraboloid. $J(x)$ has its minimum value at the optimum analysis x_a . Different x values are tried to find the smaller value of the cost function.

3. MODELLING 20 MARCH 2007 MEDITERRANEAN LOW PRESSURE SYSTEM WITH WRF (ARW)

3.1 Overview on Advanced Research WRF Modeling System

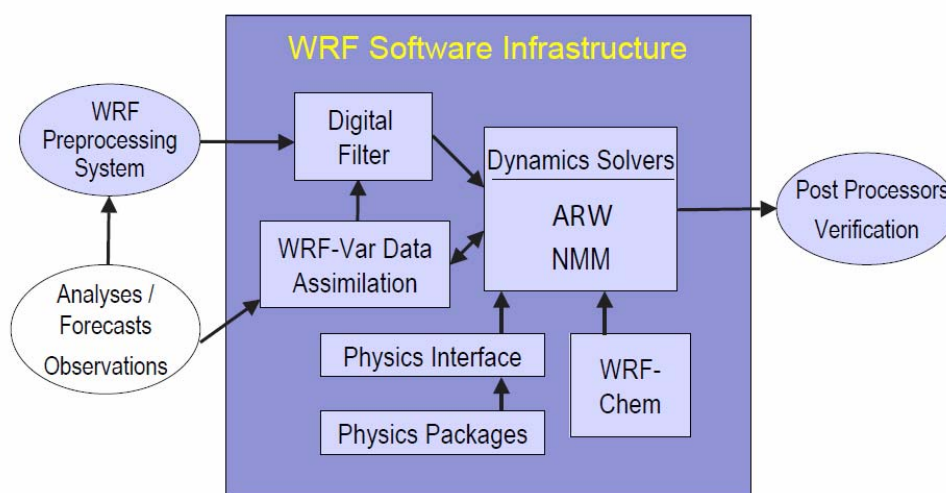


Figure 3.1 : WRF system components (Skamarock et al., 2008)

As shown in the Figure 3.1, the WRF Modeling System consists of these major programs. These are WRF Preprocessing System (WPS), ARW solver and Post-processing and Visualization tools. WPS is used primarily for real data simulations. It is used for defining simulation domains; interpolating terrestrial data, degribbing and interpolating meteorological data from another model to this simulation domain. The key component of the modeling system is ARW Solver.

The WRF model has both hydrostatic and nonhydrostatic options making it possible to work on regional and global applications. It includes complete coriolis and curvature terms, Arakawa C-grid staggering, Runge-Kutta 2nd and 3rd order time integration options, scalar-conserving flux form for prognostic variables, 2nd to 6th order advection options (horizontal and vertical), positive-definite advection option for moisture, scalar and TKE. The model also provides two-way nesting with multiple nests and nest levels, one-way nesting and moving nests. It involves map-scale factors for polar stereographic (conformal), Lambert-conformal, Mercator

(conformal) projections, latitude and longitude which can be rotated. Other features of the model are mass-based terrain following coordinate, vertical grid-spacing can vary with height, grid analysis nudging and observation nudging, digital filter initialization, full physics options for land-surface, planetary boundary layer, atmospheric and surface radiation, microphysics and cumulus convection, upper boundary absorption and Rayleigh damping. Lateral boundary conditions of the model are periodic, symmetric, and open radiative for idealized cases and specified with relaxation zone for real cases. There are a lot of idealized examples in the model package (Wang et al., 2008).

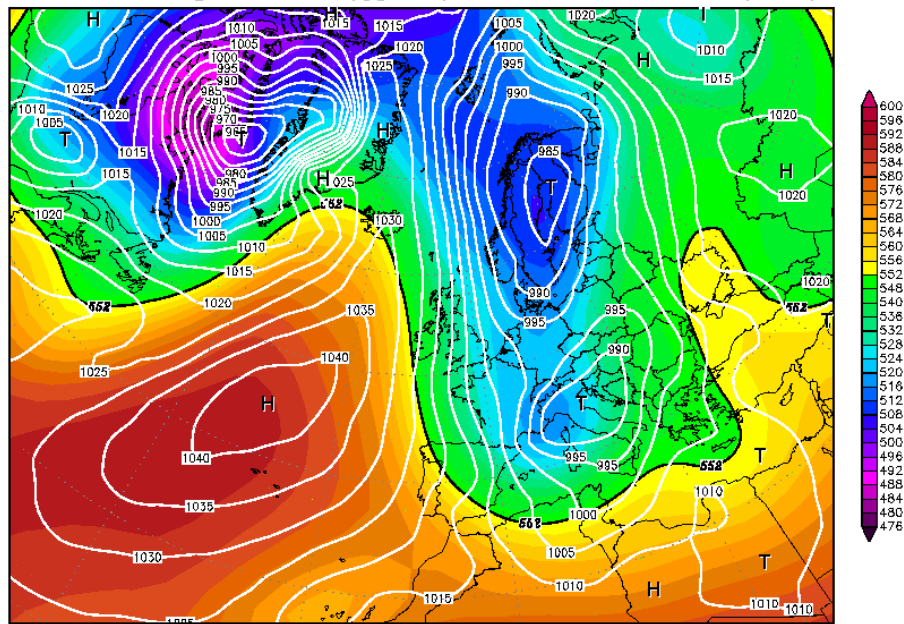
A number of Post-processing and Visualization programs are supported, some of them are RIP4 (based on NCAR Graphics), NCAR Graphics Command Language (NCL), GrADS and Vis5D (Wang et al., 2008).

3.2 Description of the Case

The Mediterranean Sea is a relatively data-sparse region and the weather systems that form and propagate over this region frequently affect the weather conditions of Turkey. For these reasons, the 20 March 2007 Mediterranean low pressure system is chosen as a case to evaluate COSMIC GPS-RO data impact during its lifecycle. In 20 March 2007, a deep low-pressure centre occurred over the Mediterranean Sea near northern Italy and later affected a large area of the central and eastern Mediterranean region downstream.

20MAR2007 00Z

500 hPa Geopotential (gpm) und Bodendruck (hPa)

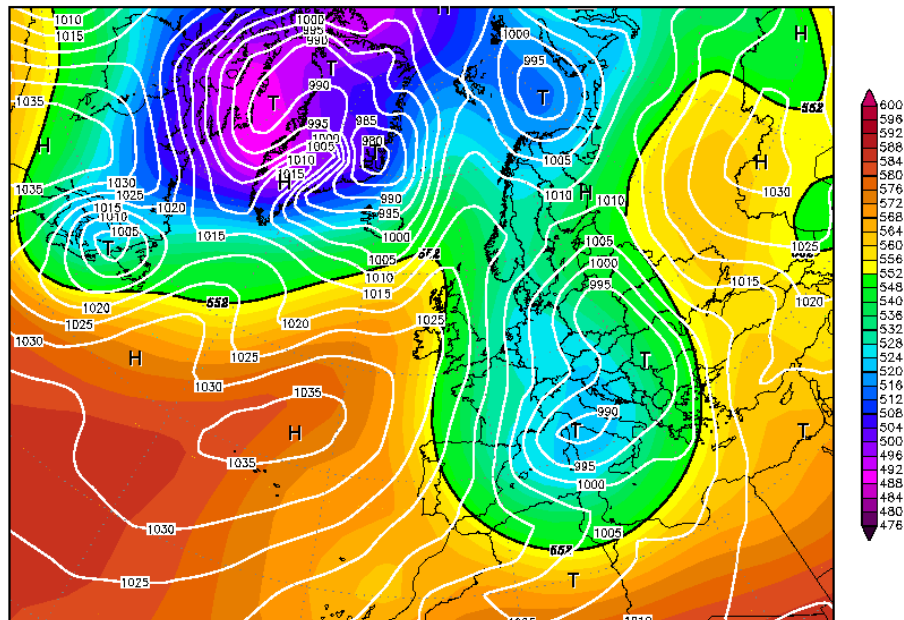


Daten: Reanalysis des NCEP
(C) Wetterzentrale
www.wetterzentrale.de

Figure 3.2 : 500 hPa Geopotential Height and Sea Level Pressure (hPa), 20 March 2007

21MAR2007 00Z

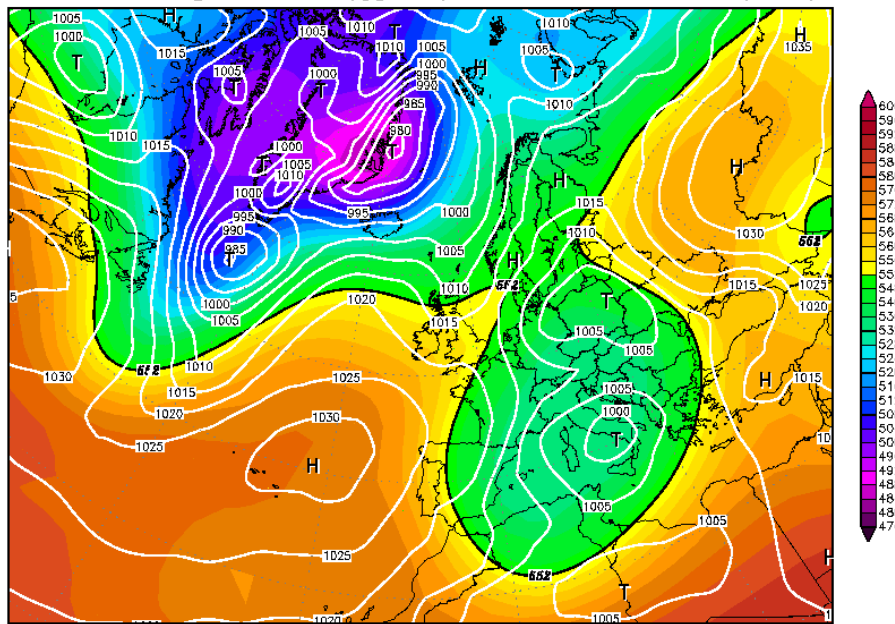
500 hPa Geopotential (gpm) und Bodendruck (hPa)



Daten: Reanalysis des NCEP
(C) Wetterzentrale
www.wetterzentrale.de

Figure 3.3 : 500 hPa Geopotential Height and Sea Level Pressure (hPa), 21 March 2007

22MAR2007 00Z
 500 hPa Geopotential (gpm) und Bodendruck (hPa)



Daten: Reanalysis des NCEP
 (C) Wetterzentrale
 www.wetterzentrale.de

Figure 3.4 : 500 hPa Geopotential Height and Sea Level Pressure (hPa), 22 March 2007

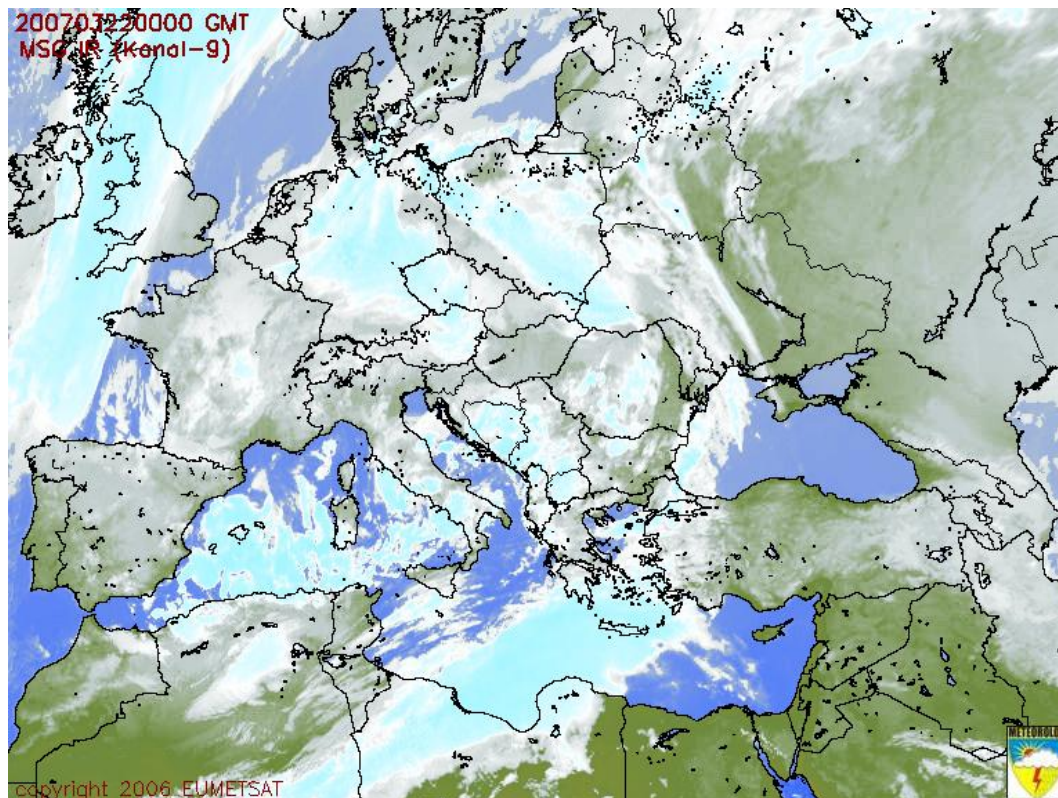


Figure 3.5 : Satellite image for the region on 22.03.2007 00:00 GMT (Turkish State Meteorological Service)

According to the NCEP Reanalysis data, there is a deep low pressure center over Sweden at the surface chart on 19.03.2007, 00:00 GMT. The sea level pressure goes as low as 960 hPa, creating a very high gradient of isobars at the environmental area. Also at 500 hPa, the contour gradient is strong surrounding the center, especially on Atlantic, between the Asor high and Island Low. On the north of Italy, the low makes a through, which will create the Mediterranean Low afterwards. The sea level pressure also makes a small centre over the Alps.

On 20.03.2007 00:00 GMT, the 500 hPa through over Italy becomes a low centre, and also at the surface level, a 990-hPa low pressure centre occurs in a wide area, effecting the region. However, the main low pressure center over Scandinavia is filling, as the central pressure decreases to 985 hPa.

On 21.03.2007 00:00 GMT, the northern low goes to northeast, when the low over Italy changes its pattern, and effecting easter parts. The central value does not change. Also the 500 hPa low is not as deep as the previous day. However, the gradient pushes the high ridge northwards, over Anatolia and Black Sea. Warm air is carried with this ridge Siberia inlands.

Looking at the 552 dam contour at 500 hPa level on 22.03.2007 00:00 GMT, the Mediterranean low seems to be separated from the mother low. The central value of 500 hPa low goes down to 532 dam, where the sea level pressure becomes 1000 hPa in south of Italy.

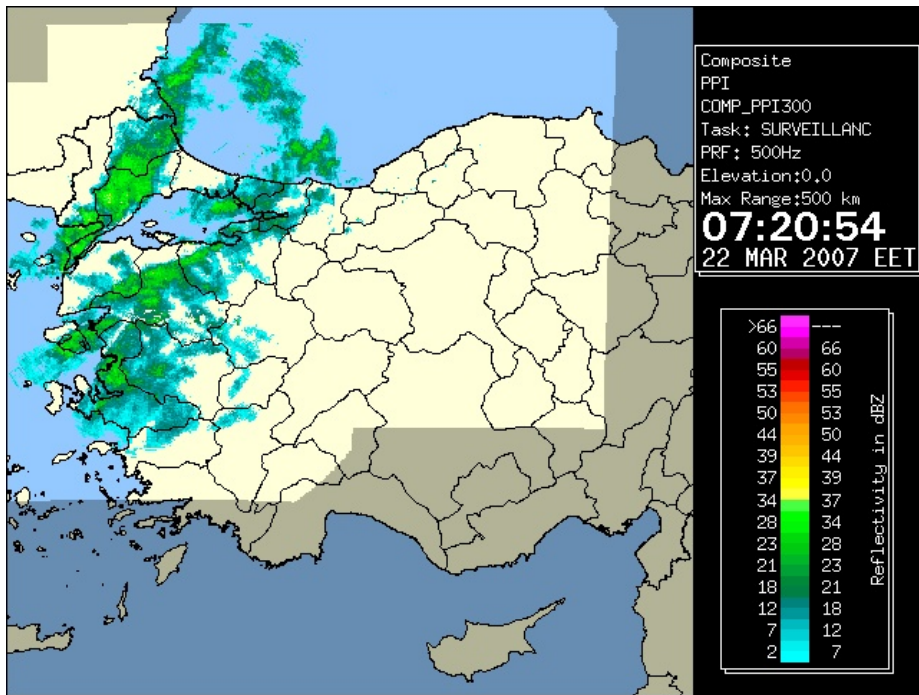


Figure 3.6 : Radar image on 22.03.2007 00:00 GMT (Turkish State Meteorological Service)

Mediterranean

Valid: 06 UTC Thu 22 Mar 07 (09 LDT Thu 22 Mar 07) Fcst: 18 h

Total precip. in past 06 h

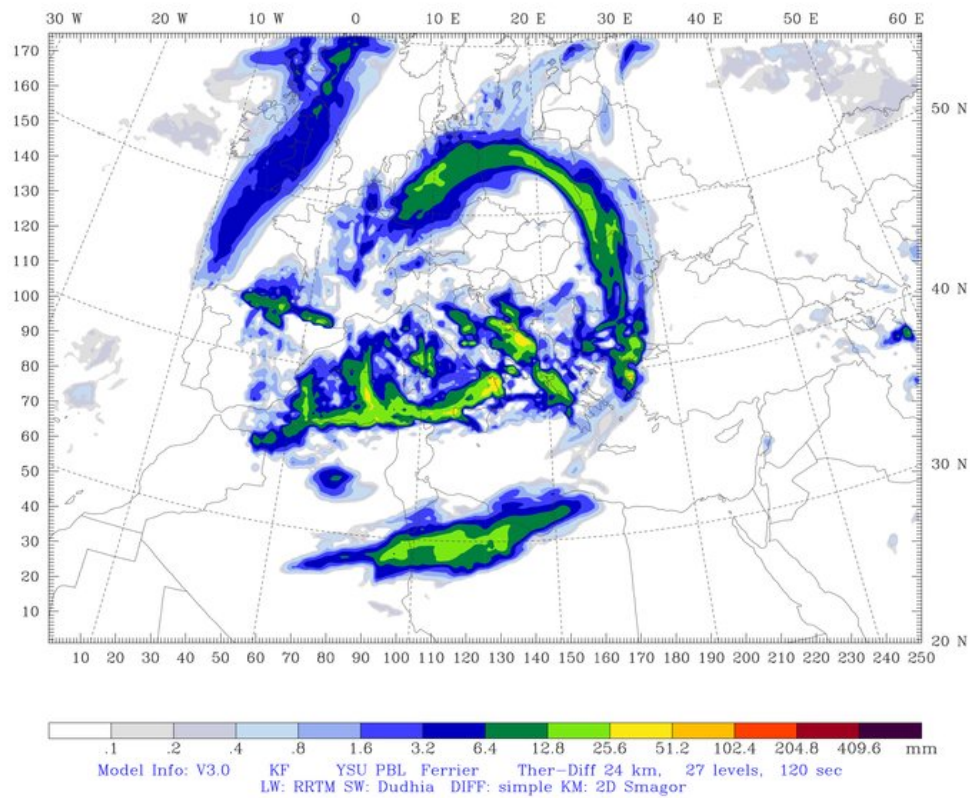


Figure 3.7 : WRF 18 h forecasts of total precipitation in past 6 hours valid at 06 UTC 22 March 2007

This low pressure center makes huge amounts of precipitation around the area, reaching western Turkey on 22.03.2007. As seen from the precipitation observations, the model seems succesful simulating the precipitation. The high amounts of precipitation near Çanakkale could be predicted accurately by the model.

3.2.1 GPS-RO data availability

Cosmic data availability can be checked by using CDAAC (COSMIC Data Analysis and Archive Center). In figure 3.4. cosmic data avaiability during the case is shown. X axis of the graphic represents days from 18 March 2007 to 24 March 2007 and the Y axis represents the numbers of the GPS occultations per day. Minimum number of occultations seen at 20 March 2007 during this period (1500 per day).

In figure 3.5 total occultation distribution for 2007.077 to 2007.083 (18 March 2007 to 24 March 2007) is shown. As seen in the figure, occultation distribution is uniform and there are many occultations over the Mediterranean Sea.

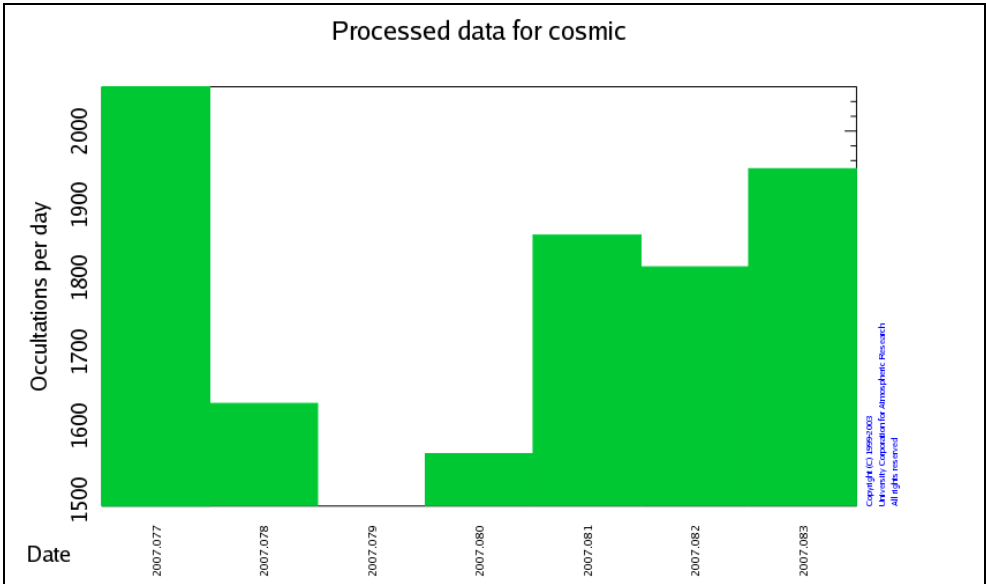


Figure 3.9 : Cosmic data availability during the formation and propagation period of the 20 March 2007 Mediterranean low pressure system.

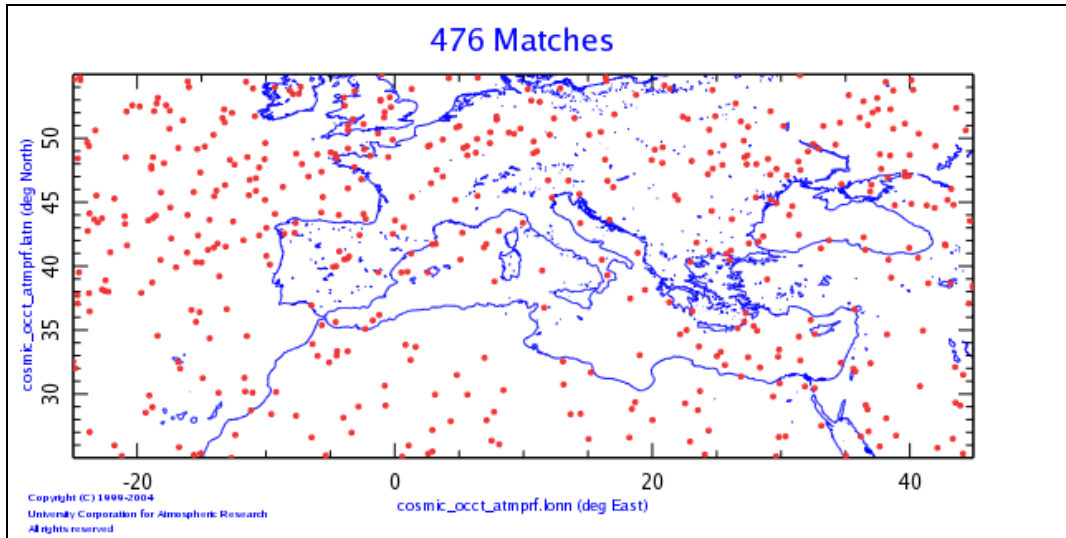


Figure 3.10 : Total occultation distribution for 2007.077 to 2007.083 (18 March 2007 to 24 March 2007)

3.3 Sensitivity to Physical Parameterizations

In order to model the 19 March 2007 low pressure system accurately, numerous WRF-ARW forecast experiments are carried out by using different physics options. WRF offers multiple physics options that can be combined in many ways. The choices vary with each major WRF release. Parameterizations tried in this study are outlined below in the Table 3.1. Default values are kept for other physical options.

Table 3.1: Parameterizations tried in sensitivity analysis (Wang et al., 2008)

Microphysics (mp_physics)
<u>WRF Single-Moment 3-class scheme:</u> A simple efficient scheme with ice and snow processes suitable for mesoscale grid sizes (3).
<u>Eta microphysics:</u> (Ferrier microphysics) The operational microphysics in NCEP models. A simple efficient scheme with diagnostic mixed-phase processes (5).
Cumulus Parameterization (cu_physics)
<u>Kain-Fritsch scheme:</u> Deep and shallow convection sub-grid scheme using a mass flux approach with downdrafts and CAPE removal time scale (<i>cu_physics</i> = 1).
<u>Betts-Miller-Janjic scheme.</u> Operational Eta scheme. Column moist adjustment scheme relaxing towards a well-mixed profile (2).
<u>Grell-Devenyi ensemble scheme:</u> Multi-closure, multi-parameter, ensemble method with typically 144 sub-grid members (3).
<u>Grell 3d ensemble cumulus scheme.</u> Scheme for higher resolution domains allowing for subsidence in neighboring columns (5). New in Version 3.0.

Longwave Radiation (ra_lw_physics)
<u>RRTM scheme</u> : Rapid Radiative Transfer Model. An accurate scheme using look-up tables for efficiency. Accounts for multiple bands, trace gases, and microphysics species (<i>ra_lw_physics</i> = 1).
<u>GFDL scheme</u> : Eta operational radiation scheme. An older multi-band scheme with carbon dioxide, ozone and microphysics effects (99).
Shortwave Radiation (ra_sw_physics)
<u>Dudhia scheme</u> : Simple downward integration allowing efficiently for clouds and clear-sky absorption and scattering. When used in high-resolution simulations, sloping and shadowing effects may be considered (<i>ra_sw_physics</i> = 1).
<u>GFDL shortwave</u> : Eta operational scheme. Two-stream multi-band scheme with ozone from climatology and cloud effects (99).

Table 3.2: 8 different physics options variations used in WRF runs of sensitivity analysis

	1	2	3	4	5	6	7	8
Cu_physics (1)	■				■		■	■
Cu_physics (2)		■						
Cu_physics (3)			■			■		
Cu_physics (5)				■				
Mp_physics (3)	■	■	■					
Mp_physics (5)				■	■	■	■	■
Ra_lw_physics (1)	■	■	■	■	■	■		
Ra_lw_physics (99)							■	■
Ra_sw_physics (1)	■	■	■	■	■	■	■	
Ra_sw_physics (99)								■

For verification of the parameterizations, GFS analyses are used. Forecasts with different parameterization variations are compared to GFS analyses valid at same forecast times. Root-mean square error (RMSE) and mean error statistics are calculated for the prognostic model variables.

Finally Kain-Fritsch cumulus, Eta microphysics, Rapid Radiative Transfer Model longwave radiation, and Dudhia Scheme shortwave radiation parameterization schemes are chosen for the 20 March 2007 low-pressure system, as they resulted in the smallest RMSE and mean error values. RMSE and mean error summary statistics for these parameterizations are shown below in Table 3.3. Verification results of all other parameterization variations are in the appendices.

Table 3.3: RMSE and mean error statistics of verification of the most accurate WRF forecast with Kain-Fritsch Scheme, Eta microphysics, Rapid Radiative Transfer Model Scheme, Dudhia Scheme Physics Options.

VARIABLES	RMSE	MEAN ERROR
T	-1.02912545	3.32360053
QVAPOR	0.00000655	0.00047368
QCLOUD	0.00000107	0.00001579
QRAIN	0.00000037	0.00000671
U	0.04802153	3.59374094
V	-0.18827605	3.62177825
W	-0.00010738	0.0549823
PH	-101.634079	269.7882996
PHB	0	0
MUB	0	0
U10	0.18096046	2.57141304
V10	0.03492462	2.87172651

All simulations that have been performed in this study for sensitivity analysis are visualized by using RIP 4. Some of them are here. Figure 3.11 to 3.14 show the differences between the sea level temperature forecasts and observations (GFS analysis) of sensitivity test elements for t+36 hours. In general, all model configurations have a negative bias over southern central Europe, where the low pressure centre is located. The least errors seem as -11 hPa at the Grell-Devenyi Ensemble scheme test, plotted at Figure 3.13. A positive bias exist over Anatolia and environment, as well as northern Algeria on all plots. The Eta microphysics test has the best approximation over this area.

Seyda Valid: 12 UTC Tue 20 Mar 07 (15 LDT Tue 20 Mar 07) Fcst: 36 h
 Sea-level pressure (diff. from case=real, time= 0.00)

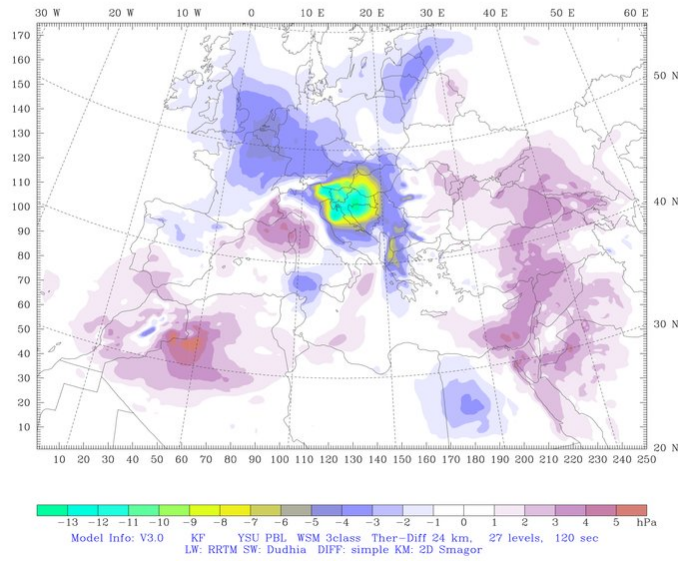


Figure 3.11 : Mean sea level pressure difference of the forecast and the observation at 12z on 20.03.2007 with usage of Kain-Fritsch Scheme, WRF Single-Moment 3-class scheme , Rapid Radiative Transfer Model Scheme, Dudhia Scheme Physics Options

Seyda Valid: 12 UTC Tue 20 Mar 07 (15 LDT Tue 20 Mar 07) Fcst: 36 h
 Sea-level pressure (diff. from case=real, time= 0.00)

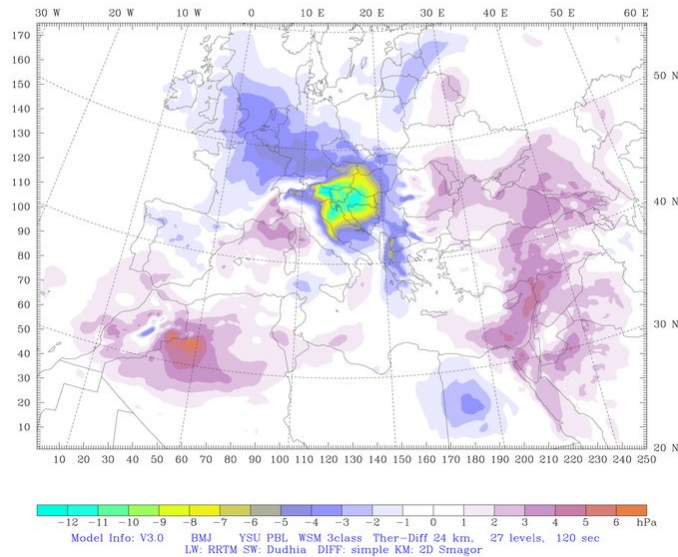


Figure 3.12 : Mean sea level pressure difference of the forecast and the observation at 12z on 20.03.2007 with usage of Betts-Miller-Janjic scheme , WRF Single-Moment 3-class scheme , Rapid Radiative Transfer Model Scheme, Dudhia Scheme Physics Options

Seyda Fcst: 36 h
 Valid: 12 UTC Tue 20 Mar 07 (15 LDT Tue 20 Mar 07)
 Sea-level pressure
 (diff. from case=real, time= 0.00)

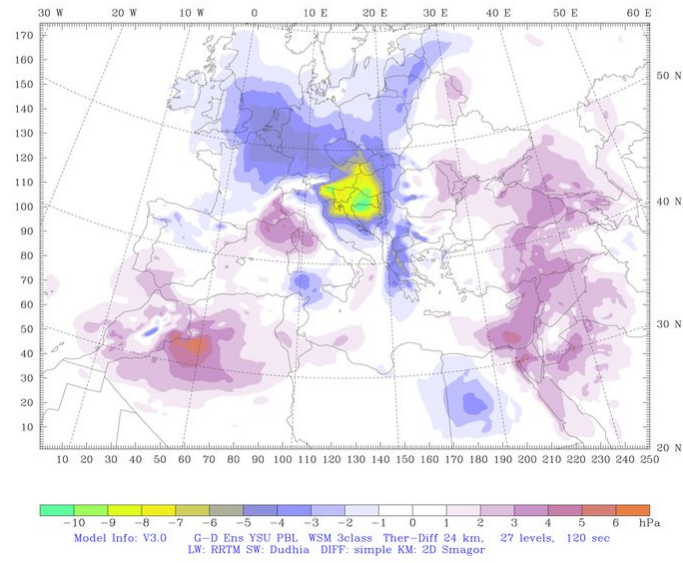


Figure 3.13 : Mean sea level pressure difference of the forecast and the observation at 12z on 20.03.2007 with usage of Grell-Devenyi ensemble scheme, WRF Single-Moment 3-class scheme , Rapid Radiative Transfer Model Scheme, Dudhia Scheme Physics Options

Seyda Fcst: 36 h
 Valid: 12 UTC Tue 20 Mar 07 (15 LDT Tue 20 Mar 07)
 Sea-level pressure
 (diff. from case=real, time= 0.00)

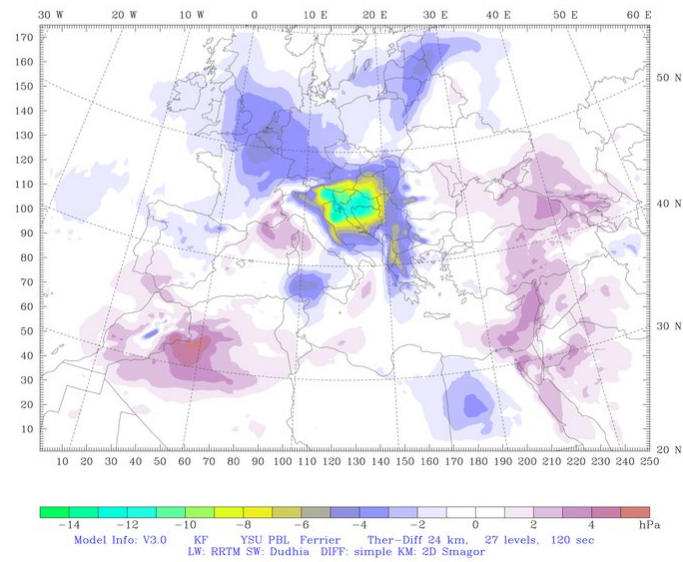


Figure 3.14 : Mean sea level pressure difference of the forecast and the observation at 12z on 20.03.2007 with usage of Kain-Fritsch Scheme, Eta microphysics, Rapid Radiative Transfer Model Scheme, Dudhia Scheme Physics Options

Figure 3.15 to 3.18 are plotted for the comparison of 850 hPa temperature forecasts to the GFS analysis, taken as observations. These figures are for initial time + 36 hours, too. All four runs indicate that model is successful in temperature prediction at this level. However, there are errors in some regions, similar in each. The temperature field was underestimated over southerastern Europe, as well as northwestern Sahara. The three cumulus parameterization tests show an important error in underestimating the field exceeding 8 C over the border between Algeria and Morocco, where the Ferrier microphysics (plotted as Figure 3.18) has an effect of decreasing the error near 4 C. However, it must be noted that this microphysics scheme slightly increases the positive bias over eastern Anatolia and Croatia, with respect to WRF Single-Moment 3-class scheme. The cumulus schemes do not seem to have an important impact to remark, on 850 hPa temperature.

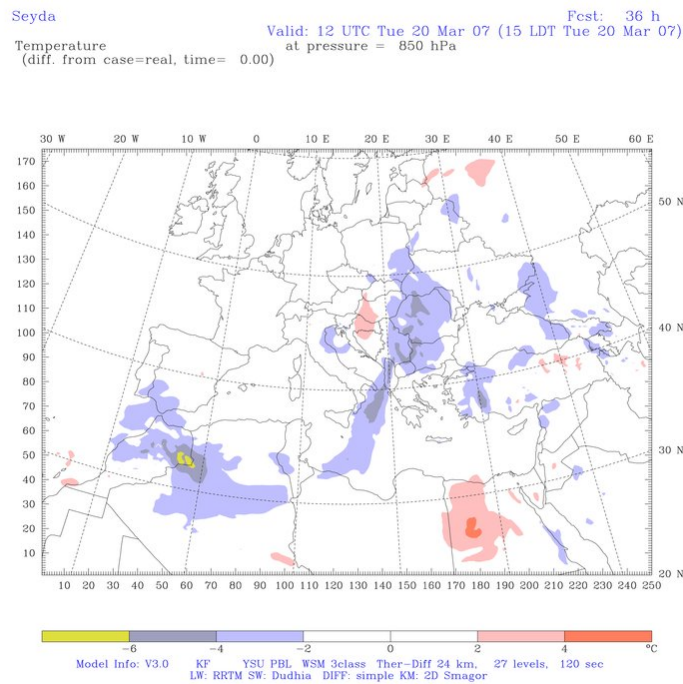


Figure 3.15 : Temperature (at 850 hPa level) difference of the forecast and the observation at 12z on 20.03.2007 with usage of Kain-Fritsch Scheme, WRF Single-Moment 3-class scheme , Rapid Radiative Transfer Model Scheme, Dudhia Scheme Physics Options

Seyda Fcst: 36 h
 Valid: 12 UTC Tue 20 Mar 07 (15 LDT Tue 20 Mar 07)
 Temperature at pressure = 850 hPa
 (diff. from case=real, time= 0.00)

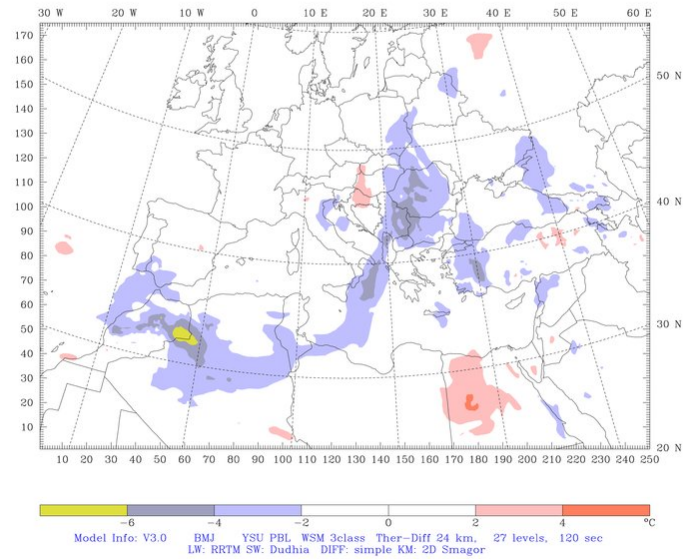


Figure 3.16 : Temperature (at 850 hPa level) difference of the forecast and the observation at 12z on 20.03.2007 with usage of Betts-Miller-Janjic scheme , WRF Single-Moment 3-class scheme , Rapid Radiative Transfer Model Scheme, Dudhia Scheme Physics Options

Seyda Fcst: 36 h
 Valid: 12 UTC Tue 20 Mar 07 (15 LDT Tue 20 Mar 07)
 Temperature at pressure = 850 hPa
 (diff. from case=real, time= 0.00)

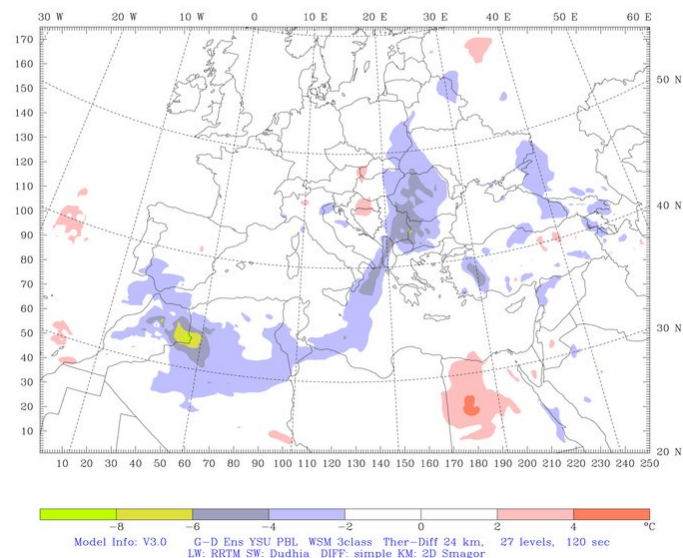


Figure 3.17 : Temperature (at 850 hPa level) difference of the forecast and the observation at 12z on 20.03.2007 with usage of Grell-Devenyi ensemble scheme, WRF Single-Moment 3-class scheme , Rapid Radiative Transfer Model Scheme, Dudhia Scheme Physics Options

Seyda Fest: 36 h
 Valid: 12 UTC Tue 20 Mar 07 (15 LDT Tue 20 Mar 07)
 Temperature at pressure = 850 hPa
 (diff. from case=real, time= 0.00)

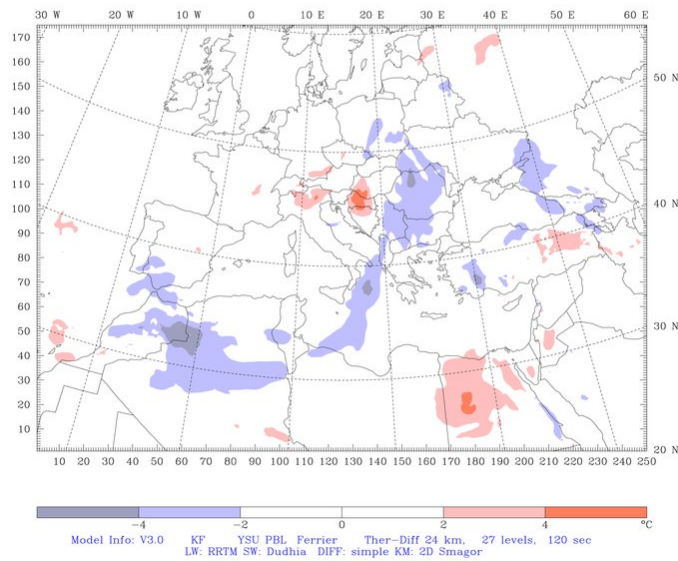


Figure 3.18 : Temperature (at 850 hPa level) difference of the forecast and the observation at 12z on 20.03.2007 with usage of Kain-Fritsch Scheme, Eta microphysics, Rapid Radiative Transfer Model Scheme, Dudhia Scheme Physics Options

700 hPa relative humidity difference between the forecasts and observations for each 4 sensitivity test elements are seen on Figure 3.19 to 3.22, for t+36 hours. It is obvious that Betts-Miller-Janjic convective scheme (Figure 3.20) has a positive bias over western Europe, where Grell-Devenyi Ensemble scheme (Figure 3.21) shows a negative bias. Keim-Fritsch scheme used for the control run (Figure 3.19) seems a bit more accurate with respect to others, but also indicate a similarity to the Grell-Devenyi ensemble scheme. Concerning the eastern part of the studied area, all runs agree with underestimating the humidity as local spots, at this level. Looking at Figure 3.22, it can be said that using Ferrier microphysics did not make a huge difference on relative humidity, compared to WRF Single-Moment 3-class schemes.

Seyda Valid: 12 UTC Tue 20 Mar 07 (15 LDT Tue 20 Mar 07) Fcst: 36 h
 Relative humidity (w.r.t. water) at pressure = 700 hPa
 (diff. from case=real, time= 0.00)

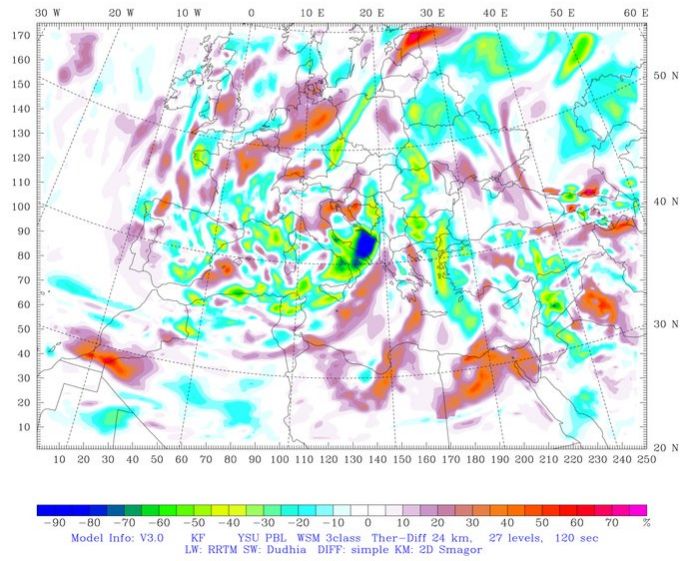


Figure 3.19 : Relative Humidity (at 700 hPa level) difference of the forecast and the observation at 12z on 20.03.2007 with usage of Kain-Fritsch Scheme, WRF Single-Moment 3-class scheme, Rapid Radiative Transfer Model Scheme, Dudhia Scheme Physics Options

Seyda Valid: 12 UTC Tue 20 Mar 07 (15 LDT Tue 20 Mar 07) Fcst: 36 h
 Relative humidity (w.r.t. water) at pressure = 700 hPa
 (diff. from case=real, time= 0.00)

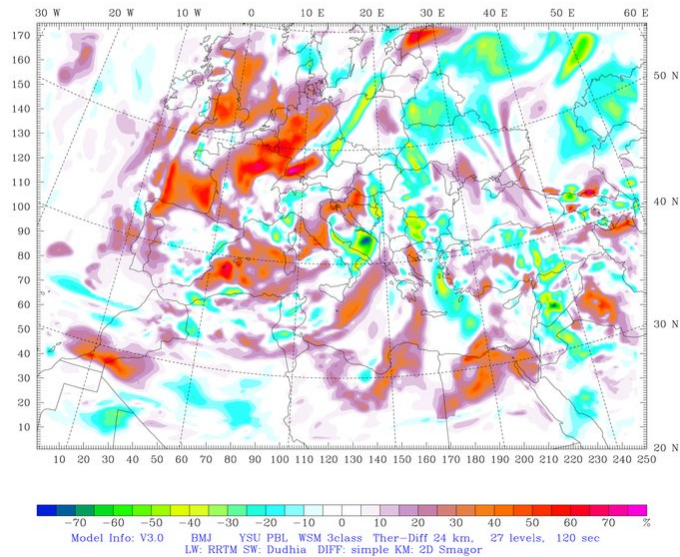


Figure 3.20 : Relative Humidity (at 700 hPa level) difference of the forecast and the observation at 12z on 20.03.2007 with usage of Betts-Miller-Janjic Scheme, WRF Single-Moment 3-class scheme, Rapid Radiative Transfer Model Scheme, Dudhia Scheme Physics Options

Seyda Valid: 12 UTC Tue 20 Mar 07 (15 LDT Tue 20 Mar 07) Fcst: 36 h
 Relative humidity (w.r.t. water) at pressure = 700 hPa
 (diff. from case=real, time= 0.00)

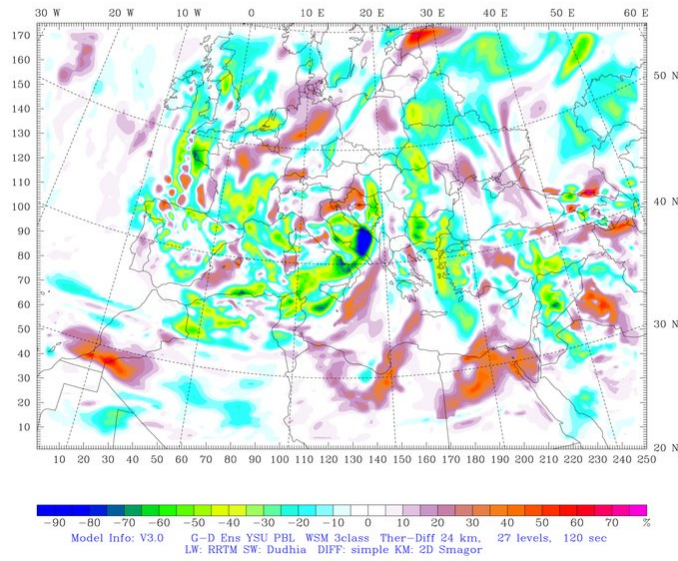


Figure 3.21 : Relative Humidity (at 700 hPa level) difference of the forecast and the observation at 12z on 20.03.2007 with usage of Grell-Devenyi Ensemble Scheme, WRF Single-Moment 3-class scheme, Rapid Radiative Transfer Model Scheme, Dudhia Scheme Physics Options

Seyda Valid: 12 UTC Tue 20 Mar 07 (15 LDT Tue 20 Mar 07) Fcst: 36 h
 Relative humidity (w.r.t. water) at pressure = 700 hPa
 (diff. from case=real, time= 0.00)

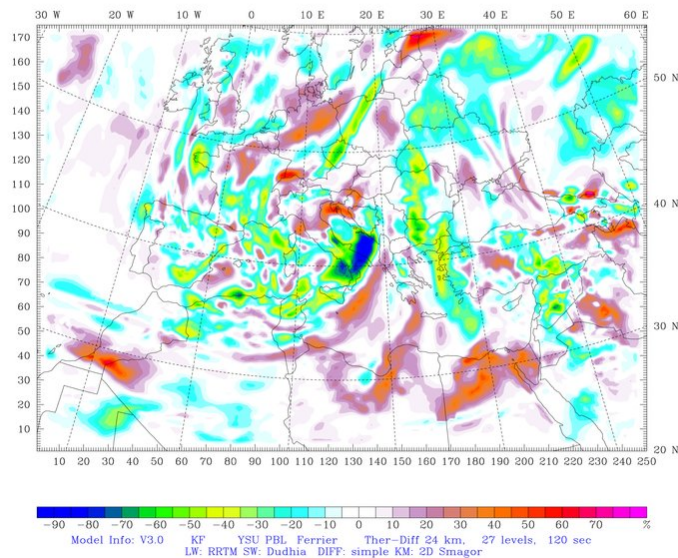


Figure 3.22 : Relative Humidity (at 700 hPa level) difference of the forecast and the observation at 12z on 20.03.2007 with usage of Kain-Fritsch Scheme, Ferrier microphysics, Rapid Radiative Transfer Model Scheme, Dudhia Scheme Physics Options

4. ASSIMILATION OF GPS-RO BY USING WRF- 3DVAR

4.1 GPS Radio Occultation

When radio signal passes through the atmosphere it changes, i.e. it is occulted by the atmosphere. By detection of a change in a radio signal, physical properties of a planetary atmosphere can be defined. The technique used for measuring the physical properties of a planetary atmosphere which relies on the detection of a change in a radio signal is called radio occultation.

When electromagnetic radiation passes through an atmosphere, it is refracted. The magnitude of the refraction depends on the temperature and water vapor concentration in the atmosphere. The amount of bending cannot be measured directly at radio frequencies. Doppler shift of the signal given the geometry of the emitter and receiver is used for the calculation of bending. The amount of bending can be related to the refractive index by using an Abel transform on the formula relating bending angle to refractivity. With the neutral atmosphere assumption by using atmospheric refractivity temperature, pressure and water vapour can be calculated, since radio occultation data has applications in meteorology (Kursinski et al 1997, Melbourne et al 1994). If radio occultation missions rely on radio signals from Global Positioning System satellites, the technique is called. GPSRO. The GPS signals are received on low earth orbit (LEO) satellites.

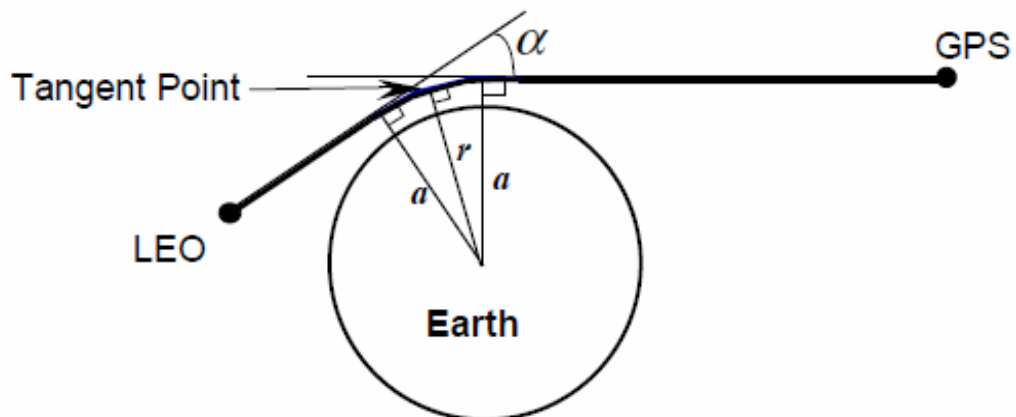


Figure 4.1 : Geometry of a typical GPS occultation (Kuo et al., 2000)

GPS radio occultation data have four main characteristics. There is no instrument drift in this system. Effects of aerosols, clouds and precipitation are minimal, this data has a very high vertical resolution, and relatively uniform global coverage. The same region of the Earth is sampled once every 100 min because the COSMIC system with a constellation of eight low-Earth orbiting (LEO) satellites has a global “refresh rate” of about 100 min. Moreover, COSMIC data is usually available to the operational centers within three hours of observations. These features provide some significant advantages over radiosondes and space-based sounders. When used together with these complementary systems, COSMIC data offers an opportunity to improve significantly the skill of weather prediction models. However, despite these advantages, the use of GPS radio occultation data in a global analysis is not a trivial matter. First of all, the raw measurements of GPS radio limb soundings are the phase delays and amplitudes of the GPS radio signals. It takes a number of steps to reduce the data to the traditional meteorological variables of temperature, pressure and water vapor. Because of the ray traversing geometry, the GPS radio occultation data has unique characteristics, which are very different from the point measurement of a radiosonde or an “area-average” measurement of a microwave sounder. A single GPS radio occultation measurement represents a weighted average over a "pencil-like" volume (the Fresnel volume). The effective horizontal scale of the measurement along the ray is approximately several hundred km, while the cross-ray scale is quite small (~1 km). Another important issue is related to the fact that over regions with significant vertical refractivity gradients, more than one ray may arrive at a given receiver at the same time, a problem known as multipath propagation (Gorbunov and Gurvich 1998). Under such conditions, the retrieved refractivity profiles may contain significant errors. To assimilate GPS radio occultation data effectively into a weather prediction model, one needs to correctly process them and to properly account for the measurement characteristics and measurement errors (Rocken et al., 2000)

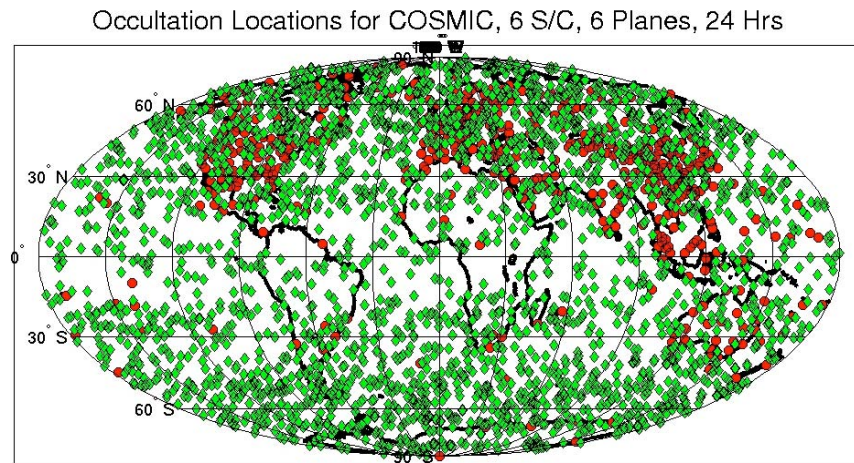


Figure 4.2 : Coverage of COSMIC GPS RO sounding in one day, Green dots are COSMIC soundings. Red dots are radiosonde stations (Marshall and Yoe, 2005)

4.1.1 Brief description of the COSMIC system

The space segment of the COSMIC includes the eight LEO satellites and the GPS constellation. A low earth orbit is generally defined as an orbit within the locus extending from the Earth's surface up to an altitude of 2,000 km. Given the rapid orbital decay of objects below approximately 200 km, the commonly accepted definition for LEO is between 160 - 2,000 km (100 - 1,240 miles) above the Earth's surface. As mentioned before, the GPS signals are received on low earth orbit (LEO) satellites. Data from LEO satellites are transmitted to the high-latitude ground stations in Fairbanks and Kiruna. Then the data is transferred to the COSMIC Data Analysis and Archive Center (CDAAC) in Boulder, Colorado. The CDAAC also receives data from a global network of ground GPS and TBB receiving sites (the fiducial network). The CDAAC processes and archives all received data and forward these data to scientific and operational users. All data and products at CDAAC are also sent to Taiwan Analysis Center for COSMIC (TACC). TACC performs its own analysis of the data and distributes its products and CDAAC products to the user community in Taiwan. NSPO mission operations are responsible for constellation operations. Satellite and payload commanding are controlled by NSPO via S-band uplink from two Taiwanese ground stations (Rocken et al., 2000).

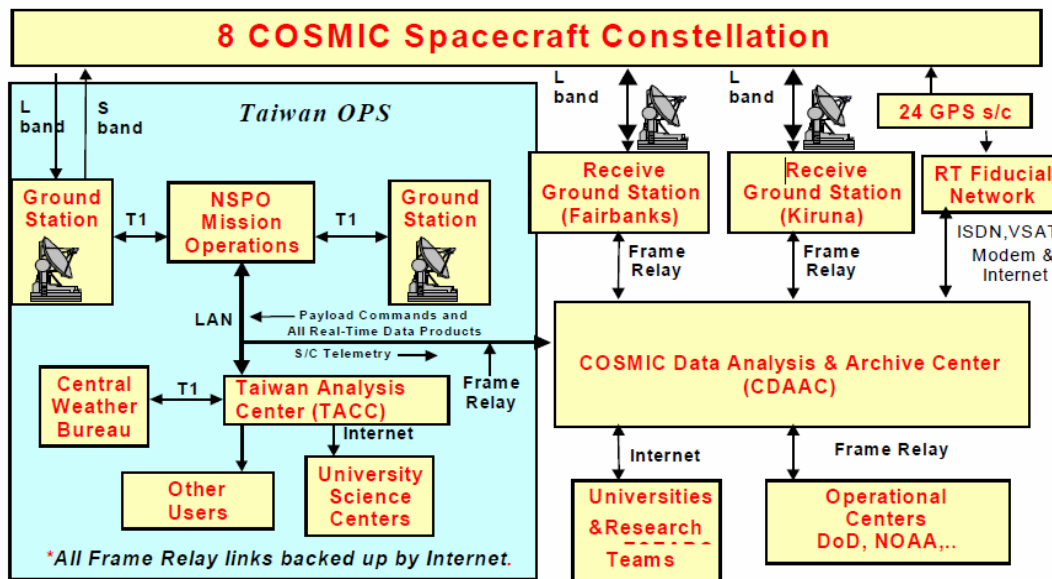


Figure 4.3 : Cosmic System Overview (Rocken et al., 2000)

4.2 WRF- 3DVAR

The WRF 3DVAR is a data assimilation system that assimilates observations into the interpolated analyses created by WPS. It is based on the incremental variational data assimilation technique and uses conjugate gradient method to minimize the cost function in the analysis control variable. The analysis is performed on un-staggered Arakawa A-grid and analysis increments are interpolated to staggered Arakawa C-grid and added to the background (first guess) to obtain a final analysis at the WRF-model grid. With the Obsproc utility, WRF 3DVAR supports both ASCII and PREPBUFR formatted conventional observation data. It includes a utility (“gen_be”) to generate the climatological background error covariance estimate via the NMC method or ensemble perturbations (Parrish and Derber, 1992). It has a verification package both with respect to observations and analysis. Finally, a utility program is included to update WRF boundary conditions to reflect changes to boundary tendencies.

4.2.1 Running WRF- 3DVAR

The WRF-Var system runs with three input files: A WRF first guess/boundary input file from either WPS/real (cold-start) or WRF (warm-start), observations (in ASCII or PREBUFR format), and a background error statistics file containing the background error covariances. The “wrfda.log” (or “rsl.out.0000” if running in distributed-memory mode) contains important WRF-Var runtime log information.

Table 4.1: Information about WRF-Var input files (Wang et al., 2008)

Input Data	Format	Created By
First Guess	NETCDF	WRF Preprocessing System (WPS) and real.exe or WRF
Observations	ASCII (PREPBUFR also possible)	Observation Preprocessor (OBSPROC)
Background Error Statistics	Binary	WRF-Var gen_be utility /Default CV3

WRF-Var generates numerous diagnostic files and an output file (wrfvar_output) after a successful run.

Before performing a WRF model integration with a WRF-Var analysis, the values and tendencies for each of predicted variables for the first time period in the lateral boundary condition file for domain-1 (wrfbdy_d01) must be updated to be consistent with the new WRF-Var initial condition (analysis). This procedure is performed by the WRF-Var utility “da_updated_bc”. Finally, the output file of WRF-Var is used as the wrfinput_d01 file for new WRF run.

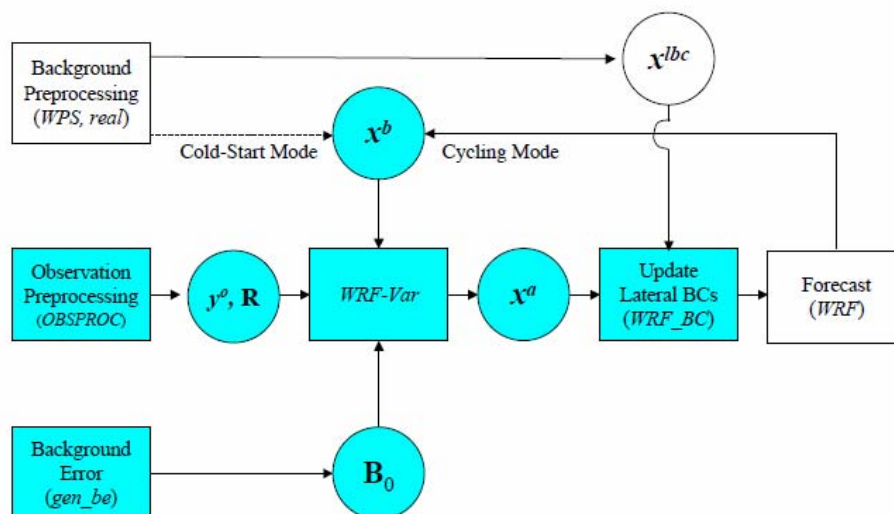


Figure 4.4 : The relationship between datasets (circles), and algorithms (rectangles) of the ARW system (Skamarock et al., 2008)

4.2.2 Observation preprocessing (OBSPROC)

For this study, the needed COSMIC wetPrf data are downloaded and prepared for Obsproc (WRF 3DVAR Observation Preprocessor) by decoding them to little_r format from NETCDF format by using wefPrf decoder.

Then OBSPROC is run for several time windows and analysis times during the case. By using OBSPROC, observations outside the time range and domain (horizontal and top) are removed and observational errors based on a pre-specified error file are assigned. Observation files to be used by WRF-Var are also generated by OBSPROC in ASCII or BUFR format.

In this study, a time window of 6 hours is used to assimilate observations at any given analysis time. So, for example, to prepare the observation file at the analysis time 00Z of a given day, all the observations between ± 3 hours are processed, as illustrated in figure 4.5, which means that the observations between 21Z of previous day and 03Z of same day will be treated as simultaneous valid at 00Z.

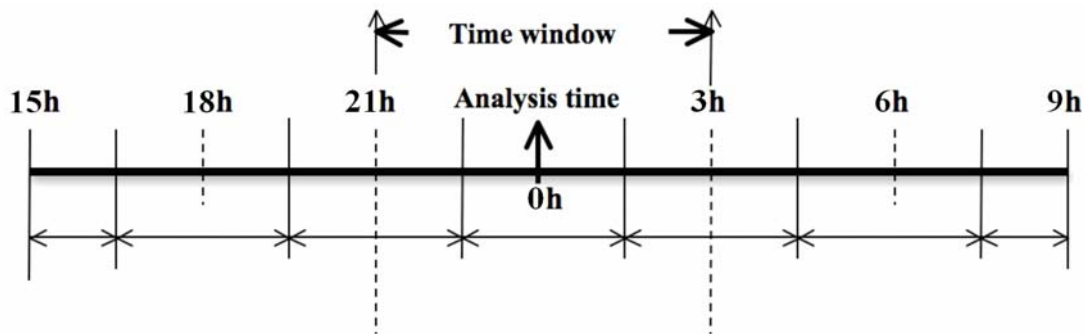


Figure 4.5 : Time window description for 3D-VAR

In Table 4.2, the number of horizontal locations of the GPS-RO soundings for each time window during the case is shown. While these numbers may appear to be small to have impact on the forecast skills, it should be noted that the vertical resolution of a typical GPS sounding is very high.

Table 4.2 : Number of GPS-RO soundings for each time window during the case

Time_analysis	time_window_min	Time_window_max	GPSRF
2007-03-19_00:00	2007-03-18_21:00	2007-03-19_03:00	8
2007-03-19_06:00	2007-03-19_03:00	2007-03-19_09:00	36
2007-03-19_12:00	2007-03-19_09:00	2007-03-19_15:00	26
2007-03-19_18:00	2007-03-19_15:00	2007-03-19_21:00	12
2007-03-20_00:00	2007-03-19_21:00	2007-03-20_03:00	9
2007-03-20_06:00	2007-03-20_03:00	2007-03-20_09:00	26
2007-03-20_12:00	2007-03-20_09:00	2007-03-20_15:00	25
2007-03-20_18:00	2007-03-20_15:00	2007-03-20_21:00	15
2007-03-21_00:00	2007-03-20_21:00	2007-03-21_03:00	11
2007-03-21_06:00	2007-03-21_03:00	2007-03-21_09:00	21
2007-03-21_12:00	2007-03-21_09:00	2007-03-21_15:00	30
2007-03-21_18:00	2007-03-21_15:00	2007-03-21_21:00	15
2007-03-22_00:00	2007-03-21_21:00	2007-03-22_03:00	20
2007-03-22_06:00	2007-03-22_03:00	2007-03-22_09:00	32
2007-03-22_12:00	2007-03-22_09:00	2007-03-22_15:00	29
2007-03-22_18:00	2007-03-22_15:00	2007-03-22_21:00	11
2007-03-23_00:00	2007-03-22_21:00	2007-03-23_03:00	15

The 3DVAR_OBSPROC can also be used to plot the data distribution of GPSRO soundings by using MAP_plot. In Figure 4.6 a sample Map_PLOT output which show the GPS-RO occultations for given time window is shown. The analysis time of this sample is 2007-03-19_00:00, the time window minimum is 2007-03-18_21:00 and the time window maximum is 2007-03-19_03:00. There are only 8 GPS-RO soundings in this time window. MAP_plot outputs for other time windows are shown in the appendices.

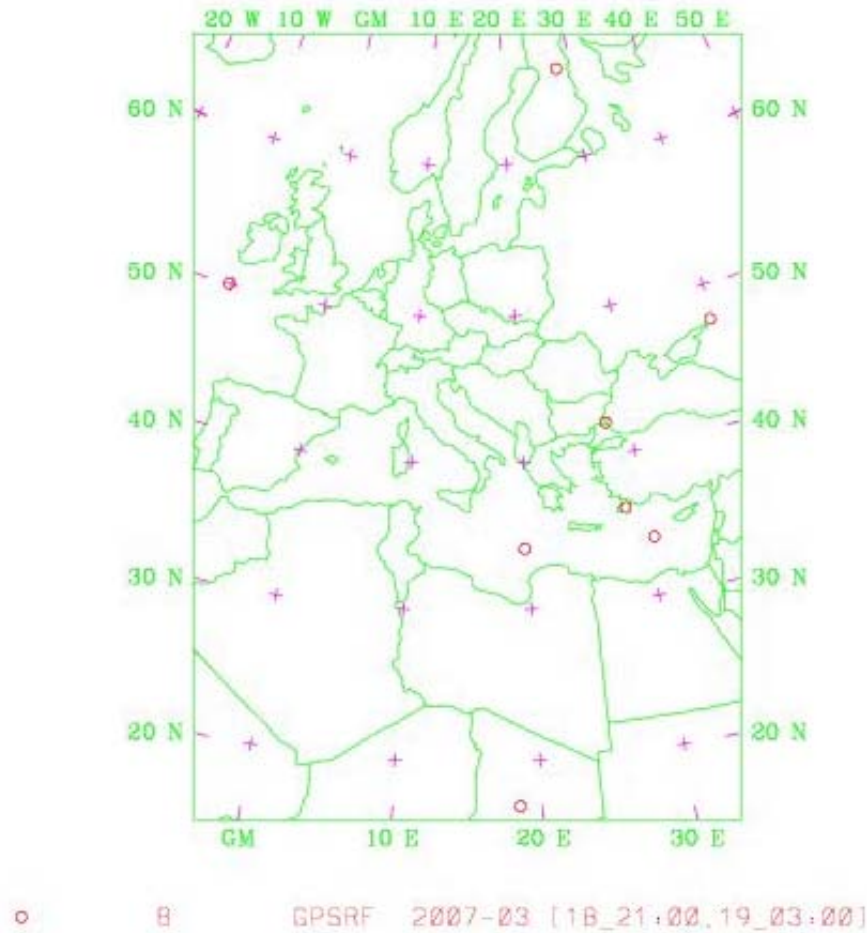


Figure 4.6: Map_PLOT output which show the GPS-RO Occultations for given time window

4.2.3 Background error statistics (gen_be)

Variational data assimilation systems use forecast (first guess or background) error covariances as an input to define analysis. Especially in data-sparse areas of the globe the impact of background error covariances is very important.

The “NMC-method” is used in 3/4D-Var systems for definition of background error covariances. In this method forecast error covariances are approximated using forecast difference statistics (Skamarock et al., 2008).

WRF-Var offers a utility (“gen_be”) which generates background error statistics (the “be.dat” file). A series of WRF forecasts are provided to the gen_be program. They are used to generate model perturbations, used as a proxy for estimates of forecast error. For the NMC method, the model perturbations are differences between forecasts (e.g. T+24 minus T+12 is typical for regional applications, T+48 minus

T+24 for global) valid at the same time. Climatological estimates of background error may then be obtained by averaging such forecast differences over a period of time (e.g. one month). It is important to include forecast differences from at least 00Z and 12Z through the period, to remove the diurnal cycle (Skamarock et al., 2008). The inputs to gen_be are NetCDF WRF forecast output ("wrfout") files at specified forecast ranges. To avoid unnecessary large single data files, it is assumed that all forecast ranges are output to separate files. By setting the WRF namelist.input options history_interval=720, and frames_per_outfile=1, necessary output datasets are obtained.

In this study, BE statistics using the NMC method with (T+24)-(T+12) forecast differences are calculated. For gen_be inputs, a total of 55 one-day WRF forecasts (initialized at 00Z and 12Z of respective days) are run expanding a 27-day period between 00Z 15 February and 12Z 14 March 2007. This period is just prior to the occurrence of the 20 March 2007 low-pressure system of interest and so the background error covariances thus generated are expected to reflect relevant climatological perturbations.

4.2.4 WRF-Var diagnostics

Diagnostic files which contain useful information about the performance of data assimilation are generated by WRF-Var. In this section contents of some of them are mentioned. WRF-Var users are advised to check these diagnostic files to see if the assimilation results appear to be sensible. Two of these diagnostic files are cost_fn and grad_fn. These ASCII formatted files contain the WRF-Var cost and gradient function values, for the first and last iterations. By editing namelist.input file as CALCULATE_CG_COST_FN = true, values of gradient and cost function are listed for each iteration; this can be helpful for visualization purposes. Another diagnostic file is gts_omb_oma which contains information about all of the observations used by the WRF-Var. This is also a ASCII formatted file and each observation is stored with its observed value, quality flag, observation error, observation minus background (OMB), and observation minus analysis (OMA). For both analysis and forecast verification purposes this information is very useful. Furthermore, namelist.output and statistics are the other diagnostic files of WRF-Var which contain information about a WRF-Var run. The namelist.output file is a consolidated list of all the namelist options used. The statistics file is a text file which contains

OMB (OI) and OMA (AO) statistics (minimum, maximum, mean and standard deviation) for each observation type and variable. Other contents of the statistics file are analysis minus background (A-B) statistics, i.e. statistics of the analysis increments for each model variable at each model level.

The analysis file of WRF-Var is a WRF (NetCDF) formatted file called `wrfvar_output`. It is used as the input file “`wrfinput_d01`” of any subsequent WRF runs after lateral boundary and/or low boundary conditions are updated.

5. RESULTS AND DISCUSSION

WRF is run for eleven analysis times with (i) GFS initial and boundary conditions only, and (ii) with GPS-RO observations assimilated in addition to the conventional GFS analyses. The 6, 12, 18 and 24 hour forecast results are verified against GPS-RO soundings. In total, 44 forecasts with GPS-RO assimilation and 44 forecasts with no GPS-RO assimilation initial conditions are compared.

For assimilation of FORMOSAT-3/COSMIC GPSRO data Local (Refractivity) observation operator in WRFVar (3DVar) is used.

In the neutral atmosphere by neglecting of small terms related to liquid or frozen water, the refractivity N is related to atmospheric pressure, P , temperature, T , water vapor partial pressure, P_w (Kuo et al. 2000).

$$N = 77.6 \times \frac{P}{T} + 3.73 \times 10^5 \times \frac{pq}{T^2(0.622 + 0.378q)} \quad (5.1)$$

5.1 Overall Average RMS and Mean Errors

We verify our forecasts with COSMIC GPSRO data by using 3DVar. OMB (OI) statistics (RMSE and mean error) are calculated. A sample statistics file output is shown in the appendices. Table 5.1 shows all RMS and mean errors (analysis and forecast) computed at each forecast time (6, 12, 18, 24) for all 11 analysis times. Average RMS and mean errors for 6, 12, 18, 24 hour forecasts are calculated.

The quality of the assimilation results can be evaluated based on the innovations, or observation-minus-forecast differences, defined by:

$$d_i^f = y_i - \overline{H_i(\mathbf{x}^f)} \quad (5.2)$$

where the subscript i indicates quantities related to the i th observation valid at a given time t , y is the observed variable, \mathbf{x} is the state vector of the forecast model, the superscript f indicates a quantity based on a forecast valid at time t , an overbar denotes the ensemble mean, and H is the GPS-RO observation operator that maps the state vector onto the observations. Since d^f compares the ensemble-mean short-range forecast to new observations, it provides a measure of the quality of the

forecast, and the analysis that produced the forecast. All statistics mentioned here will be computed for with-assimilation and no-assimilation of GPS-RO observations separately.

The first statistic is the *mean error*, $\langle d \rangle$, which is the average of all M innovations at a given time:

$$\langle d^f \rangle = \frac{1}{M} \sum_{i=1}^M d_i^f = \frac{1}{M} \sum_{i=1}^M (y_i - \overline{H_i(\mathbf{x}^f)}) \quad (5.3)$$

A second statistic is the *root-mean-square (rms) error*, $\langle r^f \rangle$, computed as follows:

$$\langle r^f \rangle = \sqrt{\frac{1}{M} \sum_{i=1}^M d_i^{f2}} \quad (5.4)$$

For vertical profiles of these two statistics, further binning of observation into height intervals is performed.

Since 00Z and 12Z GFS analyses already include information from the radiosonde network, more impact from the additional GPS-RO observations was expected for 06Z or 18Z analysis times. Therefore, average RMS and mean errors are also computed separately for 00Z/12Z and 06Z/18Z initial times. All calculation results are shown in table 5.1.

Table 5.1:Verification results for each forecast

	19_00	19_06	19_12	19_18	20_00	20_06	20_12	20_18	21_00	21_06	21_12	ORT	ORT	VAR	MAX	MIN	
	1	2	3	4	5	6	7	8	9	10	11	ALL	00-12Z	06-18Z			
6HR RMSE A	1.5210	1.5509	1.5143	1.6145	1.7587	1.6190	1.6911	1.8013	1.3053	1.6695	1.9327	1.6430	1.6248	1.6844	0.0295	1.9327	1.3053
12HR RMSE A	1.6655	1.4330	1.8410	1.8902	1.6449	1.6408	1.6190	1.5788	1.7320	2.1282	2.1832	1.8093	1.7712	1.8845	0.0582	2.1832	1.4330
18HR RMSE A	1.6188	1.6275	1.8011	1.6682	1.7269	2.1824	1.3593	1.8775	2.1094	2.2256	2.1094	1.8087	1.7523	1.8705	0.0805	2.2256	1.3593
24HR RMSE A	1.8175	1.7823	1.6153	1.8069	2.1245	1.3250	1.9434	1.9630	2.1487	1.9464	1.8501	1.8670	1.8822	1.8438	0.0398	2.1487	1.5250
6HR RMSE F	1.5435	1.5495	1.5183	1.5879	1.7921	1.6054	1.7921	1.8341	1.3074	1.6908	1.9476	1.6551	1.6321	1.7005	0.0348	1.9476	1.3074
12HR RMSE F	1.7235	1.4852	2.0107	1.8583	1.6437	1.7138	1.6496	1.5999	1.7457	2.1449	2.2243	1.8297	1.8024	1.8841	0.0603	2.2243	1.4852
18HR RMSE F	1.6178	1.8131	1.7982	1.6295	1.7809	2.2691	1.3099	1.9281	2.1258	2.3225	1.8829	1.8369	1.7927	1.9033	0.0909	2.3225	1.3099
24HR RMSE F	1.8290	1.7802	1.6735	1.8552	2.0625	1.4727	1.9064	1.9181	2.1247	1.9759	1.8735	1.8670	1.8806	1.8463	0.0357	2.1247	1.4727
6HR BIAS A	-0.2751	-0.1816	-0.2110	-0.0964	-0.1547	-0.4673	0.0033	0.2428	-0.1559	-0.2997	-0.2313	-0.1831	-0.1881	-0.1715	0.0350	0.2428	-0.4673
12HR BIAS A	-0.2011	-0.2175	0.0150	-0.1196	-0.3825	-0.0064	-0.3832	-0.3076	-0.2680	-0.4172	-0.1730	-0.2556	-0.2465	-0.2741	0.0215	0.0150	-0.4172
18HR BIAS A	-0.3455	-0.1308	-0.1142	-0.4005	0.0793	0.2431	-0.1852	-0.2605	-0.4524	-0.0691	-0.4524	-0.2391	-0.2039	-0.2788	0.0521	0.2431	-0.4524
24HR BIAS A	-0.1857	1.7823	-0.2983	0.1212	0.1347	-0.1433	-0.3090	-0.3739	-0.2164	-0.3548	-0.4992	-0.2817	-0.2998	-0.2470	0.4415	1.7823	-0.4992
6HR BIAS F	-0.2731	-0.1825	-0.2009	-0.1016	-0.1724	-0.4532	-0.1014	0.2248	-0.1151	-0.3216	-0.2385	-0.2049	-0.2123	-0.1899	0.0308	0.2248	-0.4532
12HR BIAS F	-0.1918	-0.2207	0.0271	-0.0996	-0.3940	-0.0200	-0.2378	-0.3189	-0.2378	-0.4421	-0.1515	-0.2486	-0.2340	-0.2784	0.0232	0.0271	-0.4421
18HR BIAS F	-0.3783	-0.0906	-0.1153	-0.3559	0.0673	0.1489	-0.1730	-0.2751	-0.4660	-0.0452	-0.4169	-0.2667	-0.2681	-0.2645	0.0419	0.1489	-0.4660
24HR BIAS F	-0.2647	-0.1172	-0.3403	0.0895	0.2035	-0.1634	-0.3157	-0.3573	-0.1987	-0.3402	-0.4756	-0.2828	-0.3038	-0.2427	0.0434	0.2035	-0.4756

In Figures 5.1, 5.2, 5.3, 5.4, 5.5 and 5.6, calculation results are shown as graphics. Green lines represent forecast errors from initial conditions with GPS-RO assimilated, and red lines represent forecast errors from initial conditions without GPS-RO assimilated.

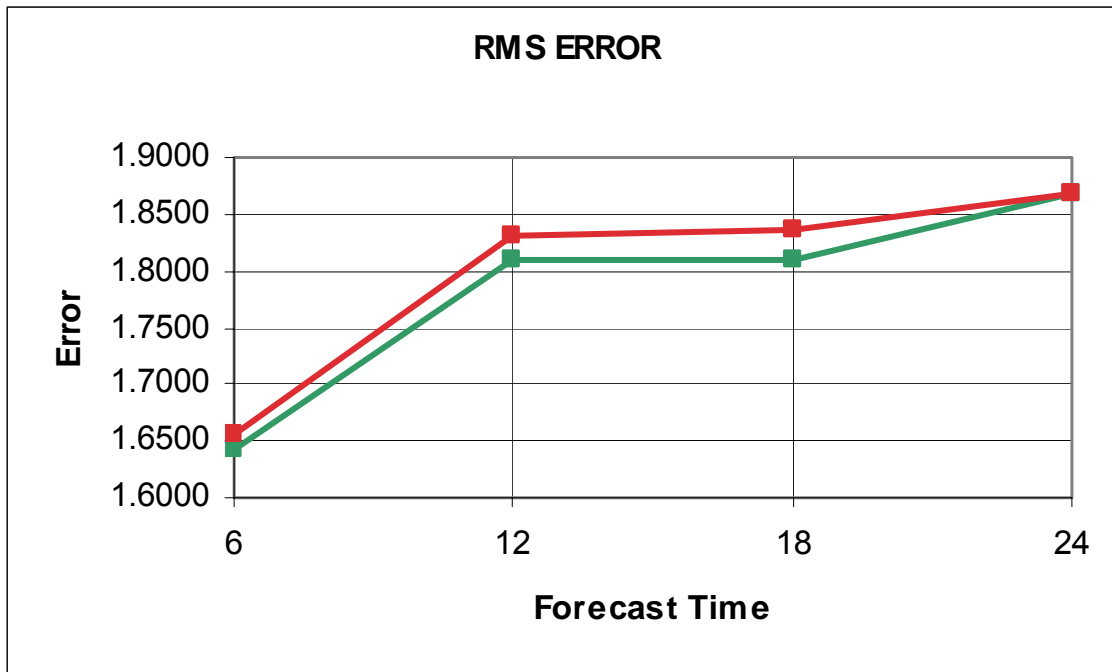


Figure 5.1 : Average RMS errors for 6, 12, 18, 24 hour forecasts of the study

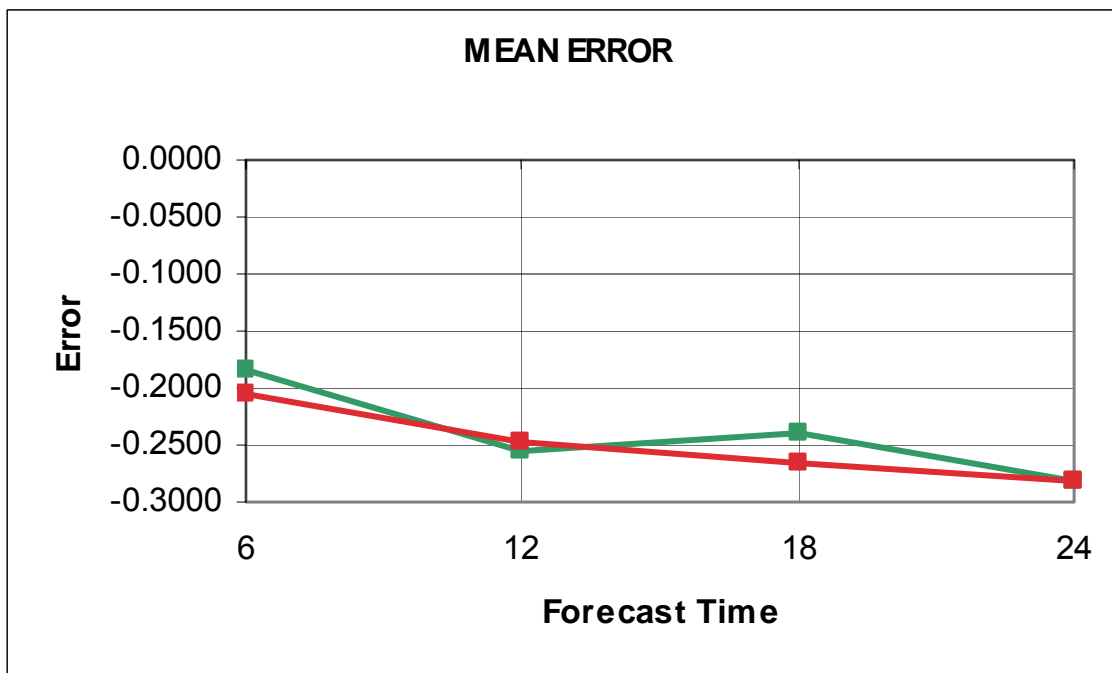


Figure 5.2 : Average mean errors for 6, 12, 18, 24 hour forecasts of study

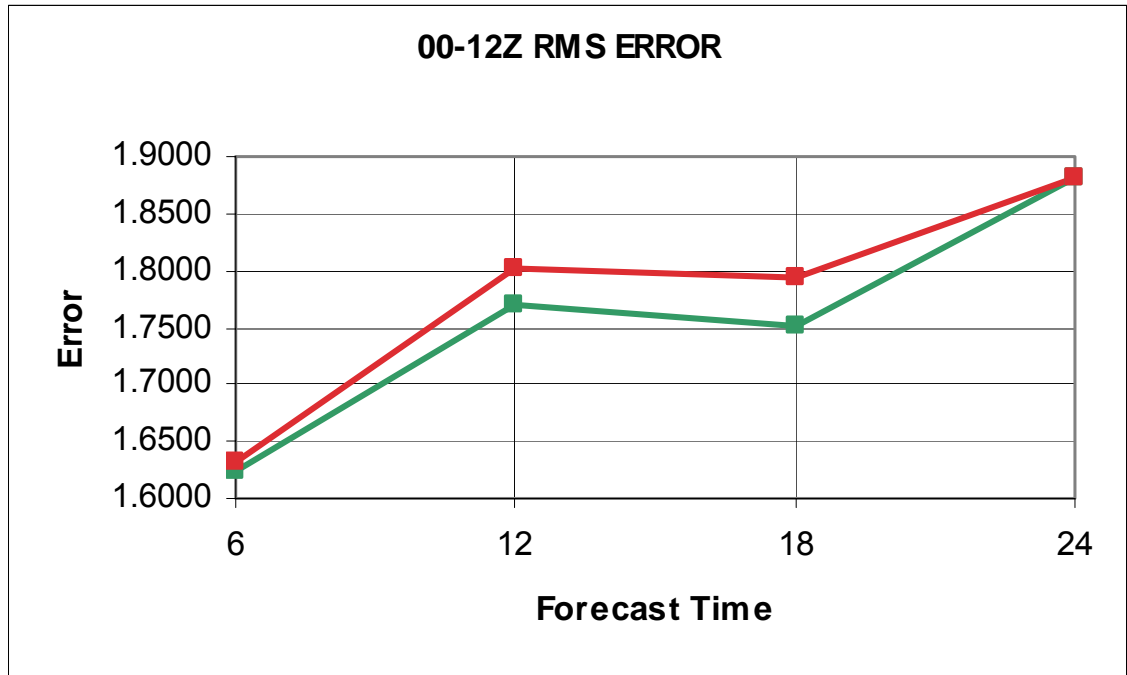


Figure 5.3 : Average RMS errors for 6, 12, 18, 24 hour forecasts with initial times 00Z or 12Z

In Figure 5.1, a slight decrease of the globally-averaged RMSE can be seen when GPS-RO observations are assimilated. An improvement in the mean error is also observed for the 6, 18, and 24-hour forecast times (Figure 5.2). Contrary to expectations, assimilation of GPS-RO has a stronger impact on forecasts which were initialized at 00Z or 12Z, as opposed to 06Z and 18Z. This is shown in Figures 5.3 through 5.6.

In conclusion, improvements in short-term forecasts (up to 24 hours) with the assimilated GPS-RO data are observed and the benefits of assimilating GPS-RO data in addition to the traditional observations assimilated by the GFS system are presented.

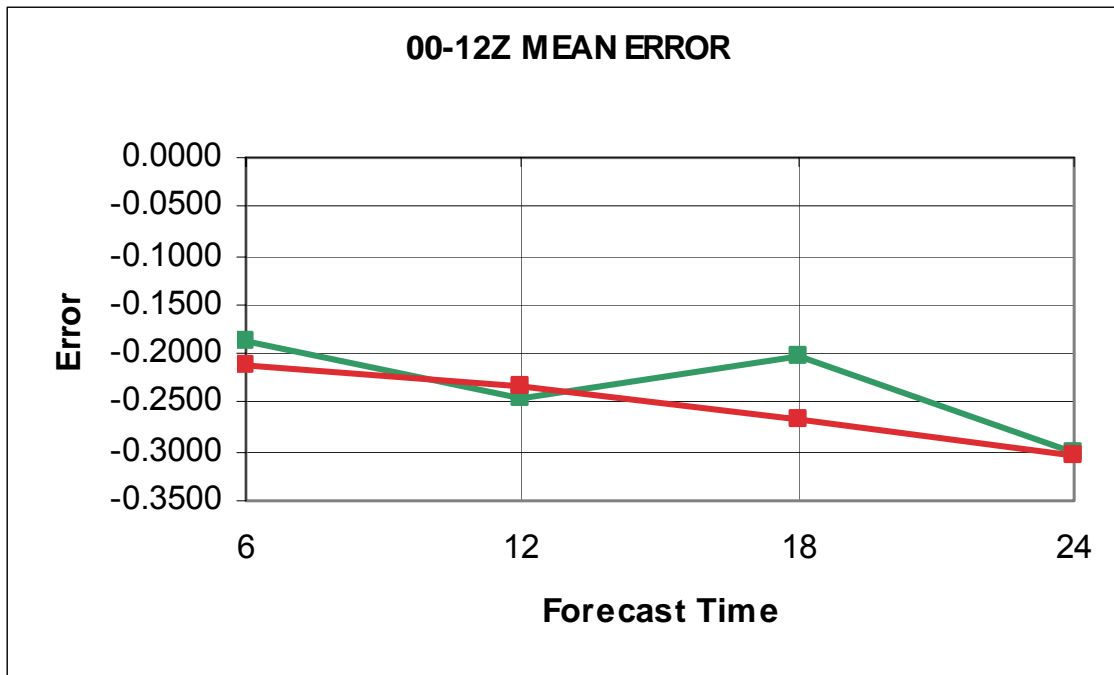


Figure 5.4 : Average mean errors for 6, 12, 18, 24 hour forecasts with initial times 00Z or 12Z

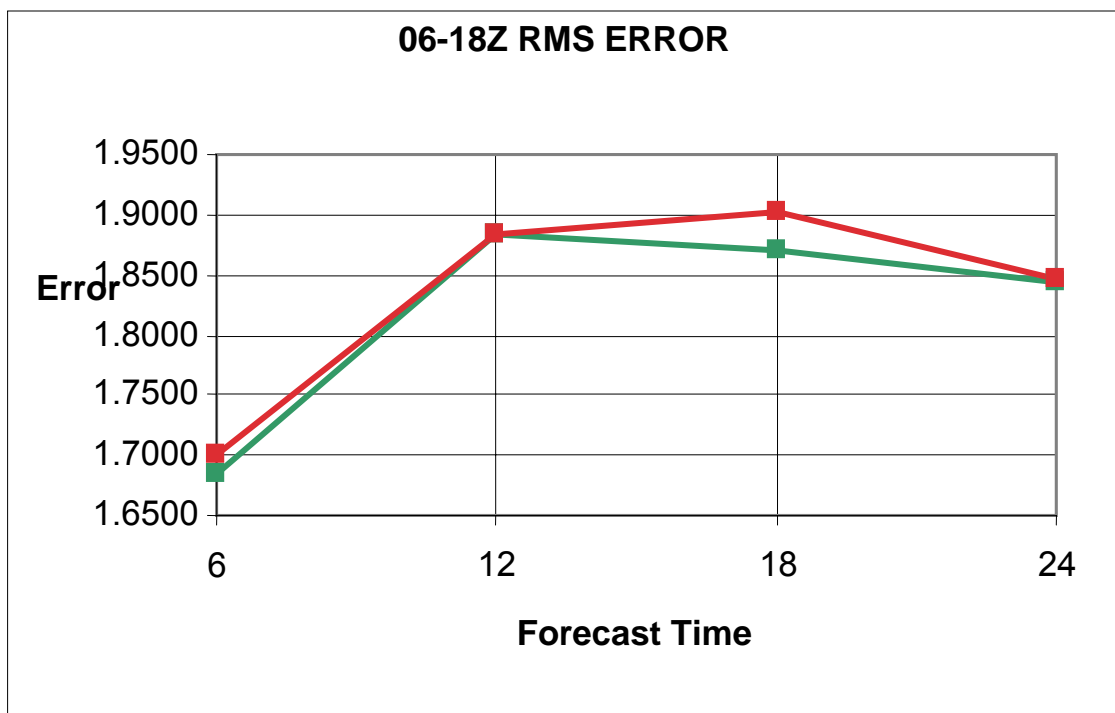


Figure 5.5 : Average RMS errors for 6 ,12 ,18, 24 hr forecasts with initial 06 or 18Z

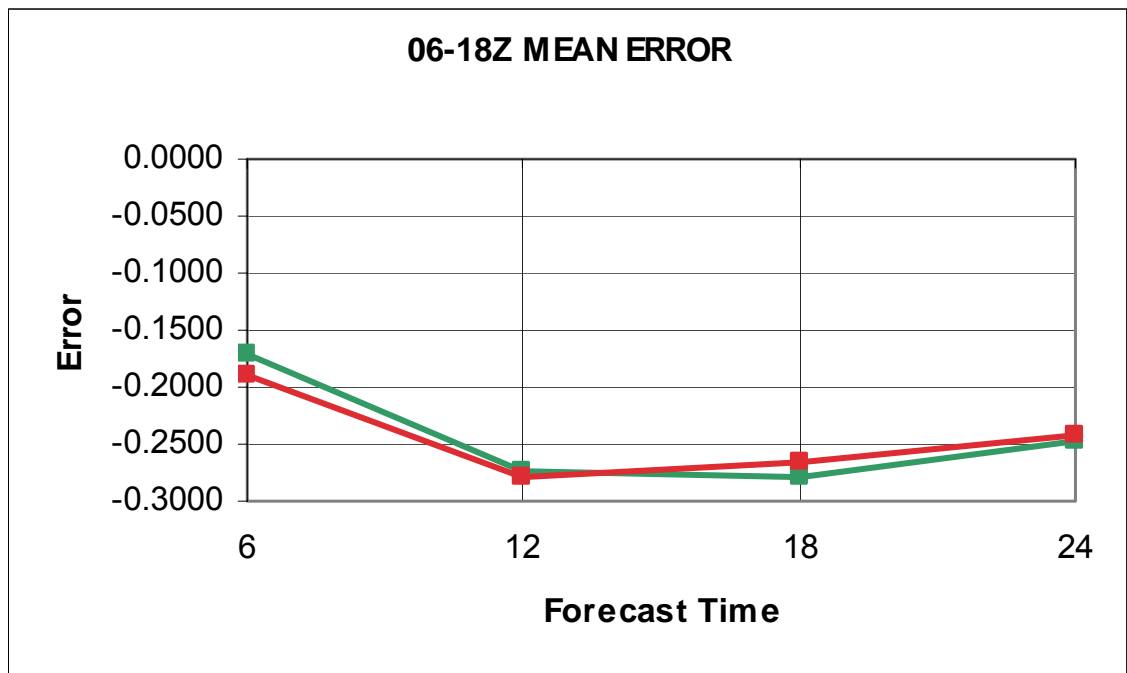


Figure 5.6 : Average mean errors for 6, 12, 18, 24 hour forecasts with initial times 06Z or 18Z

5.2 Vertical Average RMS and Mean Error Gradients

In addition to overall averages of RMS and mean errors, average RMS and mean errors are also calculated for all model vertical levels. In Figures 5.1 through 5.6, the maximum reduction in average RMS and mean errors were seen for the 18-hour forecasts, therefore in this section we focus on vertical profiles of error differences for the 18-hour forecasts only. For easier comparison, we directly plot differences in RMS and mean errors between initializations without and with GPS-RO observations. Positive numbers imply an improvement in errors by the assimilation of GPS-RO observations.

In Table 5.2, overall vertical distribution statistics are presented for RMS and mean error differences, while tables 5.3 and 5.4 focus on initial times grouped as 00Z/12Z and 06Z/18Z, respectively.

Table 5.2: Vertical average RMS and mean error gradients of all 18 hour forecasts for both GPS-RO assimilated and not assimilated initial conditions

Height	S_AS	OMB_RMSE	OMB_MEAN_	S	OMB_RMSE	OMB_MEAN
		_AS	AS		No	No
		With	With			With
		Assimilation	Assimilation			Assimilation
19500	825	0.14242963	-0.019383515	829	0.144086537	-0.016487308
18500	1380	0.158254897	-0.010961862	1380	0.154730959	-0.010177467
17500	1380	0.174184069	-0.021084266	1380	0.176932549	-0.017963557
16500	1380	0.205029118	0.00104199	1380	0.206989721	0.002329278
15500	1380	0.252557888	-0.043182911	1380	0.250230991	-0.044751743
14500	1380	0.325714809	-0.079927973	1380	0.315653298	-0.079098447
13500	1380	0.384844872	-0.049321446	1380	0.380356116	-0.051314808
12500	1380	0.42308324	0.116750241	1380	0.419677712	0.125137306
11500	1380	0.563768136	0.281444852	1380	0.570120992	0.307654327
10500	1380	0.697079738	0.335318648	1380	0.704533455	0.352358594
9500	1380	0.63471741	0.178760651	1380	0.631029419	0.166801654
8500	1377	0.676156126	0.017238975	1377	0.66121751	-0.000804578
7500	1360	0.868394118	-0.101585242	1360	0.850287814	-0.117352967
6500	1357	1.001735275	-0.291757779	1357	0.999850724	-0.312552184
5500	1347	1.592686892	-0.448174142	1347	1.580653813	-0.469477397
4500	1329	2.250485954	-0.758230909	1329	2.26025453	-0.780508746
3500	1288	3.270368478	-0.900354593	1298	3.365422134	-1.004594808
2500	1211	3.71138258	-0.594099586	1227	3.766471958	-0.618667997
1500	1056	4.449785489	-0.675159055	1062	4.514581088	-0.572396783
500	472	5.844273	-2.166536377	471	5.885547032	-2.168586545

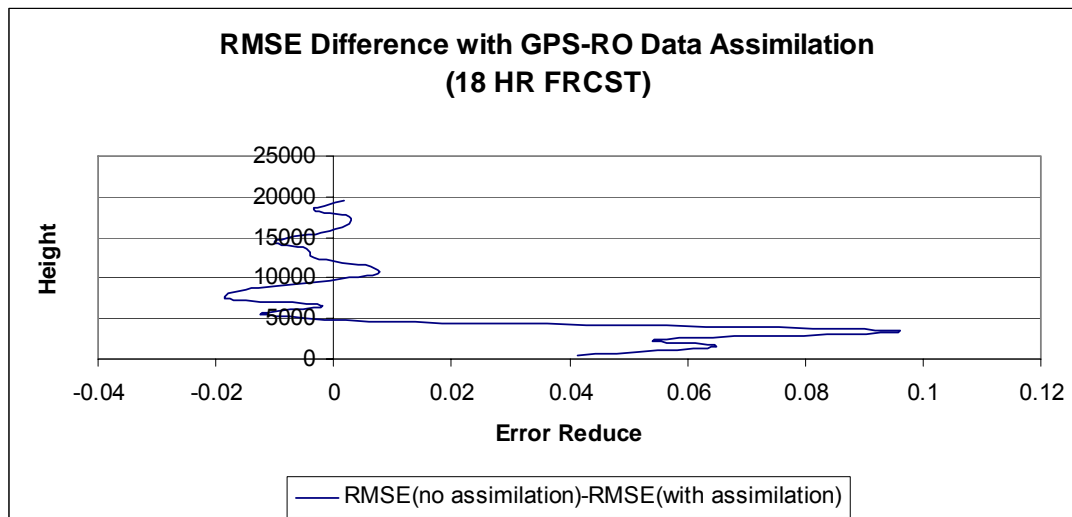


Figure 5.7 : Vertical average RMSE difference gradient for all 18 hour forecasts

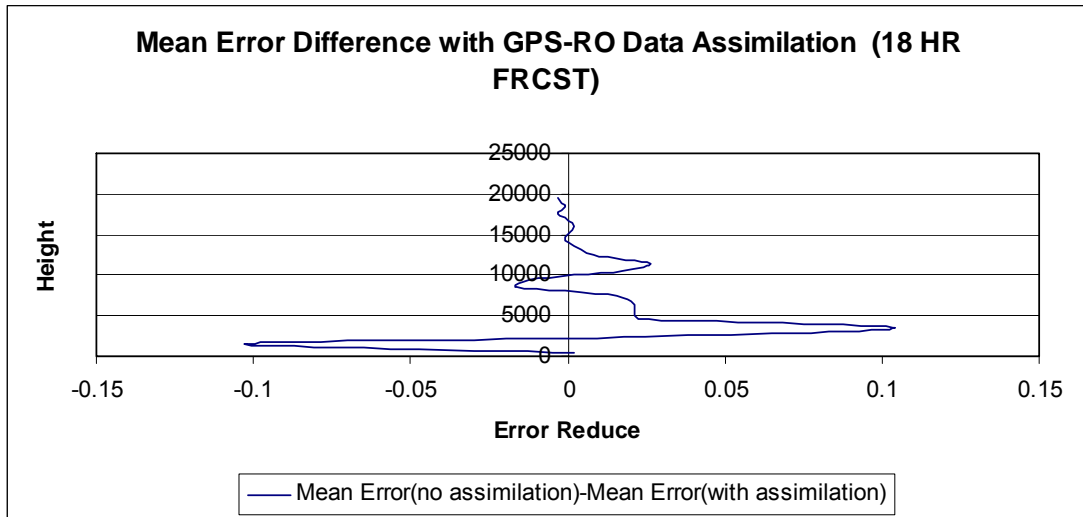


Figure 5.8 : Vertical average mean error difference gradient for all 18 hour forecasts

Figures 5.7, 5.8, 5.9, 5.10, 5.11, and 5.12 are the graphical representations of vertical RMS or mean error differences for the 18-hour forecasts. The x axes of the graphics represent error differences and the y axes represent heights. Error differences are calculated as follows;

$$\text{RMSE (no assimilation)} - \text{RMSE (with assimilation)} \quad (5.1)$$

$$\text{Abs. Mean Err. (no assimilation)} - \text{Abs. Mean Err. (with assimilation)} \quad (5.2)$$

Therefore, positive values indicate positive effects of the GPS-RO data assimilation on the forecasts.

Table 5.3: Vertical average RMS and mean error gradients of 18 hour forecasts with initial times 00Z or 12Z for both GPS-RO assimilated and not assimilated initial conditions

Height	S_AS	OMB_RMSE	OMB_MEAN_	S	OMB_RMSE	OMB_MEAN
		AS	AS		No	No
		With	With			No
		Assimilation	Assimilation			Assimilation
19500	443	0.150976091	-0.004335527	446	0.15181612	-0.002743887
18500	740	0.166614971	-0.006698584	740	0.161974837	-0.007712184
17500	740	0.174532928	-0.021822217	740	0.173165177	-0.018817927
16500	740	0.206350783	0.01498527	740	0.207833441	0.014126858
15500	740	0.243340767	-0.011726328	740	0.242445023	-0.019312097
14500	740	0.308119782	-0.049935281	740	0.302767968	-0.059149791
13500	740	0.366659691	-0.047899109	740	0.363538566	-0.043827246
12500	740	0.426112471	0.101895861	740	0.421585484	0.121982568
11500	740	0.55105733	0.238031379	740	0.557897981	0.268457956
10500	740	0.740794994	0.357788939	740	0.742528021	0.36992735
9500	740	0.675093743	0.28003696	740	0.664449174	0.260579144
8500	740	0.679625711	0.144629168	740	0.665480374	0.118777054
7500	740	0.8473993	0.001943948	740	0.829790176	-0.031390178
6500	740	0.932222837	-0.246620733	740	0.935645387	-0.2922696
5500	740	1.669230563	-0.381072414	740	1.651653859	-0.443593698
4500	730	2.290322389	-0.771211688	730	2.276720707	-0.850892363
3500	713	3.063693331	-1.050859901	714	3.11510397	-1.115932041
2500	690	3.376345176	-0.804828066	690	3.445583844	-0.832345284
1500	597	4.736756656	-0.854231401	597	4.699215589	-0.825009216
500	272	5.333251374	-1.270916958	270	5.33163293	-1.262285381

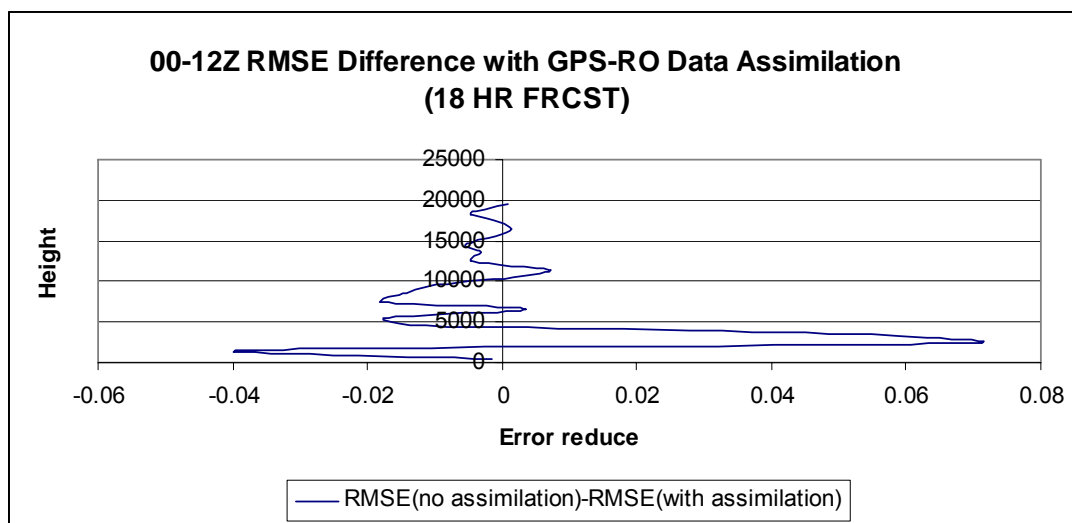


Figure 5.9 : Vertical average RMSE difference gradient for 18 hour forecasts with initial times 00Z or 12Z

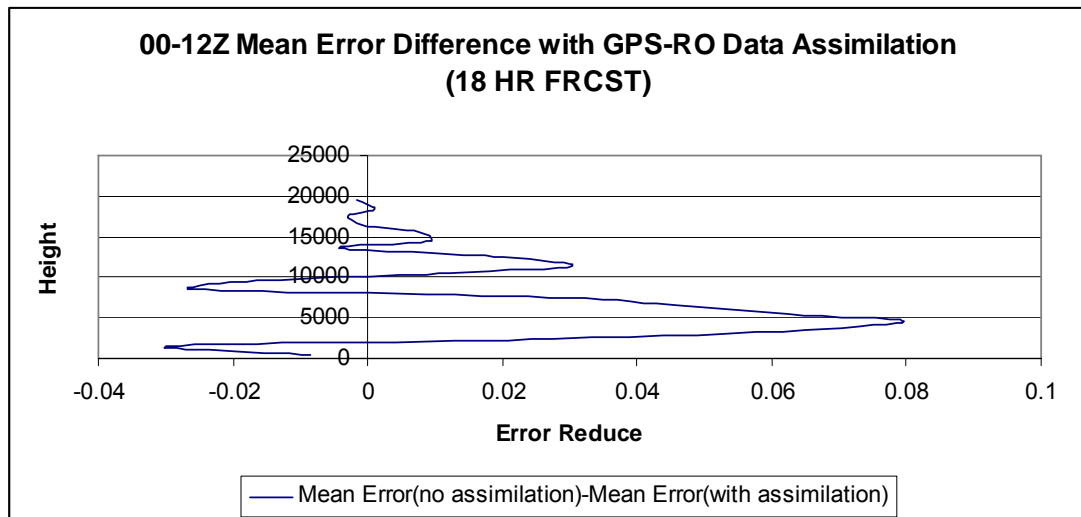


Figure 5.10 : Vertical average mean error difference gradient for 18 hour forecasts with initial times 00Z or 12Z

Results in Figures 5.7 through 5.12 confirm our findings of overall improvements in the RMS and mean errors as was shown in Figures 5.1 through 5.6 because larger positive areas are spanned in the vertical profiles than negative areas, implying that the net effects of assimilating GPS-RO observations are positive.

Table 5.4: Vertical average RMS and mean error gradients of 18 hour forecasts with initial times 06Z or 18Z for both GPS-RO assimilated and not assimilated initial conditions

Height	S	OMB_RMSE		OMB_MEAN_		S	OMB_RMSE		OMB_MEAN	
		AS	AS	AS	S		No Assimilation	No Assimilation	No Assimilation	No Assimilation
		With Assimilation		With Assimilation			No Assimilation		No Assimilation	
19500	382	0.131826377	-0.036834454	383	0.134526957	-0.032491395				
18500	640	0.148001051	-0.015891277	640	0.145907595	-0.01302795				
17500	640	0.173779828	-0.02023101	640	0.181190952	-0.016975692				
16500	640	0.203490242	-0.015079927	640	0.206009862	-0.011311673				
15500	640	0.262812529	-0.079554585	640	0.258941842	-0.074166334				
14500	640	0.344942063	-0.114607024	640	0.329925224	-0.10216408				
13500	640	0.404854509	-0.050966023	640	0.398918568	-0.0599723				
12500	640	0.419553428	0.133925619	640	0.417460982	0.128784973				
11500	640	0.578116732	0.331641681	640	0.583934994	0.352975131				
10500	640	0.642838769	0.309337375	640	0.657872493	0.332044719				
9500	640	0.584566062	0.061659918	640	0.590032857	0.058371431				
8500	637	0.672103037	-0.130749632	637	0.656230592	-0.139722017				
7500	620	0.892806398	-0.225152339	620	0.874123759	-0.219953715				
6500	617	1.079216094	-0.345892972	617	1.071794719	-0.336878136				
5500	607	1.494076673	-0.529978556	607	1.489526087	-0.501032483				
4500	599	2.200962801	-0.742411263	599	2.240023598	-0.694732385				
3500	575	3.509784251	-0.71372801	584	3.648200135	-0.868473601				
2500	521	4.113307158	-0.315015802	537	4.142456398	-0.344110589				
1500	459	4.04619739	-0.442247964	465	4.265834115	-0.248075015				
500	200	6.474858143	-3.384578788	201	6.556367935	-3.386006019				

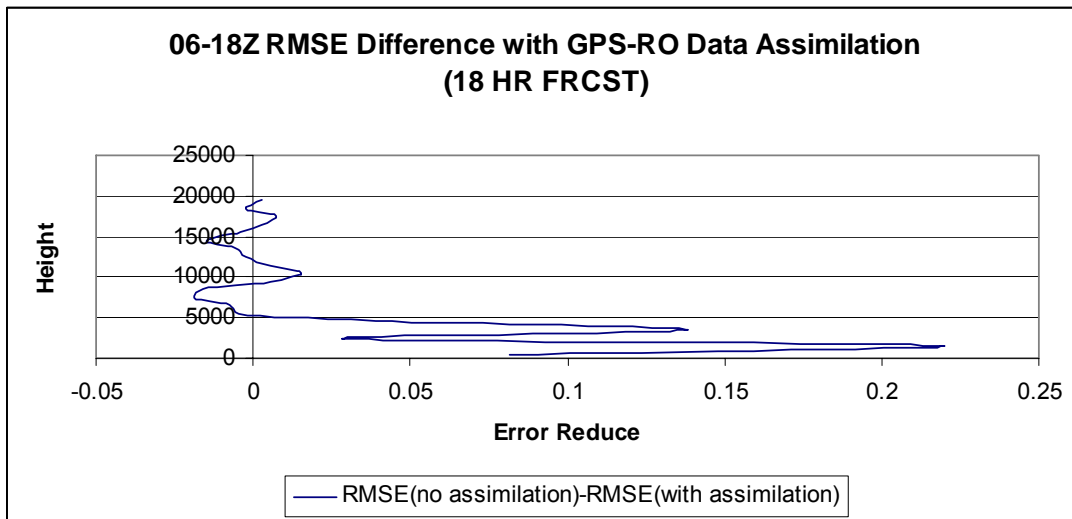


Figure 5.11: Vertical average RMSE difference gradient for 18 hour forecasts with initial times 06Z or 18Z

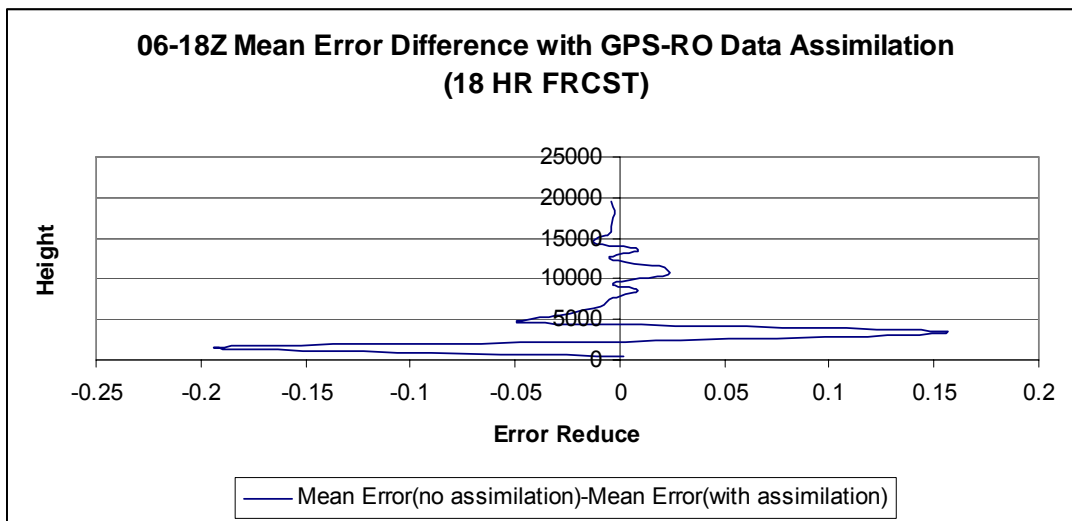
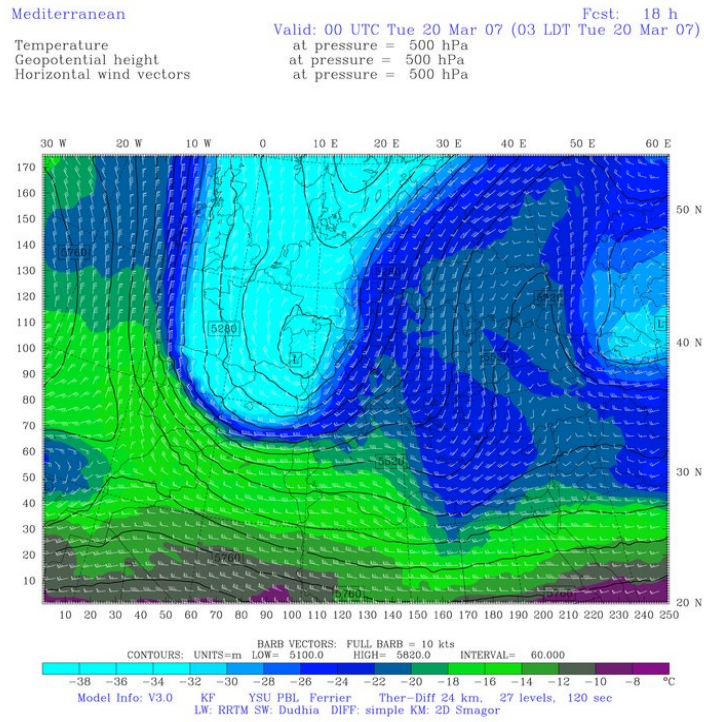


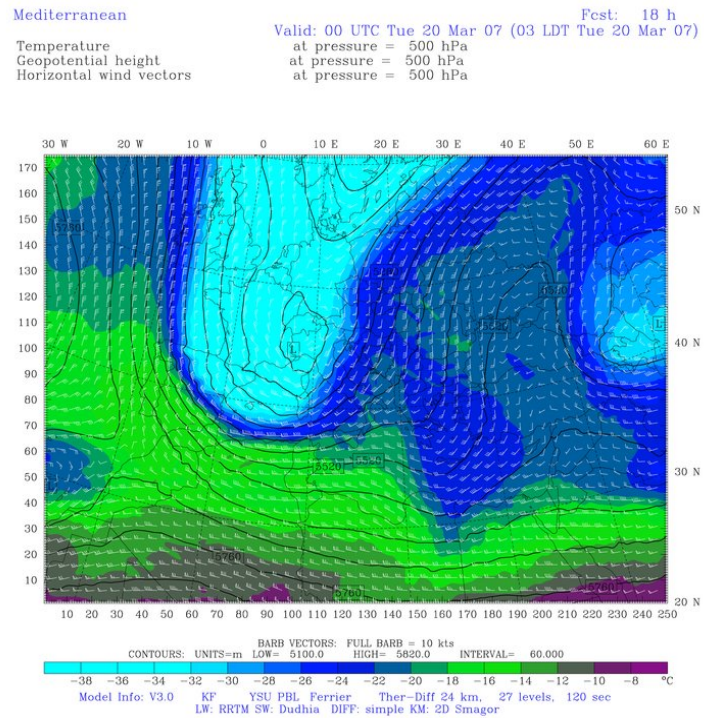
Figure 5.12 : Vertical average mean error difference gradient for 18 hour forecasts with initial times 06Z or 18Z

An interesting finding is that most of the systematic large impacts are limited to the lower levels of the troposphere close to the surface. This could indicate that most positive impact of the assimilation of GPS-RO observations could occur in the boundary layer where model uncertainty, especially for moisture, is the greatest.

5.3 Examples of Positive Impact of Data Assimilation on Forecasts



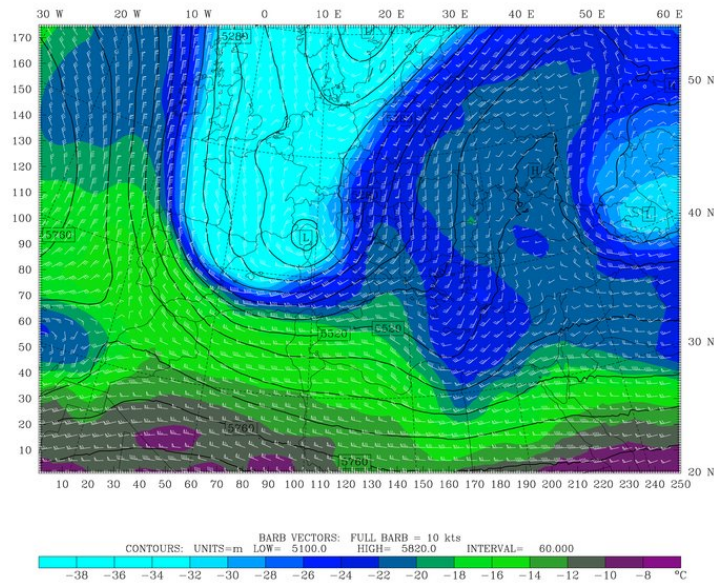
(a)



(b)

Mediterranean
Temperature
Geopotential height
Horizontal wind vectors

Fcst: 0 h
Valid: 00 UTC Tue 20 Mar 07 (03 LDT Tue 20 Mar 07)
at pressure = 500 hPa
at pressure = 500 hPa
at pressure = 500 hPa



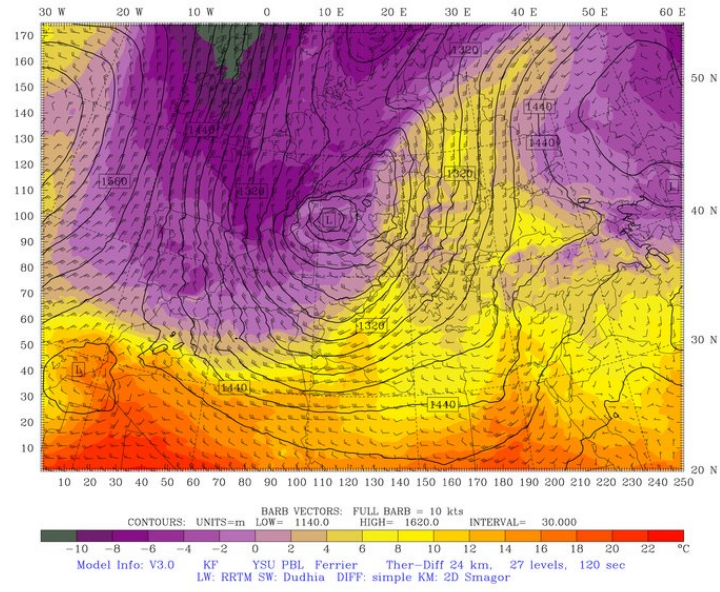
(c)

Figure 5.13: (a) 20.03.2007 00:00 GMT forecast without assimilation, initialized at 19.03.2007 06:00 GMT. (b) 20.03.2007 00:00 GMT forecast with GPS-RO assimilation, initialized at 19.03.2007 06:00 GMT. (c) 20.03.2007 00:00 GMT analysis of GFS.

Comparing the 18-hours forecasts of the runs with GFS input, it is seen that the run with GPS-RO assimilation is more successful than the one without assimilation at 500 hPa level. Figure 5.13 (a) shows the 20.03.2007 00:00GMT forecast of the run without GPS-RO assimilation, where Figure 5.13 (b) is the forecast of the same moment with assimilation. Figure 5.13 (c) is the GFS input, which represent the observations. The general patterns of geopotential height and temperature seem same, except smoother curves of the GFS input, which is because of the resolution issue. When looking up the small differences of temperarute patterns like the small warm cell over Romania, cold cell on Black Sea, it is clear that the run with assimilation has a better accuracy.

Mediterranean
Temperature
Geopotential height
Horizontal wind vectors

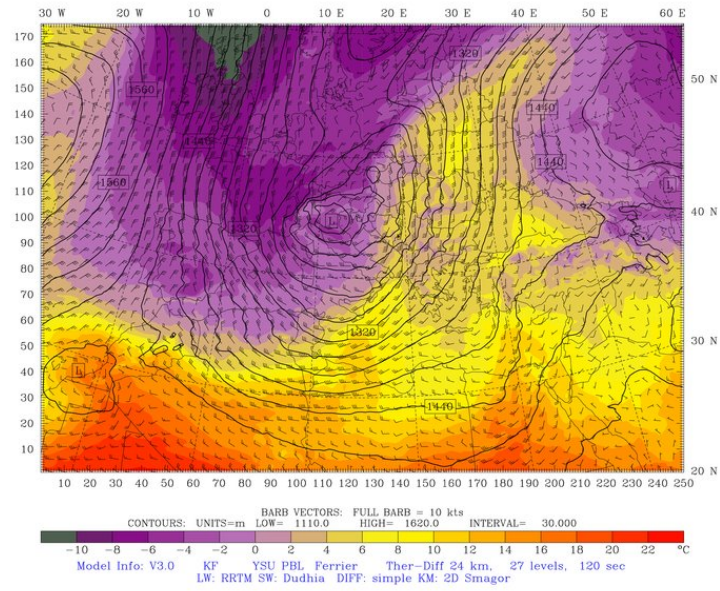
Valid: 06 UTC Tue 20 Mar 07 (09 LDT Tue 20 Mar 07)
Fcst: 18 h
at pressure = 850 hPa
at pressure = 850 hPa
at pressure = 850 hPa



(a)

Mediterranean
Temperature
Geopotential height
Horizontal wind vectors

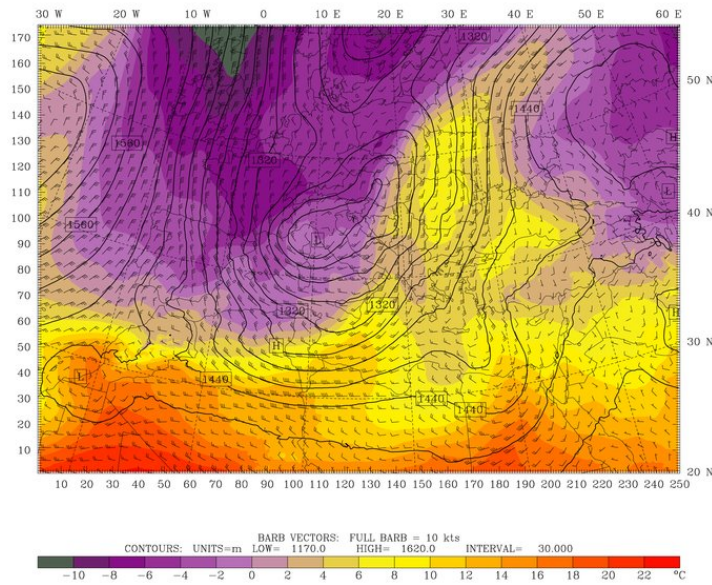
Valid: 06 UTC Tue 20 Mar 07 (09 LDT Tue 20 Mar 07)
Fcst: 18 h
at pressure = 850 hPa
at pressure = 850 hPa
at pressure = 850 hPa



(b)

Mediterranean
Temperature
Geopotential height
Horizontal wind vectors

Valid: 06 UTC Tue 20 Mar 07 (09 LDT Tue 20 Mar 07)
Fest: 0 h
at pressure = 850 hPa
at pressure = 850 hPa
at pressure = 850 hPa



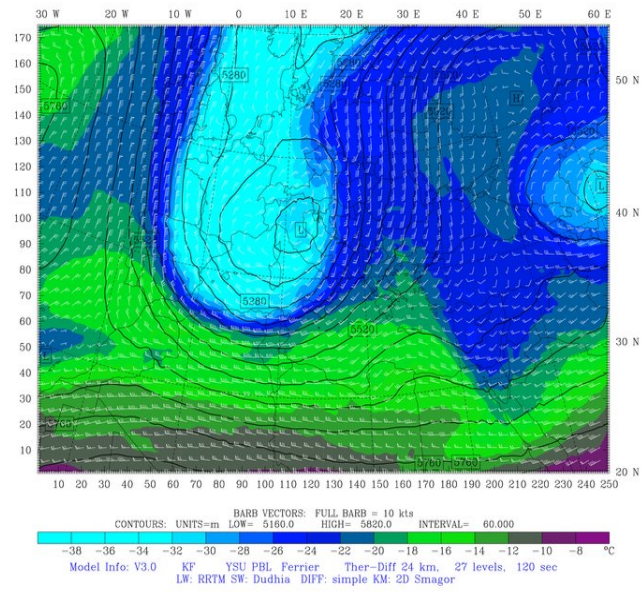
(c)

Figure 5.14: (a) 20.03.2007 06:00 GMT forecast without assimilation, initialized at 19.03.2007 12:00 GMT. (b) 20.03.2007 06:00 GMT forecast with GPS-RO assimilation, initialized at 19.03.2007 12:00 GMT. (c) 20.03.2007 06:00 GMT analysis of GFS.

To have a look at the accuracy of the Mediterranean Low, 850 hPa geopotential height values can be a good criteria, since it is approximately the top of the atmospheric boundary layer. 850 hPa forecast of 20.03.2007 06:00 GMT is seen at Figure 5.14 (a) without and Figure 5.14 (b) with assimilation. Figure 5.14 (c) is the GFS input.

Mediterranean
Temperature
Geopotential height
Horizontal wind vectors

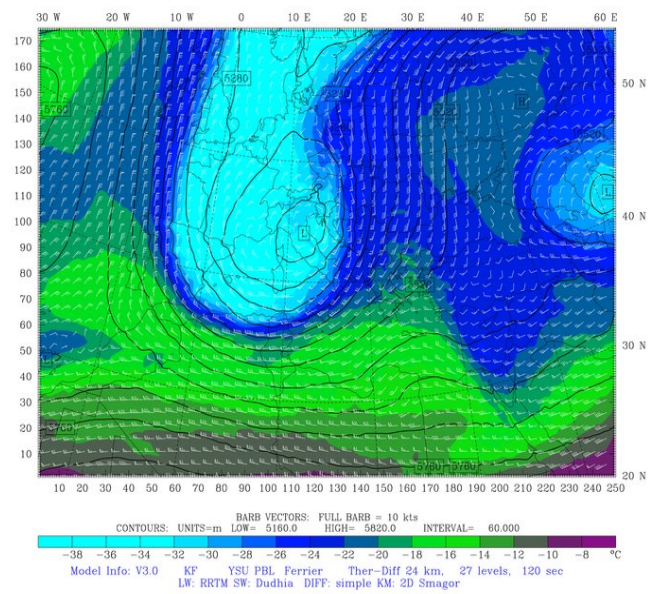
Valid: 12 UTC Tue 20 Mar 07 (15 LDT Tue 20 Mar 07)
Fest: 18 h
at pressure = 500 hPa
at pressure = 500 hPa
at pressure = 500 hPa



(a)

Mediterranean
Temperature
Geopotential height
Horizontal wind vectors

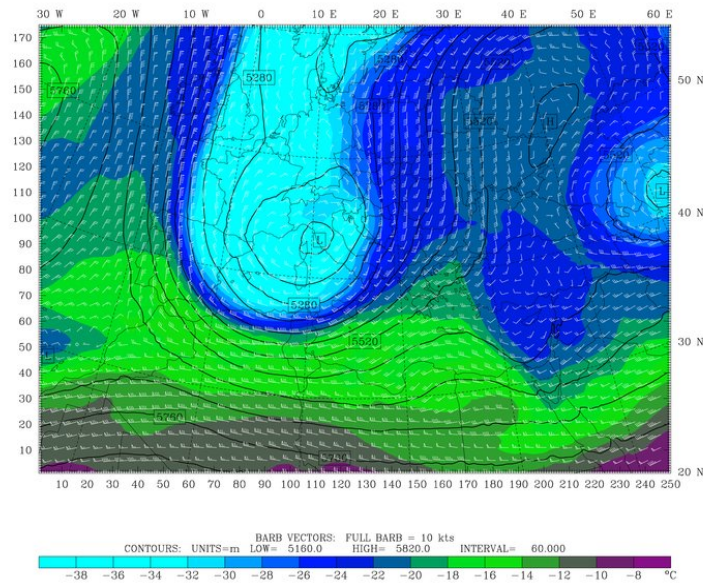
Valid: 12 UTC Tue 20 Mar 07 (15 LDT Tue 20 Mar 07)
Fest: 18 h
at pressure = 500 hPa
at pressure = 500 hPa
at pressure = 500 hPa



(b)

Mediterranean
Temperature
Geopotential height
Horizontal wind vectors

Valid: 12 UTC Tue 20 Mar 07 (15 LDT Tue 20 Mar 07)
Fest: 0 h
at pressure = 500 hPa
at pressure = 500 hPa
at pressure = 500 hPa



(c)

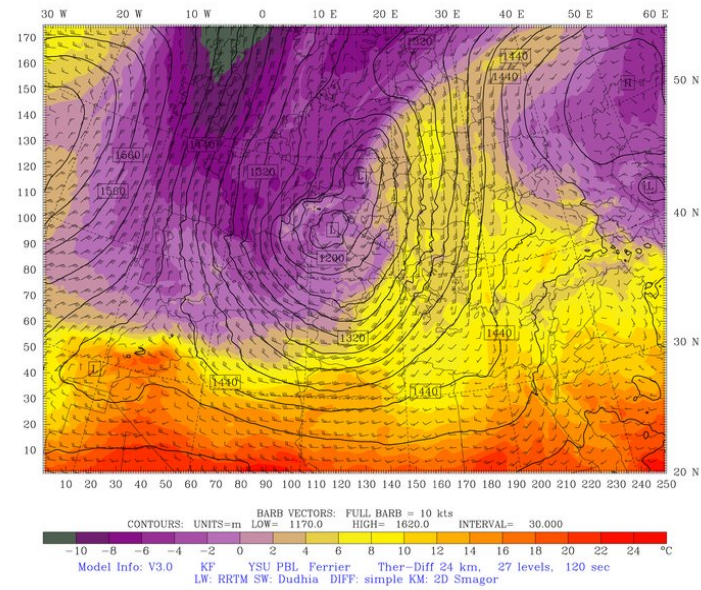
Figure 5.15: (a) 20.03.2007 12:00 GMT forecast without assimilation, initialized at 19.03.2007 18:00 GMT. (b) 20.03.2007 12:00 GMT forecast with GPS-RO assimilation, initialized at 19.03.2007 18:00 GMT. (c) 20.03.2007 12:00 GMT analysis of GFS.

The closed contour of low centre at 500 hPa on north of Italy has a value of 516 dam in both of the forecasts, at 20.03.2007 12:00 GMT. The observation plot also has the same value, although the closed contour seems to be smaller. The forecast with assimilation is more similar to the observation, with respect to the size of the closed contour of the low centre.

Mediterranean

Valid: 12 UTC Tue 20 Mar 07 (15 LDT Tue 20 Mar 07) Fcst: 18 h
at pressure = 850 hPa
at pressure = 850 hPa
at pressure = 850 hPa

Temperature
Geopotential height
Horizontal wind vectors

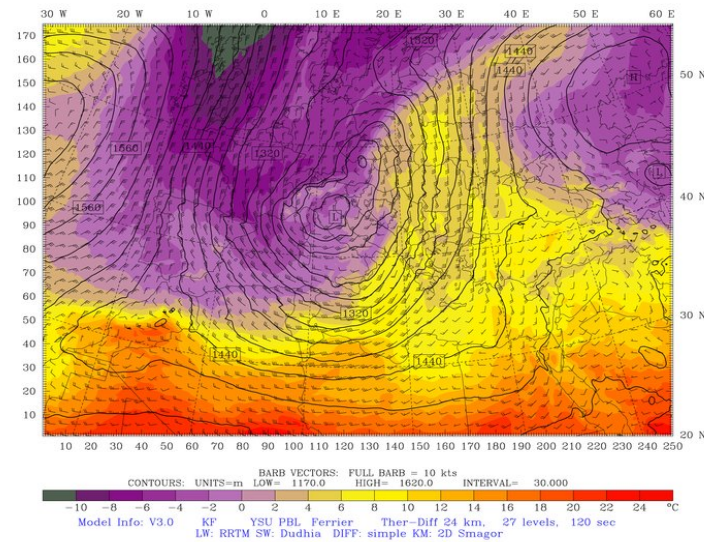


(a)

Mediterranean

Valid: 12 UTC Tue 20 Mar 07 (15 LDT Tue 20 Mar 07) Fcst: 18 h
at pressure = 850 hPa
at pressure = 850 hPa
at pressure = 850 hPa

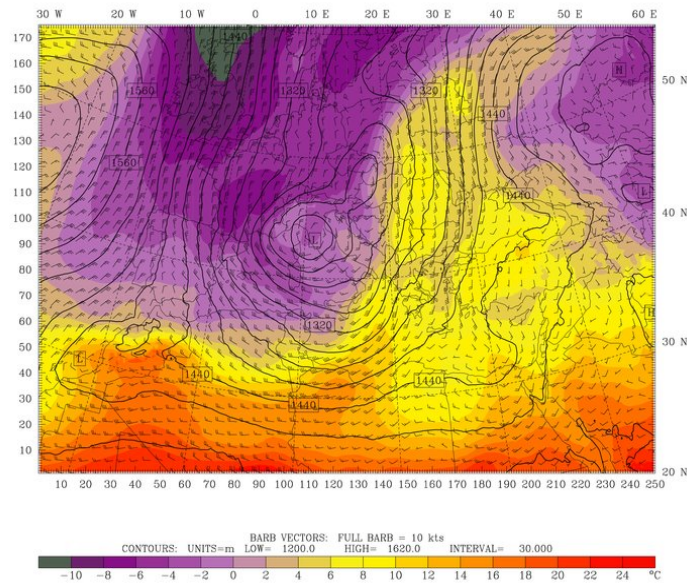
Temperature
Geopotential height
Horizontal wind vectors



(b)

Mediterranean
Temperature
Geopotential height
Horizontal wind vectors

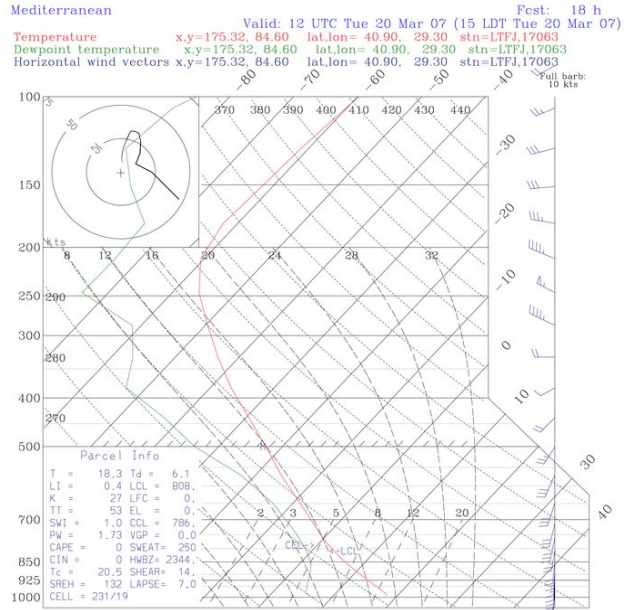
Valid: 12 UTC Tue 20 Mar 07 (15 LDT Tue 20 Mar 07)
Fest: 0 h
at pressure = 850 hPa
at pressure = 850 hPa
at pressure = 850 hPa



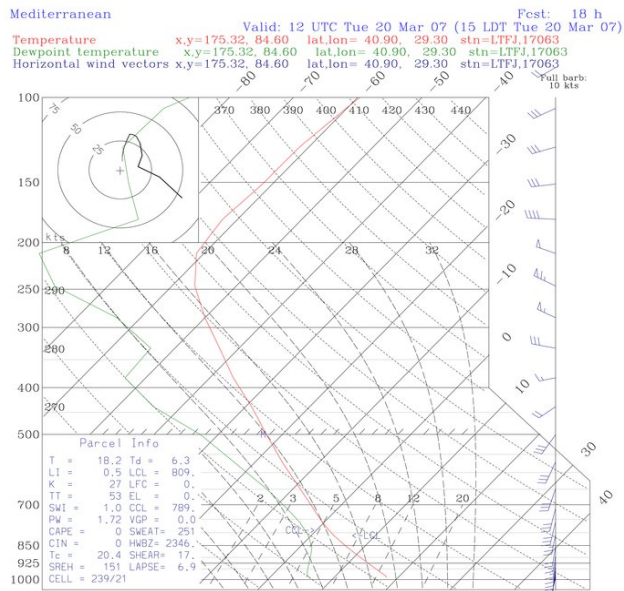
(c)

Figure 5.16: (a) 20.03.2007 12:00 GMT forecast without assimilation, initialized at 19.03.2007 18:00 GMT. (b) 20.03.2007 12:00 GMT forecast with GPS-RO assimilation, initialized at 19.03.2007 18:00 GMT. (c) 20.03.2007 12:00 GMT analysis of GFS.

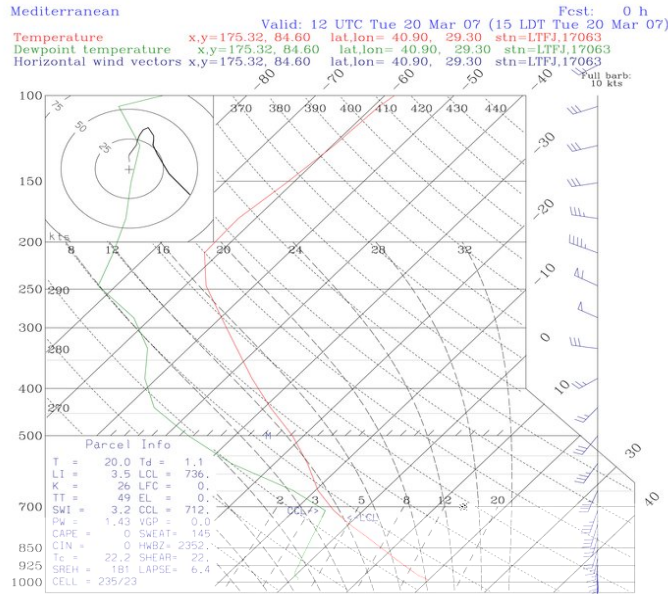
Also at 850 hPa level of the same time, it is seen that the geopotential height of the low centre is underestimated about 3 dam, 117 dam instead of 120 dam. This is a very deep low, so the amount of error is satisfactory. However, assimilation seems to be slightly improving the forecast, since the centre of the low has a higher value.



(a)



(b)



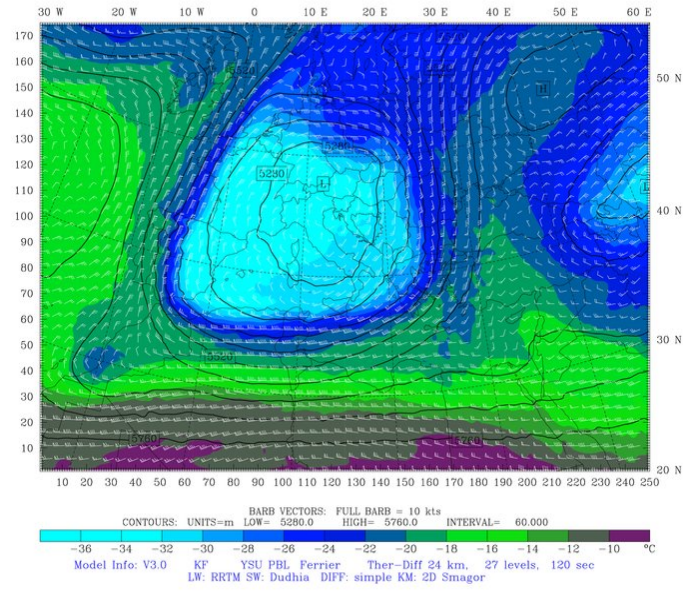
(c)

Figure 5.17: (a) 20.03.2007 12:00 GMT forecast without assimilation, initialized at 19.03.2007 18:00 GMT. (b) 20.03.2007 12:00 GMT forecast with GPS-RO assimilation, initialized at 19.03.2007 18:00 GMT. (c) 20.03.2007 12:00 GMT analysis of GFS.

For a vertical outlook, a thermodynamic diagram can give an idea. At Figure 5.17, Skew-T log-p diagrams of Istanbul Sabiha Gokcen Airport are shown, as the forecast without and with assimilation, and observation in order. Although there is not huge difference between the temperature profiles, it is absolutely clear that the Dew Point Temperature profile is much more accurate at the diagram of forecast with assimilation, especially at the higher levels of the troposphere. The forecasts of thermodynamic values and indexes are also improved with assimilation in general.

Mediterranean
Temperature
Geopotential height
Horizontal wind vectors

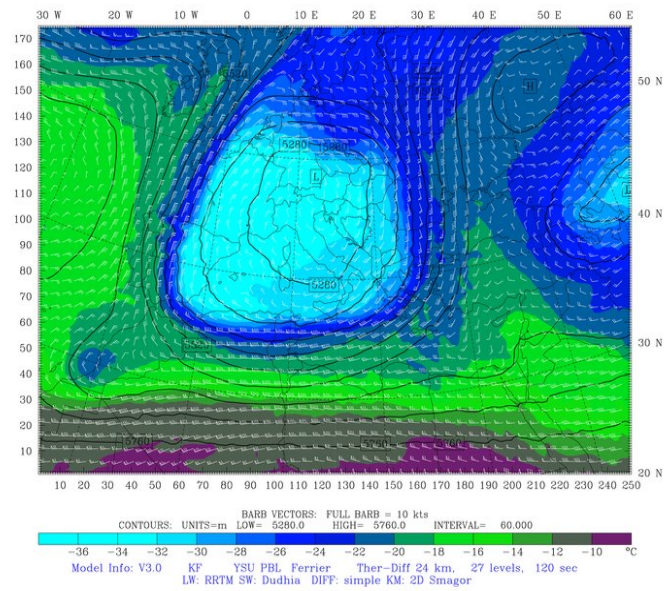
Fcst: 18 h
Valid: 12 UTC Wed 21 Mar 07 (15 LDT Wed 21 Mar 07)
at pressure = 500 hPa
at pressure = 500 hPa
at pressure = 500 hPa



(a)

Mediterranean
Temperature
Geopotential height
Horizontal wind vectors

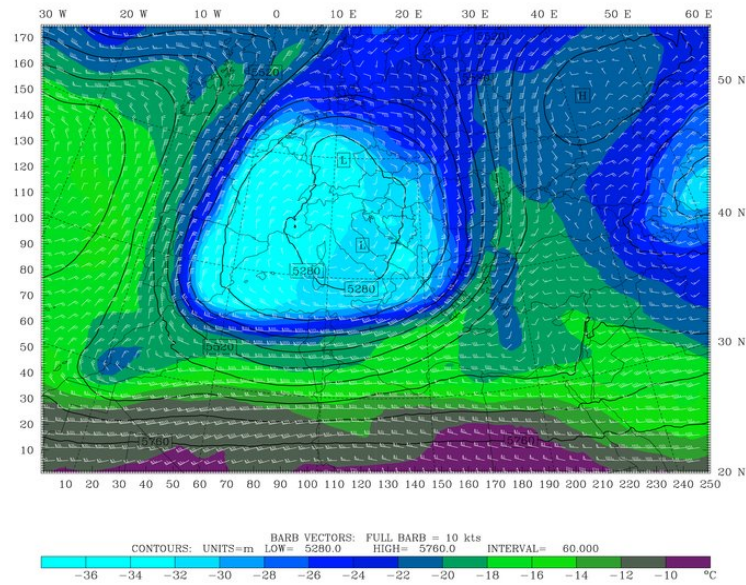
Fcst: 18 h
Valid: 12 UTC Wed 21 Mar 07 (15 LDT Wed 21 Mar 07)
at pressure = 500 hPa
at pressure = 500 hPa
at pressure = 500 hPa



(b)

Mediterranean
Temperature
Geopotential height
Horizontal wind vectors

Valid: 12 UTC Wed 21 Mar 07 (15 LDT Wed 21 Mar 07)
Fcst: 0 h
at pressure = 500 hPa
at pressure = 500 hPa
at pressure = 500 hPa



(c)

Figure 5.18: (a) 21.03.2007 12:00 GMT forecast without assimilation, initialized at 20.03.2007 18:00 GMT. (b) 21.03.2007 12:00 GMT forecast with GPS-RO assimilation, initialized at 20.03.2007 18:00 GMT. (c) 21.03.2007 12:00 GMT analysis of GFS.

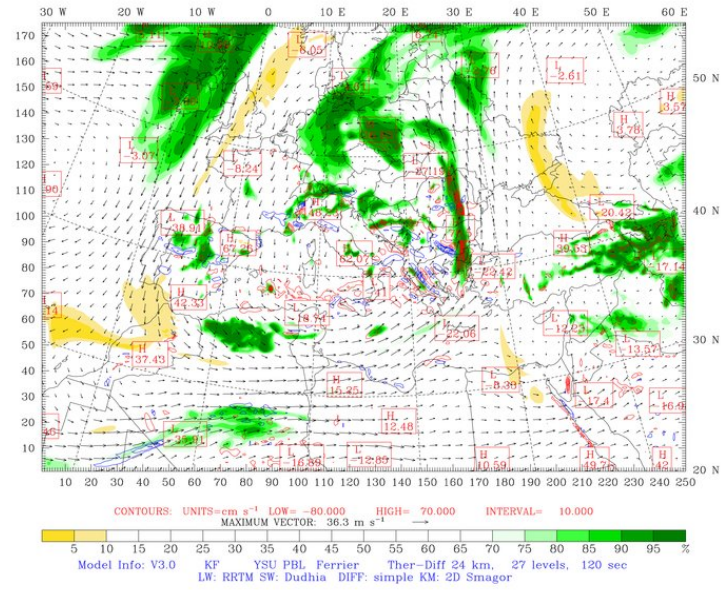
500 hPa forecasts of 21.03.2007 12:00 GMT also indicate that the assimilation improved the 500 hPa temperature. Especially the -20 C isotherm of the forecast with assimilation on Western Black Sea has a similar pattern with the observation.

Mediterranean

Fcst: 18 h

Relative humidity (w.r.t. water)
Horizontal wind vectors
Vertical velocity

Valid: 12 UTC Wed 21 Mar 07 (15 LDT Wed 21 Mar 07)
at pressure = 700 hPa
at pressure = 700 hPa
at pressure = 700 hPa



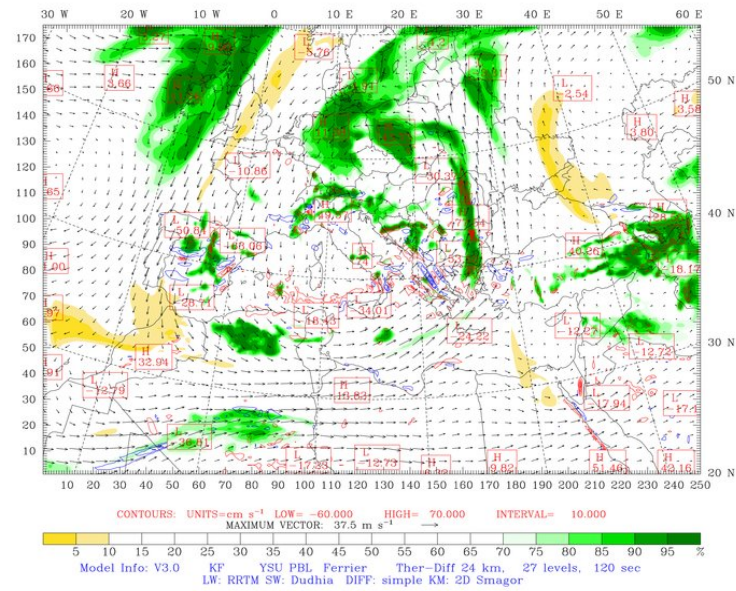
(a)

Mediterranean

Fcst: 18 h

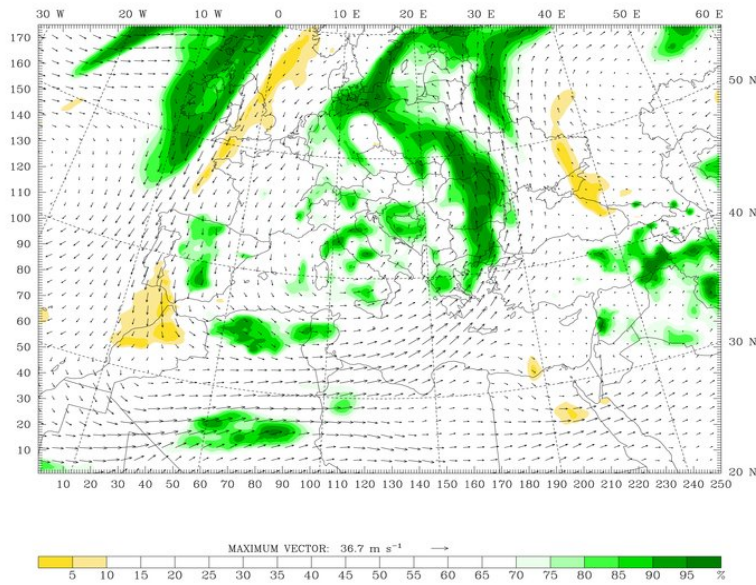
Relative humidity (w.r.t. water)
Horizontal wind vectors
Vertical velocity

Valid: 12 UTC Wed 21 Mar 07 (15 LDT Wed 21 Mar 07)
at pressure = 700 hPa
at pressure = 700 hPa
at pressure = 700 hPa



(b)

Mediterranean Fcst: 0 h
 Valid: 12 UTC Wed 21 Mar 07 (15 LDT Wed 21 Mar 07)
 Relative humidity (w.r.t. water) at pressure = 700 hPa
 Horizontal wind vectors at pressure = 700 hPa
 Vertical velocity at pressure = 700 hPa



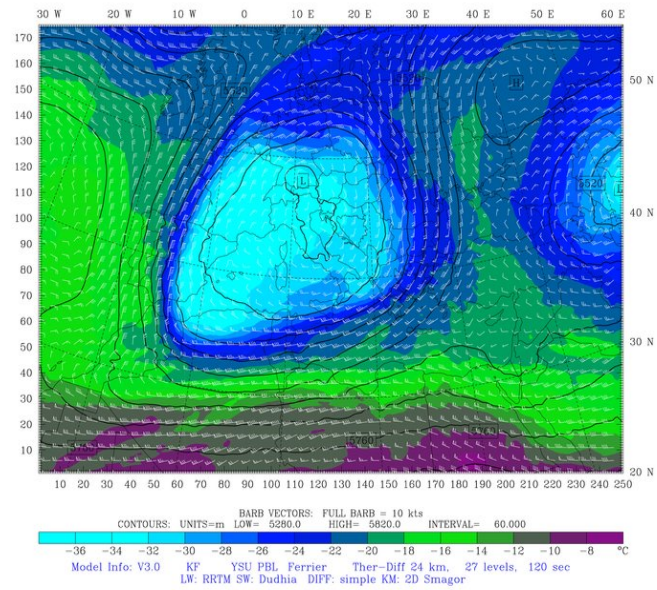
(c)

Figure 5.19: (a) 21.03.2007 12:00 GMT forecast without assimilation, initialized at 20.03.2007 18:00 GMT. (b) 21.03.2007 12:00 GMT forecast with GPS-RO assimilation, initialized at 20.03.2007 18:00 GMT. (c) 21.03.2007 12:00 GMT analysis of GFS.

At 700 hPa of the same time, the relative humidity over the same area is also better estimated with the run with GPS-RO assimilation.

Mediterranean

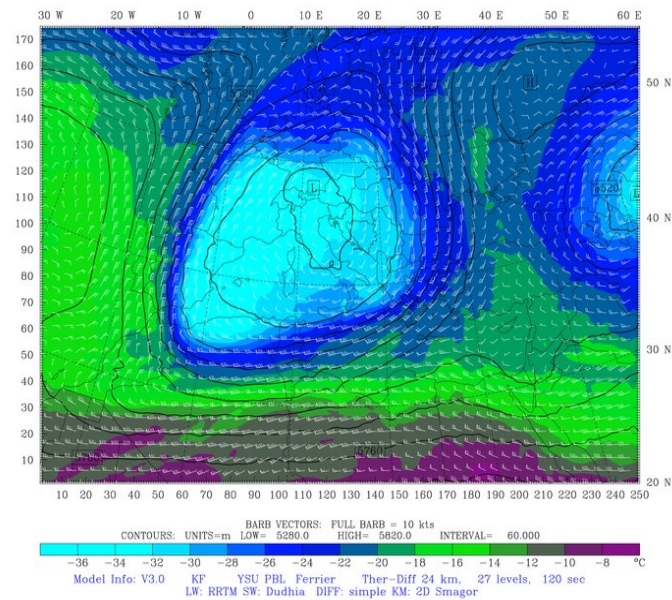
Valid: 18 UTC Wed 21 Mar 07 (21 LDT Wed 21 Mar 07)
Fcst: 18 h
Temperature at pressure = 500 hPa
Geopotential height at pressure = 500 hPa
Horizontal wind vectors at pressure = 500 hPa



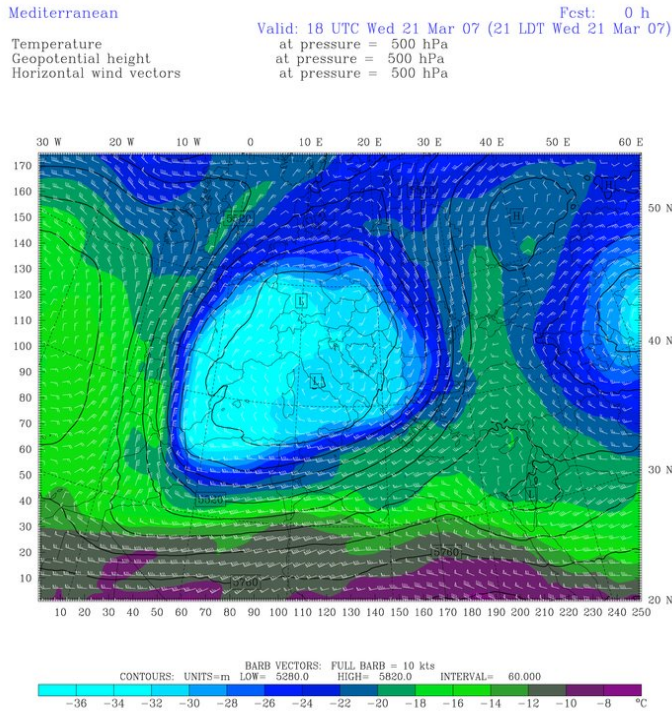
(a)

Mediterranean

Valid: 18 UTC Wed 21 Mar 07 (21 LDT Wed 21 Mar 07)
Fcst: 18 h
Temperature at pressure = 500 hPa
Geopotential height at pressure = 500 hPa
Horizontal wind vectors at pressure = 500 hPa



(b)



(c)

Figure 5.20: (a) 21.03.2007 18:00 GMT forecast without assimilation, initialized at 21.03.2007 00:00 GMT. (b) 21.03.2007 18:00 GMT forecast with GPS-RO assimilation, initialized at 21.03.2007 00:00 GMT. (c) 21.03.2007 18:00 GMT analysis of GFS.

500 hPa forecasts of 21.03.2007 18:00 GMT show a higher accuracy of temperature with assimilation. The isotherms in front of the low centre over Eastern Mediterranean and Western Anatolia has a similar pattern to that of the observation.

In conclusion, experiments were conducted to assimilate GPS-RO data for the 19 March Mediterranean low pressure system. In general, the COSMIC GPS-RO data assimilation showed positive impacts on the forecasts, especially within the boundary layer.

In this study limited amount of data are assimilated to the model and also because of some constraints (experience, time, cpu) the assimilation was not made in cycling mode. Only impacts of one time assimilation are shown for different analysis times and different forecast hours. To see a more consistent impact, cycling of observations should be carried out. Furthermore, as most of the impact of GPS-RO observations were seen to be limited to the boundary layer, greater vertical model resolution especially at lower levels may also contribute to further improving results. Finally,

for more conclusive and statistically significant results, these experiments should be repeated for a number of other Mediterranean low-pressure systems.

REFERENCES

- Bevis, M., Businger, S., Herring T. A., Rochen, C., Anthes, R. A. and Ware, R. H.**, 1992. GPS meteorology: remote sensing of atmospheric water vapor using the global positioning system. *Journal of Geophysical Research*, **97**, 15,787-15,801.
- Bouttier, F., Courtier, P.**, 1999. Data assimilation concepts and methods. *ECMWF Training Course Notes*
- Duan, J., Bevis, M., Fang, P., Bock, Y., Chiswell, S. R., Businger, S., Rocken, C., Solheim, F. S., Van Hove, T., Ware, R. H., McClusky, S. Herring, T. A., and King, R. W.**, 1996. GPS meteorology: direct estimation of the absolute value of precipitable water, *Journal of Applied Meteorology*, **35**, 830-838.
- Gorbunov, M.E., and A.S.**, 1998. Gurvich, Microlab-1 experiment: Multipath effects in the lower troposphere, *Journal of Geophysical Research*, **103**, 13819-13826.
- Liu, H., Anderson, J., Kuo, Y-H., Snyder, C. and Caya, A.**, 2007. Evaluation of a Nonlocal Quasi-Phase Observation Operator in Assimilation of CHAMP Radio Occultation Refractivity with WRF, *Monthly Weather Review*, **136**, 242- 256.
- Kalnay, E.**, 2003. *Atmospheric Modeling, Data Assimilation and Predictability*, Cambridge University Press, United Kingdom.
- Kuo, Y-H., Sokolovskiy, S., Anthes, A., Vandenberghe1, F.**, 2000. Assimilation of GPS Radio Occultation Data for Numerical Weather Prediction, *Special issue of Terrestrial, Atmospheric and Oceanic Science*, 11(1), 157-186, March 2000.
- Kuo, Y.-H., Zou, X., and Huang, W.**, 1997. The impact of GPS data on the prediction of an extratropical cyclone: An observing system simulation experiment, *Journal of Dynamics of Atmospheres and Oceans*, **27**, 439-470.
- Kursinski, E. R.,Hajj, G. A., Schofield, T., Linfield, R. P. and Hardy, K. R.**, 1997. Observing Earth's atmosphere with radio occultation measurements using the Global Positioning System. *Journal of Geophysical Research*, **102**, 23.429-23.465.
- Leroy, S.**, 1997. The measurement of geopotential heights by GPS radio occultation, *Journal of Geophysical Research*, **102 (D6)**, 6971-6986.
- Lorenc, A. C.**, 1986. Analysis methods for numerical weather prediction. *The Quarterly Journal of the Royal Meteorological Society*, **112**, 1177–1194.
- Lynch, P.**, 2008. Origins of Computer Weather Prediction and Climate Modeling, *Journal of Computational Physics*, **227**, 3431–3444.

- Marshall, J. L., Yoe, J.**, 2005. 2nd *GPSRO Data Users Workshop*, Lansdowne, Virginia August 22-24 2005.
- Melbourne, W. G., Davis, E. S., Duncan, C. B., Hajj, G. A., Hardy, K. R., Kursinski, E. R., Meehan, T. K., Young, L. E. and Yunck, T. P.**, 1994. The Application of Spaceborne GPS to Atmospheric Limb Sounding and Global Change Monitoring, *NASA/ Jet Propulsion Laboratory Publication*, 94-18.
- Nutter, P. A., Mullen, S. L., and Baumhefner, D. P.**, 1998. The Impact of Initial Condition Uncertainty on Numerical Simulations of Blocking, *Monthly Weather Review*, **126**, 2482–2502.
- Parrish, D.F., and Derber, J. C.**, 1992. The National Meteorological Center’s Spectral Statistical Interpolation analysis system. *Monthly Weather Review*, **120**, 1747–1763.
- Rabier, F., Klinker, E., Courtier, P., and Hollingsworth, A.**, 1996. Sensitivity of forecast errors to initial conditions, *The Quarterly Journal of the Royal Meteorological Society*, **122**, 121-150.
- Rocken, C., Van Hove, T., Johnson, J., Solheim, S., Ware, R. H., Bevis, M., and Chiswell, R.**, 1995. GPS/STORM – GPS sensing of atmospheric water vapor for meteorology. *Journal of Atmospheric and Oceanic Technology*, **12**, 468-478.
- Rocken, C., Anthes, R., Exner, M., Hunt, D., Sokolovskiy, S., Ware, R., Gorbunov, M., Schreiner, W., Feng, D., Herman, B., Kuo, Y. and Zou, X.**, 1997. Analysis and validation of GPS/MET data in the neutral atmosphere, *Journal of Geophysical Research*, **102 (D25)**, 29849-29866.
- Rocken, C., Kuo, Y.-H., Schreiner, W., Hunt, D., Sokolovskiy, S.**, 2000. COSMIC System Description, *Special issue of Terrestrial, Atmospheric and Oceanic Science*, **11(1)**, 21-52, March 2000.
- Skamarock, W.C., Klemp, J.B., Dudhia, J., Gill, D.O., Barker, D.M., Duda, M.G., Huang, X-Y., Wang, W., Powers, J.G.**, 2008. *A Description of the Advanced Research WRF Version 3*.
- Talagrand, O.**, 1997. Assimilation of observations, an introduction, *Journal of the Meteorological Society of Japan Special Issue*, **75**, 1B, 191-209.
- Url-1** <<http://www.cosmic.ucar.edu>>, accessed at 23.01.2009
- Url-2** < <http://www.wetterzentrale.de/topkarten/fsreaeur.html>>, accessed at 15.09.2008
- Url-3** < http://en.wikipedia.org/wiki/GPS_Radio_occultation>, accessed at 11.12.2008
- Wang, W., Barker, B., Bruyère, C., Duda, M., Dudhia, J., Gill, D., Michalakes, J. and Rizvi, S.**, 2008. *ARW Version 3 Modeling System User’s Guide*.
- Ware, R., Exner, M., Feng, D., Gorbunov, M., Hardy, K., Herman, B., Kuo, Y., Meehan, T., Melbourne, W., Rocken, C., Schreiner, W., Sokolovskiy, S., Solheim, F., Zou, X., Anthes, R., Businger, S.**

and Trenberth, K., 1996. GPS sounding of the atmosphere from low Earth orbit: Preliminary results, *Bulletin of the American Meteorological Society*, **77**, 19-40.

APPENDICES

APPENDIX A.1 : A sample WRF namelist used in this study.

```
&time_control
run_days           = 4,
run_hours          = 0,
run_minutes        = 0,
run_seconds        = 0,
start_year         = 2007, 2006, 2006,
start_month        = 03, 05, 05,
start_day          = 19, 25, 25,
start_hour         = 00, 00, 00,
start_minute       = 00, 00, 00,
start_second       = 00, 00, 00,
end_year           = 2007, 2006, 2006,
end_month          = 03, 05, 05,
end_day            = 23, 27, 27,
end_hour           = 00, 00, 00,
end_minute         = 00, 00, 00,
end_second         = 00, 00, 00,
interval_seconds   = 21600
input_from_file    = .true.,.true.,.true.,
history_interval   = 180, 60, 30,
frames_per_outfile = 1000, 1000, 1000,
restart            = .false.,
restart_interval   = 5000,
io_form_history    = 2
io_form_restart    = 2
io_form_input      = 2
io_form_boundary   = 2
debug_level        = 0
/

&domains
time_step          = 120,
time_step_fract_num = 0,
time_step_fract_den = 1,
max_dom            = 1,
s_we               = 1, 1, 1,
e_we               = 250, 121, 186,
s_sn               = 1, 1, 1,
e_sn               = 175, 106, 136,
```

```

s_vert          = 1, 1, 1,
e_vert          = 28, 28, 28,
num_metgrid_levels = 27
dx              = 24000, 8000, 1600,
dy              = 24000, 8000, 1600,
grid_id         = 1, 2, 3,
parent_id       = 0, 1, 2,
i_parent_start  = 1, 64, 16,
j_parent_start  = 1, 25, 62,
parent_grid_ratio = 1, 3, 5,
parent_time_step_ratio = 1, 3, 5,
feedback        = 1,
smooth_option   = 0
/

```

```

&physics
mp_physics      = 5, 3, 3,
ra_lw_physics   = 1, 1, 1,
ra_sw_physics   = 1, 1, 1,
radt            = 24, 24, 24,
sf_sfclay_physics = 1, 1, 1,
sf_surface_physics = 1, 1, 1,
bl_pbl_physics  = 1, 1, 1,
bldt            = 0, 0, 0,
cu_physics      = 1, 1, 0,
cudt            = 5, 5, 5,
isfflx          = 1,
ifsnow          = 0,
icloud          = 1,
surface_input_source = 1,
num_soil_layers = 5,
ucmcall         = 0,
mp_zero_out     = 0,
maxiens         = 1,
maxens          = 3,
maxens2         = 3,
maxens3         = 16,
ensdim          = 144,
slope_rad       = 0,
topo_shading    = 0,
/

```

```

&fdda
/

```

```

&dynamics
w_damping       = 0,
diff_opt        = 1,
km_opt          = 4,
diff_6th_opt    = 0,

```

```

diff_6th_factor      = 0.12,
base_temp            = 290.
damp_opt             = 0,
zdamp                = 5000., 5000., 5000.,
dampcoef             = 0.01, 0.01, 0.01
khdif                = 0, 0, 0,
kvdif                = 0, 0, 0,
non_hydrostatic     = .true., .true., .true.,
pd_moist             = .true., .true., .true.,
pd_scalar            = .true., .true., .true.,
/

```

```

&bdy_control
spec_bdy_width      = 5,
spec_zone           = 1,
relax_zone          = 4,
specified            = .true., .false., .false.,
nested              = .false., .true., .true.,
/

```

```

&grib2
/

```

```

&namelist_quilt
nio_tasks_per_group = 0,
nio_groups = 1,
/

```


APPENDIX A.2 : A sample WPS namelist used in this study.

```
&share
wrf_core = 'ARW',
max_dom = 1,
start_date = '2007-03-19_00:00:00','2006-05-25_00:00:00','2006-05-25_00:00:00'
end_date = '2007-03-23_00:00:00','2006-05-27_00:00:00','2006-05-27_00:00:00'
interval_seconds = 21600
io_form_geogrid = 2,
/
```

```
&geogrid
parent_id = 1, 1, 2,
parent_grid_ratio = 1, 3, 5,
i_parent_start = 1, 64, 16,
j_parent_start = 1, 25, 62,
e_we = 200, 121, 186,
e_sn = 135, 106, 136,
geog_data_res = '10m','2m','30s'
dx = 24000,
dy = 24000,
map_proj = 'lambert',
ref_lat = 37.50,
ref_lon = 16.50,
truelat1 = 32.5,
truelat2 = 42.5,
stand_lon = 16.5,
geog_data_path = '/home/seyda/WRF/geog'
/
```

```
&ungrib
out_format = 'WPS',
prefix = 'FILE',
/
```

```
&metgrid
fg_name = 'FILE'
io_form_metgrid = 2,
/
```

```
&mod_levs
press_pa = 201300 , 200100 , 100000 ,
          95000 , 90000 ,
          85000 , 80000 ,
          75000 , 70000 ,
          65000 , 60000 ,
          55000 , 50000 ,
          45000 , 40000 ,
```

35000 , 30000 ,
25000 , 20000 ,
15000 , 10000 ,
5000 , 1000

APPENDIX A.3 : RMSE and mean error summery statistics for all parameterization variations which are tried in this study.

Table A.1 : RMSE and MEAN ERROR Statistics for Variables of cu_physics=1, mp_physics= 3 Parameterizations Verifications

VARIABLES	RMSE	MEAN ERROR
T	-1.15019834	3.33020949
QVAPOR	0.00002737	0.00046943
QCLOUD	0.00000334	0.00002476
QRAIN	0.00000363	0.00003831
U	0.03475221	3.5845778
V	-0.18000281	3.63864303
W	-0.00017093	0.05418772
PH	-113.3644333	274.0866089
PHB	0	0
MUB	0	0
U10	0.16352661	2.5493536
V10	0.01648772	2.85321188

Table A.2 : RMSE and MEAN ERROR Statistics for Variables of cu_physics= 2, mp_physics= 3 Parameterizations Verifications

VARIABLES	RMSE	MEAN ERROR
T	-1.18545711	3.35118794
QVAPOR	0.00002962	0.00046358
QCLOUD	0.00000444	0.00003123
QRAIN	0.00000397	0.00003653
U	0.03792351	3.52816391
V	-0.18267979	3.57531977
W	-0.00022976	0.05341746
PH	-113.3691254	270.5900574
PHB	0	0
MUB	0	0
U10	0.16582671	2.4387219
V10	0.01088473	2.7901299

Table A.3: RMSE and MEAN ERROR Statistics for Variables of
cu_physics= 3, mp_physics= 3 Parameterizations Verifications

VARIABLES	RMSE	MEAN ERROR
T	-1.18437696	3.34640265
QVAPOR	0.00001694	0.000486
QCLOUD	0.00000484	0.00003368
QRAIN	0.00000334	0.00003153
U	0.02693046	3.53256631
V	-0.17960629	3.54447532
W	-0.00023393	0.05484865
PH	-115.5956802	275.1863098
PHB	0	0
MUB	0	0
U10	0.14626196	2.51050711
V10	-0.00177344	2.74141097

Table A.4 : RMSE and MEAN ERROR Statistics for Variables of
cu_physics= 5, mp_physics= 5 Parameterizations Verifications

VARIABLES	RMSE	MEAN ERROR
T	-1.14967585	3.3359251
QVAPOR	0.00002214	0.00048633
QCLOUD	0.00000282	0.00002702
QRAIN	0.00000062	0.00000664
U	0.04853318	3.52506852
V	-0.19069351	3.48065209
W	-0.00016815	0.05461417
PH	-112.7110443	273.812561
PHB	0	0
MUB	0	0
U10	0.1791248	2.53762722
V10	0.00176379	2.76128054

Table A.5 : RMSE and MEAN ERROR Statistics for Variables of
 cu_physics= 3, mp_physics= 5 Parameterizations Verifications

VARIABLES	RMSE	MEAN ERROR
T	-1.1485132	3.34255457
QVAPOR	0.00001546	0.00048482
QCLOUD	0.00000278	0.00002683
QRAIN	0.00000055	0.00000601
U	0.0473039	3.54438281
V	-0.19103283	3.50223827
W	-0.00019535	0.05558245
PH	-112.1374435	273.20578
PHB	0	0
MUB	0	0
U10	0.18147223	2.52475548
V10	0.00761019	2.74546885

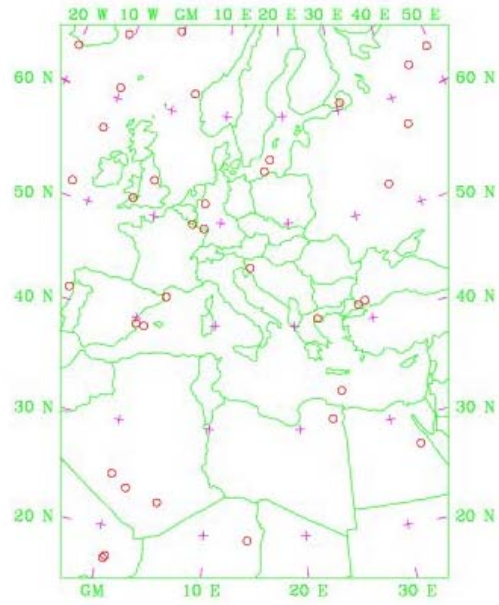
Table A.6 : RMSE and MEAN ERROR Statistics for Variables of
 cu_physics= 1, mp_physics= 5 ra_lw_physics= 99
 Parameterizations Verifications

VARIABLES	RMSE	MEAN ERROR
T	-1.06645918	3.3975873
QVAPOR	0.00000554	0.00048201
QCLOUD	0.00000121	0.00001717
QRAIN	0.00000035	0.00000629
U	0.02809247	3.56554532
V	-0.19049779	3.62455201
W	-0.00001744	0.05380011
PH	-97.69548798	265.4732971
PHB	0	0
MUB	0	0
U10	0.10272233	2.62822008
V10	0.02438727	2.87425494

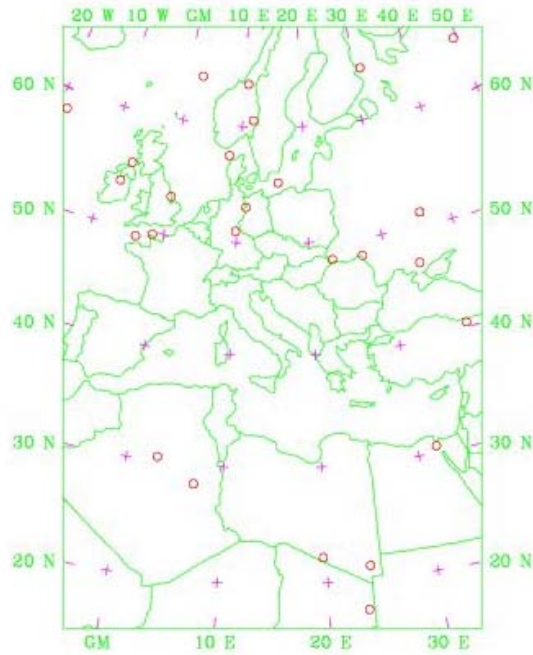
Table A.7 : RMSE and MEAN ERROR Statistics for Variables of
 cu_physics= 1, mp_physics= 5 ra_lw_physics= 99
 ra_sw_physics= 99 Parameterizations Verifications

VARIABLES	RMSE	MEAN ERROR
T	-0.82912862	2.97951436
QVAPOR	0.00001731	0.00047884
QCLOUD	0.00000113	0.00001682
QRAIN	0.00000034	0.00000623
U	0.02580584	3.51874352
V	-0.19252931	3.60837197
W	0.0000829	0.05369555
PH	-81.86911774	250.3229523
PHB	0	0
MUB	0	0
U10	0.14415355	2.561728
V10	0.05745829	2.85513711

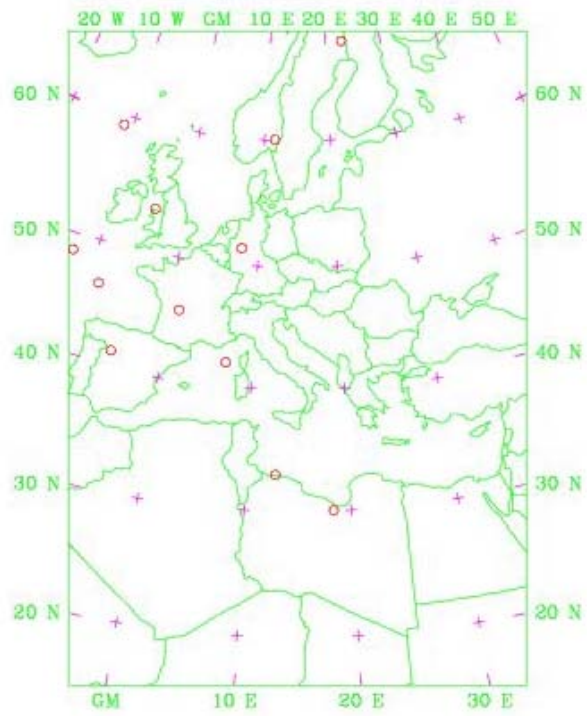
APPENDIX A.4 : Map_PLOT outputs which show the GPS-RO Occultations for given time windows



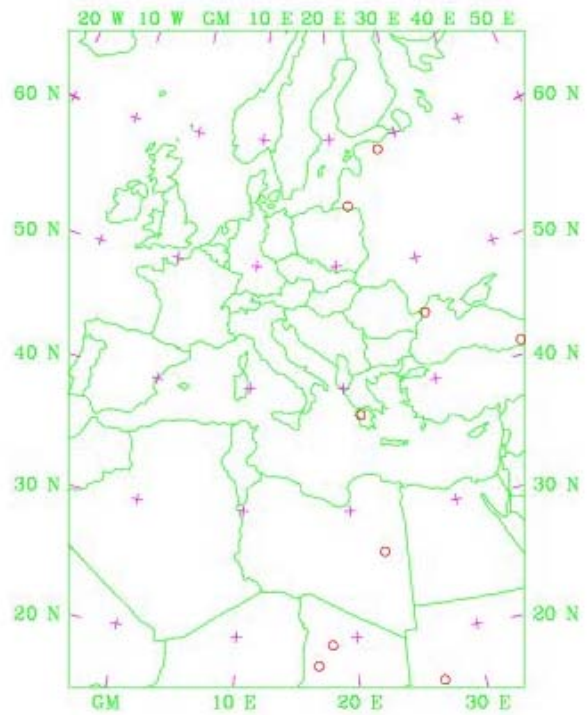
○ 36 GPSRF 2007-03 [19_03:00,19_09:00]



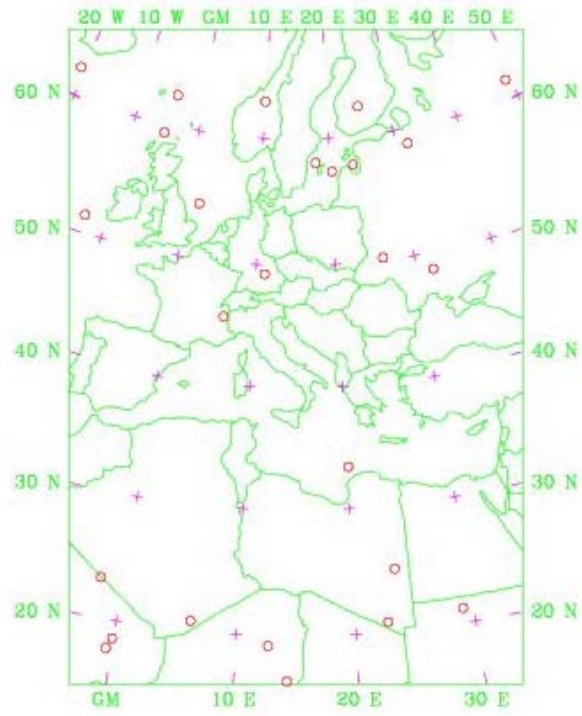
○ 26 GPSRF 2007-03 [19_09:00,19_15:00]



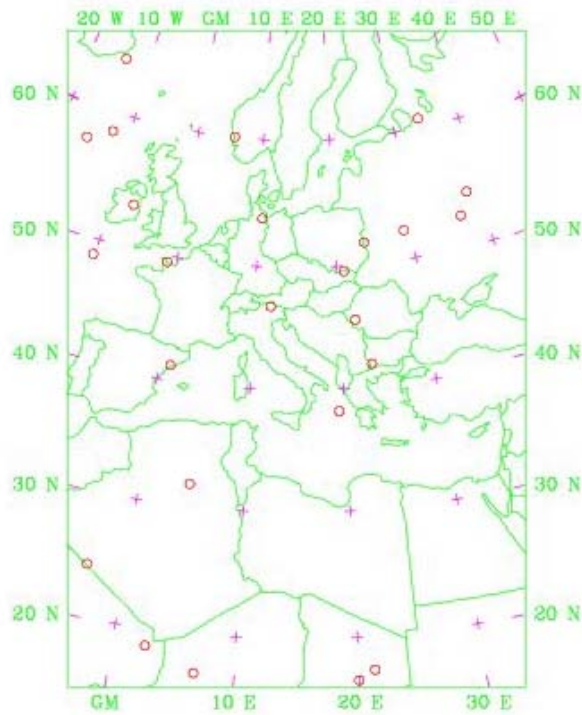
○ 12 GPSRF 2007-03 [19_15:00,19_21:00]



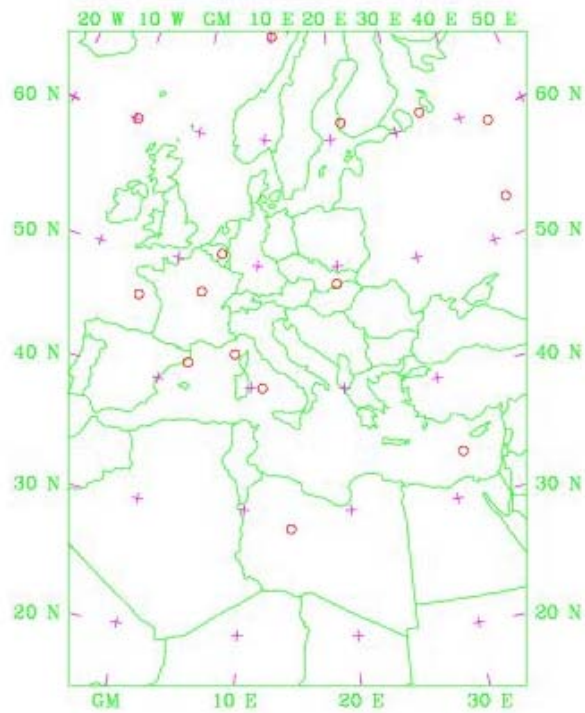
○ 9 GPSRF 2007-03 [19_21:00,20_03:00]



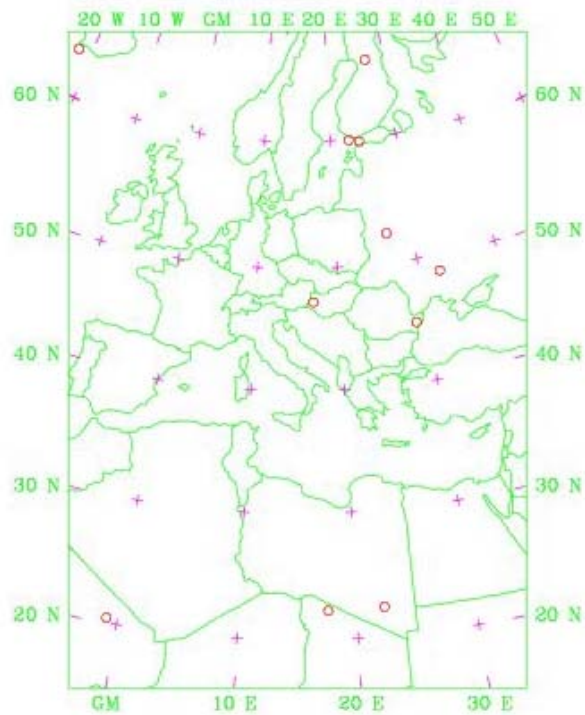
○ 26 GPSRF 2007-03 [20_03.00, 20_09.00]



○ 25 GPSRF 2007-03 [20_09.00, 20_15.00]



○ 15 GPSRF 2007-03 [20_15:00,20_21:00]



○ 11 GPSRF 2007-03 [20_21:00,21_03:00]

Figure A.1 : GPS-RO Occultation Distirubitions during the case

APPENDIX A.5 : Contents of a sample WRF-3DVAR output “statistics file”

Diagnostics of OI for gpsref

var	ref(m)	n	k
Number:	4159		
Minimum(n,k):	-10.7900	4	12
Maximum(n,k):	6.6986	10	19
Average :	-0.2731		
RMSE :	1.5435		

Diagnostics of AO for gpsref

var	ref(m)	n	k
Number:	4159		
Minimum(n,k):	-6.4673	4	12
Maximum(n,k):	4.7649	1	34
Average :	-0.0181		
RMSE :	0.6606		

Minimum of gridded analysis increments

Lvl	U	i	J	V	i	J
1	-1.2623	88	92	-1.2838	117	106
2	-1.4138	88	92	-1.4376	117	106
3	-1.5078	89	92	-1.5337	117	107
4	-1.5915	89	92	-1.6241	118	107
5	-1.639	90	92	-1.6871	118	108
6	-1.646	91	92	-1.7101	118	108
7	-1.5882	93	92	-1.6684	119	110
8	-1.4795	96	92	-1.5641	119	111
9	-1.3942	99	92	-1.4567	120	113
10	-1.4001	100	92	-1.4252	120	113
11	-1.4537	101	92	-1.4374	121	114
12	-1.5897	102	92	-1.5068	123	114
13	-1.8299	102	91	-1.6539	124	114
14	-2.1385	103	90	-1.8897	126	114
15	-2.5376	105	90	-2.2559	127	114
16	-2.8878	107	90	-2.6154	128	114
17	-3.1693	64	153	-2.9693	67	156
18	-2.9036	66	154	-2.8615	68	156
19	-2.1409	66	1	-2.1016	68	155
20	-1.687	65	1	-1.3541	86	13
21	-1.0649	64	1	-0.8538	86	12
22	-0.6118	191	174	-0.5461	77	93
23	-0.9726	97	130	-0.8565	85	121
24	-1.6257	96	129	-1.3458	88	123
25	-2.4253	98	130	-2.0054	89	123
26	-3.4543	99	131	-2.8133	89	121
27	-4.917	98	130	-3.8704	89	121
ALL	-4.917			-3.8704		

Lvl	T	i	j	p	i	J	Q	i	J
1	-0.1207	103	131	-121.8253	80	145	-4.43E-04	164	47
2	-0.1003	132	152	-120.7983	80	145	-4.86E-04	164	47
3	-0.1043	132	152	-119.4117	80	145	-5.60E-04	164	47
4	-0.1265	81	142	-117.6691	80	145	-7.58E-04	164	47
5	-0.1392	82	143	-115.5174	80	145	-9.59E-04	164	47
6	-0.1758	194	168	-112.8553	80	145	-9.77E-04	164	47
7	-0.1993	194	168	-109.7159	80	145	-8.07E-04	164	47
8	-0.2955	80	142	-105.1774	80	145	-8.71E-04	67	4
9	-0.3761	79	141	-99.3657	80	145	-9.50E-04	160	34
10	-0.4279	78	141	-93.3431	80	145	-1.17E-03	160	34
11	-0.4537	77	140	-87.0857	80	145	-9.37E-04	42	94
12	-0.4511	78	141	-78.42	80	145	-1.05E-03	71	77
13	-0.5459	77	140	-68.0238	80	145	-1.02E-03	72	77
14	-0.7663	77	140	-58.7543	80	145	-7.92E-04	71	77
15	-1.0741	79	141	-50.5105	80	145	-5.18E-04	71	77
16	-1.2534	80	142	-43.1622	80	145	-2.40E-04	72	77
17	-0.7235	101	133	-36.5993	80	145	-6.19E-05	73	77
18	-1.7553	86	90	-30.7393	80	145	-1.02E-05	74	77
19	-2.785	102	120	-25.518	80	145	-6.30E-06	103	131
20	-2.862	103	119	-20.8821	80	145	-6.02E-06	103	131
21	-2.3659	172	86	-16.7806	80	145	-3.49E-06	132	151
22	-1.3701	198	25	-13.1634	80	145	-1.28E-06	132	151
23	-1.6567	61	10	-9.9837	80	145	-3.05E-07	97	122
24	-2.5801	67	4	-7.1991	80	145	-1.40E-07	101	121
25	-3.0591	75	76	-4.7707	80	145	-1.36E-07	102	120
26	-2.1749	102	119	-2.6628	80	145	-4.14E-08	82	144
27	-2.4394	199	24	-0.8423	80	145	-7.31E-08	174	88
ALL	-3.0591			-121.8253			-1.17E-03		

Maximum of gridded analysis increments

Lvl	U	i	j	V	i	J
1	1.625	105	131	1.7828	88	127
2	1.8269	105	132	1.9872	87	126
3	1.9678	105	132	2.1073	87	126
4	2.1243	104	132	2.2117	87	126
5	2.2746	103	132	2.2421	87	125
6	2.411	101	132	2.199	86	124
7	2.4816	99	132	2.0595	85	121
8	2.4799	97	131	1.8521	84	118
9	2.465	96	131	1.7154	83	115
10	2.5166	95	131	1.732	84	115
11	2.5915	96	131	1.8295	85	117
12	2.7514	96	131	2.0591	86	118
13	3.0537	97	131	2.4293	86	119
14	3.5523	97	130	2.8512	87	120
15	4.3365	97	130	3.4067	87	120
16	5.2199	96	129	3.8755	88	120
17	5.652	96	129	4.0032	89	121
18	5.1233	96	128	3.5474	91	123
19	3.6676	97	128	2.451	93	123
20	1.9495	100	128	1.4217	97	125
21	0.7092	175	113	0.8627	44	14

22	0.602	82	83	0.533	114	120
23	0.6149	92	82	0.6083	120	112
24	1.1123	63	153	0.9847	68	156
25	1.7465	62	153	1.5032	69	157
26	2.5651	62	153	2.0759	70	158
27	3.9906	60	152	2.846	70	159
ALL	5.652			4.0032		

Lvl	T	i	J	p	i	j	Q	l	j
1	0.1247	161	36	242.6171	101	116	1.56E-04	86	89
2	0.1536	160	35	240.5571	101	116	1.68E-04	86	89
3	0.1616	160	35	237.7729	101	116	1.77E-04	86	89
4	0.1759	71	78	234.267	101	116	1.91E-04	85	89
5	0.224	74	77	229.9334	102	116	2.45E-04	194	167
6	0.211	104	118	224.5441	102	116	3.37E-04	194	167
7	0.2424	103	119	218.1171	102	116	5.36E-04	175	88
8	0.362	103	119	208.7221	102	116	4.72E-04	77	75
9	0.5672	103	118	196.7718	102	116	6.71E-04	76	76
10	0.8027	101	117	184.7041	102	116	6.92E-04	86	89
11	1.0743	101	118	172.5023	102	116	6.54E-04	86	89
12	1.314	102	119	155.7933	102	116	5.99E-04	85	90
13	1.642	103	118	135.6395	102	116	4.13E-04	85	89
14	1.8642	103	118	117.441	102	116	2.14E-04	85	89
15	1.7898	103	118	101.0739	102	116	1.57E-04	164	47
16	1.3526	71	78	86.396	102	116	9.40E-05	164	47
17	1.2771	71	77	73.2605	102	116	3.85E-05	61	10
18	0.8948	80	142	61.5307	102	116	1.41E-05	67	3
19	1.6968	80	142	51.0818	102	116	1.48E-05	102	120
20	1.2831	76	139	41.8023	102	116	1.48E-05	102	120
21	1.4741	80	142	33.591	102	116	8.83E-06	102	120
22	2.8545	185	140	26.3499	102	116	2.47E-06	102	120
23	2.258	85	89	19.9852	102	116	2.31E-07	102	120
24	1.2719	132	152	14.4111	102	116	5.35E-08	102	132
25	2.0103	43	142	9.5499	102	116	8.12E-08	80	142
26	1.7467	133	153	5.3302	102	116	7.47E-08	185	140
27	2.0063	71	135	1.6861	102	116	7.21E-08	185	140
ALL	2.8545			242.6171			6.92E-04		

Mean of gridded analysis increments

Lvl	U	V	t	P	Q
1	0.0201	0.01	0.009	10.3898	-2.81E-06
2	0.0228	0.0111	0.017	10.3002	-3.08E-06
3	0.0248	0.0117	0.022	10.1792	-3.32E-06
4	0.0271	0.0119	0.029	10.0273	-3.86E-06
5	0.0288	0.0112	0.036	9.8395	-4.33E-06
6	0.0305	0.0098	0.041	9.6057	-4.65E-06
7	0.0312	0.0076	0.051	9.3261	-4.96E-06
8	0.0302	0.0046	0.068	8.9171	-5.68E-06
9	0.0291	0.0022	0.092	8.4042	-7.88E-06
10	0.0295	0.0012	0.118	7.8997	-9.10E-06
11	0.0307	0.001	0.141	7.3987	-9.29E-06
12	0.0337	0.0013	0.164	6.714	-8.00E-06
13	0.0386	0.0018	0.187	5.8825	-6.51E-06
14	0.0434	0.0017	0.201	5.1219	-4.54E-06
15	0.0484	0.0016	0.187	4.4254	-2.35E-06

16	0.055	0.0009	0.132	3.7901	-7.77E-07
17	0.067	0.0006	0.027	3.2158	-1.01E-07
18	0.0835	0.0011	-0.111	2.7013	8.78E-09
19	0.0924	0	-0.246	2.2429	6.62E-09
20	0.0841	0.0014	-0.298	1.8358	7.32E-09
21	0.0632	0.0032	-0.219	1.4754	3.64E-09
22	0.0368	0.0019	-0.097	1.1575	5.97E-10
23	0.0089	0	-0.083	0.8779	-2.15E-10
24	-0.019	0.0041	-0.124	0.633	-1.11E-10
25	-0.0502	0.008	-0.133	0.4195	-5.47E-11
26	-0.0855	0.01	-0.121	0.2341	-2.08E-12
27	-0.1261	0.0151	-0.202	0.0741	-2.07E-10
ALL	0.0252	0.0022	-0.004	5.2996	-3.01E-06

RMSE of gridded analysis increments

Lvl	U	V	T	P	Q
1	0.3613	0.3344	0.029	42.2665	2.16E-05
2	0.4057	0.3741	0.032	41.9055	2.36E-05
3	0.4357	0.3992	0.036	41.4176	2.58E-05
4	0.4669	0.4237	0.044	40.8032	3.10E-05
5	0.4921	0.4396	0.052	40.0419	3.77E-05
6	0.5105	0.4469	0.058	39.0912	4.52E-05
7	0.511	0.4378	0.07	37.9515	5.06E-05
8	0.493	0.4133	0.094	36.2816	5.14E-05
9	0.4761	0.3931	0.135	34.1719	6.39E-05
10	0.4828	0.3982	0.18	32.0668	6.81E-05
11	0.5018	0.419	0.22	29.9501	6.32E-05
12	0.5475	0.4676	0.253	27.0464	5.87E-05
13	0.63	0.5514	0.292	23.5472	4.51E-05
14	0.7449	0.6589	0.321	20.3963	3.39E-05
15	0.9069	0.8004	0.31	17.5618	2.15E-05
16	1.0828	0.9403	0.244	15.0132	8.46E-06
17	1.1805	0.0134	0.167	12.7297	2.41E-06
18	1.1049	0.9538	0.277	10.6914	6.39E-07
19	0.8482	0.7526	0.459	8.8768	4.27E-07
20	0.5453	0.5188	0.52	7.2656	3.41E-07
21	0.3173	0.326	0.421	5.8393	1.74E-07
22	0.1736	0.2001	0.317	4.5808	4.66E-08
23	0.1865	0.1727	0.289	3.4744	8.05E-09
24	0.3284	0.2808	0.317	2.5053	4.70E-09
25	0.5443	0.4632	0.35	1.6602	3.17E-09
26	0.8268	0.6982	0.397	0.9266	3.08E-09
27	1.1814	0.9862	0.562	0.2931	3.92E-09
ALL	0.6652	0.5779	0.284	26.2642	3.40E-05

CURRICULUM VITAE



Candidate's full name: Şeyda Tanrıöver

Place and date of birth: Kayseri, 04 February 1981

Permanent Address: Istanbul Technical University, Faculty of Aeronautics and Astronautics, Department of Meteorological Engineering, 34469 Maslak/Istanbul

Universities and Colleges attended: Istanbul Technical University, Institute of Informatics
Istanbul Technical University, Faculty of Aeronautics and Astronautics

Publications:

- **Tanrıöver, S.,** Kadioğlu, M., 2009, Assimilation of GPS-RO Atmospheric Profile Data: A Case Study of a Mediterranean Low Pressure System. EGU General Assembly 2009, March 19-24, 2009 Vienna, Austria.
- Kahraman, A., **Tanrıöver, S.,** Sensitivity and Predictability Analysis of Advanced Research WRF Model (WRF-ARW) in Eastern Mediterranean Region. EGU General Assembly 2009, March 19-24, 2009 Vienna, Austria.